Colloidal Structures Through Dynamic Self-Assembly

by

Antonio Francisco Osorio Vivanco

A dissertation submitted in partial fulfillment
of the requirements for the degree of
Doctor of Philosophy
(Materials Science and Engineering)
in The University of Michigan
2013

Doctoral Committee:

Professor Sharon C. Glotzer, Chair
Professor Monica Olvera de la Cruz, Northwestern University
Professor Michael J. Solomon
Assistant Professor Anish Tuteja

Si piensas que estás vencido, lo estás.
Si piensas que no te atreves, no lo harás.
Si piensas que te gustaría ganar pero que no puedes, no lo lograrás.
Si piensas que perderás, ya has perdido.
Porque en el mundo encontrarás
que el éxito comienza con la voluntad del hombre.
Todo está en el estado mental.
Porque muchas carreras se han perdido
antes de haberse corrido,
y muchos cobardes han fracasado
antes de haber su trabajo empezado.
Piensa en grande y tus hechos crecerán.
Piensa en pequeño y quedarás atrás.
Todo está en el estado mental.
Si piensas que estás adelante, lo estás.
Tienes que pensar bien para elevarte.
Tienes que estar seguro de ti mismo
antes de intentar ganar un premio.
La batalla de la vida no siempre la gana
el hombre más fuerte, o el más ligero,
tarde o temprano, el hombre que gana
es el que cree poder hacerlo.

Adapted and translated from "Thinking" by Walter D. Wintle

For my family, whose love and support has always been an inspiration and a source of encouragement.

ACKNOWLEDGEMENTS

My deepest gratitude to my advisor, Prof. Sharon C. Glotzer. Her guidance and support during my graduate studies has strongly influenced and helped me grow professionally and personally through my time at Michigan. Particularly for allowing me such a great degree of intellectual freedom and letting me grow by learning from my own mistakes. Your support and patience has been instrumental in my development.

To my collaborators, Prof. Igal Szleifer and Prof. Monica Olvera de la Cruz, our conversations have been invaluable. I am deeply thankful for your support, patience and encouragement.

To my committee members Prof. Monica Olvera de la Cruz, Prof. Michael J. Solomon and Prof. Anish Tuteja for their time, useful suggestions and encouraging discussions.

To the Glotzer Group "peeps" for your great insights and discussion, and especially Daniel Ortiz, Pablo Damasceno, Andres Millan, Nguyen Nguyen, Dr. Ines Stuckert, Dr. Eric Jankowski and Dr. Daphne Klotsa for your friendship, collaborations and support. You have made my graduate school experience unforgettable. To our group manager, Karen Coulter, whose dedication and hard work have been of the most help through my time as a graduate student.

To my friends from the PSA, Dr. Gustavo Serrano, Javier Rios and Dr. Peter Aurora. It's been fun!

To Ayako Yamasaki, whose love and support have really helped me get to where I am today. Thank you for all the late night rides, stay-in weekends, and your infinite

patience.

To my family. My mother, Susana, whose drive and determination has always been an example and a source of encouragement. My father, Antonio, whose clear head and critical thinking still influences my decisions. My brothers, Javier and Michael and my sister Angela. My grandparents and extended family. I am truly blessed to have such a loving and supporting family with such unwavering faith in me. Thank you!

To the Rakham Graduate School and its Rackham Merit Fellowship program for their financial support. This material is based upon work supported as part of the Non-Equilibrium Energy Research Center (NERC), an Energy Frontier Research Center funded by the U.S. Department of Energy, Office of Science, Office of Basic Energy Sciences under Award Number DE-SC0000989.

TABLE OF CONTENTS

DEDICATION ii

ACKNOWLEDGEMENTS iii

LIST OF FIGURES vii

LIST OF APPENDICES xiv

ABSTRACT xv

CHAPTER

I. Introduction 1

1.1 Motivation 1
1.2 Overview 6

II. Background 9

2.1 Dynamic self-assembly 9
2.2 Reactive binary mixtures 14
2.3 Switchable colloids 19

III. Methods 22

3.1 Simulation 22
3.1.1 Langevin dynamics 22
3.1.2 Integration method 24
3.1.3 Inter-particle potentials 25
3.1.4 Validation 25
3.1.5 Particle type switching 27
3.1.6 Particle on/off switching 29
3.2 Analysis 29
3.2.1 Radial distribution function 29

3.2.2 Bond order parameter . . . 30
3.2.3 Aggregate size M_W . . . 31
3.2.4 Thermostat energy dissipation . . . 32

IV. Steady State Structures . . . 34

4.1 Introduction . . . 34
4.2 Model and methods . . . 36
4.2.1 Model . . . 36
4.2.2 Simulation Method . . . 37
4.2.3 Langevin drag coefficient (γ) selection . . . 39
4.2.4 Characterizing dynamic evolution . . . 40
4.2.5 Energy input and dissipation measurements . . . 41
4.3 Results and discussion . . . 42
4.3.1 Steady state structures . . . 42
4.3.2 Phase diagram . . . 44
4.3.3 Structure evolution . . . 47
4.3.4 Dynamics that stabilize layered structures . . . 51
4.3.5 Energy input and dissipation . . . 55
4.4 Conclusions . . . 60

V. Assembly Speed Enhancement and Transient Structures . . . 61

5.1 Introduction . . . 62
5.2 Model and methods . . . 62
5.2.1 Model . . . 62
5.2.2 Simulation method . . . 64
5.2.3 q_6 order parameter . . . 64
5.2.4 Aggregate size distribution . . . 65
5.3 Results and discussion . . . 65
5.3.1 Aggregation speed enhancement . . . 65
5.3.2 Aggregate characterization . . . 69
5.3.3 Aggregate size distribution . . . 70
5.3.4 Transient structures in dense systems . . . 73
5.4 Conclusions . . . 75

VI. Conclusions . . . 76

6.1 Summary . . . 76
6.2 Outlook . . . 78

APPENDICES . . . 80

BIBLIOGRAPHY . . . 93

LIST OF FIGURES

Figure

1.1 Representative examples of recently synthesized anisotropic particle building blocks. The particles are classified in rows by anisotropy type and increase in size from left to right according to the approximate scale at the bottom. From left to right, top to bottom: branched particles include gold[1] and CdTe[2] tetrapods. DNA-linked gold nanocrystals[3] (the small and large nanocrystals are 5nm and 10nm respectively), silica dumb-bells[4], asymmetric dimers[5] and fused clusters[6] form colloidal molecules. PbSe[7] and silver cubes[8] as well as gold[9] and polymer triangular prisms[10] are examples of faceted particles. Rods and ellipsoids of composition CdSe[11], gold[12], gibbsite[13] and polymer latex[14] are shown. Examples of patterned particles include striped spheres[15], biphasic rods[16], patchy spheres with valence[17] , AuPt nanorods[18] (the rod diameters are of the order of 200–300 nm) and Janus spheres[19]. Reproduced from reference [20]. 3

1.2 Examples of static self-assembly. (i) Crystal structure of a ribosome [21]. (ii) Self- assembled peptide-amphiphile nanofibers [22]. (iii) Electrostatic self-assembly (ESA) of polymeric microspheres on a charge-exchanging substrate modified by wet stamping [23]. (iv) ESA of macroscopic 2D crystals whose formation is mediated by charges developed by contact electrification [24]. (v) Capillary SA of polymeric plates at an interface between two liquids [25]. (vi) Self-assembled polymeric microspheres of complex internal structures [26]. Reproduced from reference [27]. 4

1.3 Examples of dynamic self-assembly in living (i-iii) and artificial systems (iv-vii). (i) Fluorescently labeled microtubules in a cell confined to a 40 m triangle on a SAM-patterned surface of gold (staining scheme: green = microtubules, red = focal adhesions, blue = actin filaments). (ii) Bacterial colony growth. (iii) School of fish [28]. (iv) Oscillon of vibrating metal beads. (v) Vortex-vortex interaction via magnetohydrodynamic dynamic self-assembly [29]. (vi) Surfactant-mediated dynamic self-assembly of gel particles floating at a liquid/air interface. Leaking of a surface-active compound the particles carry onto the interface gives rise to dynamic (repulsive) capillary forces acting between the objects. Reproduced from reference [27]. 5

2.1 Illustrations of various effects controlling the dimensions and the stability of patterns. In a, the lattices were formed by 0.86-mm disks; the lattice spacing increased with the rotational speed (800 r.p.m. in the picture on the left, 1,100 r.p.m. in the picture on the right). The pictures in b illustrate the effect of ω on the stability of aggregates. Two 1.27-mm disks were spinning on the ethylene glycol-water interface. The streamlines were visualized by placing drops of rhodamine/water solution onto the interface. In the picture on the left, the disks were rotating at $\omega = 700$ r.p.m. No dye entered a high-pressure '8-shaped' region connecting the rotating disks, and the separation between the disks did not change with time. When ω was increased to 1,100 r.p.m., the high-pressure regions produced by the disks became disjoint, as indicated by the crossing of the streamlines in the midpoint between the disks (right). Disks moved independently of each other, and the separation between them varied with time. Optical micrographs in c show hexagonally ordered aggregates formed by 570-μm PDMS disks doped with 5% magnetite, and rotating at $\omega = 1,100$ r.p.m. on a liquid-air interface 2.5 cm above the top face of the magnet. In this experiment, the liquid was a solution of 75% ethylene glycol: 25% water. Reproduced from reference [30]. 10

2.2 Dissipative self-assembly: a monomeric building block (blue) is activated by fuel consumption and is able to assemble (forming red fibers). In the assembled state it can dissipate its energy and revert to its monomeric state (blue). Energy is both consumed and dissipated in one cycle; self-assembly can occur only if sufficient energy is available. Reproduced from reference [31]. 11

2.3 Series of snapshots, taken from (a) experiment and (b) simulation, showing the evolution of 64 spheres from an initial dispersed configuration at $t = 0$, to an ordered state after 10.0 s, under horizontal vibration. By 0.1 s, the nearest spheres have interacted with each other; pairs have started to form, aligning perpendicular to the direction of oscillation. Between 0.1 and 0.4 s, short chains form; there is also a tendency for particles and chains to attach to the side walls. Between 0.4 and 1.0 s, short chains evolve to form longer ones by attaching at the ends of the nearest chain; or they attach to the sidewalls; any free particles move toward the sidewalls or attach at the ends of the nearest chain. After 2.0 s, most particles are either part of a chain or attached to the wall; there are no free particles. Thereafter the arrangement appears to be more or less stable. Reproduced from reference [32]. 13

2.4 Early-time growth factor $\omega(k)$ vs wave vector k, both with (dotted line) and without (solid line) chemistry. In the absence of chemical reactions, concentration fluctuations at all wave vectors $k < k_c$ grow. Chemical reactions introduce cutoffs both at large k and small k, so that growth occurs only for intermediate-wavelength fluctuations. Reproduced from reference [33]. 14

2.5 Concentration field for 256 lattice at a time $\tau = 2048$ following a quench to the unstable region, with reaction rates (a) $\Gamma = 0.05$ and (b) $\Gamma = 0.20$. A-rich regions are shown black and 8-rich regions are shown grey. Further evolution of the system tends to align domains, but the steady state domain width has already been selected. Reproduced from reference [33]. 15

2.6 Domain patterns obtained from numerical simulations under critical quench at $t = 10,000$ with and without hydrodynamic effects. The initial order parameter $\phi_{ini} = 0$, and the order parameter in equilibrium $\overline{\phi} = 0$. A-rich regions and B-rich regions are represented by white and black, respectively Reproduced from reference [34]. . . . 16

2.7 Morphology and the corresponding light scattering pattern of a P(S-*stat*-CMS) / PVME (50 / 50) blend irradiated at 90°C in 600 min. The scales are 10 μm and $1 \times 10^4 cm^{-1}$, respectively. Reproduced from reference [35]. 17

2.8 Simulation snapshots of the resulting steady state structures using Langevin dynamics at two different switching rates. Both images show concentric rings patterns similar to those shown in the literature. 18

2.9 Lateral photographs of light-driven motion of an olive oil droplet on a silica plate modified with CRA-CM. The olive oil droplet on a cis-rich surface moved in a direction of higher surface energy by asymmetrical irradiation with 436-nm light perpendicular to the surface. (A to C) The sessile contact angles were changed from 18 (A) to 25 (C). (D) The moving direction of the droplet was controllable by varying the direction of the photoirradiation. Reproduced from reference [36]. . 19
2.10 Idealized representation of the transition between straight (hydrophilic) and bent (hydrophobic) molecular conformations (ions and solvent molecules are not shown). The precursor molecule MHAE, characterized by a bulky end group and a thiol head group, was synthesized from MHA by introducing the (2-chlorophenyl)diphenylmethyl ester group. Reproduced from reference [37]. 20
3.1 Langevin dynamics. Coarse grained F_i^D, drag force, due to a particle's movement through a solvent and F_i^R, random force, due to thermal motion of the solvent. [Credit: Dr. Joshua Anderson] . . . 23
3.2 Typical simulation snapshots at the end of aggregation phase after one cycle of light exposure. (A,B) Monte Carlo results from reference [38]. (C,D) Langevin dynamics results. (A,C) For a range of θ with $\eta_0 = 0.037$. (B,D) For a range of η_0 with $\theta = 0.2$. Snapshots are zoomed in to show individual aggregates in detail and do not show the entire simulation box. The contrast (bold or faded) of particles is used to indicate the depth of particles from the top plane (close or farther). 26
3.3 (a,c) Number average aggregate size (M_n) and (b,c) polydispersity(PD) of the aggregates at the end of the aggregation phase after one cycle of light exposure. (a,b) At temperature θ for $\eta_0 = 0.037$. (c,d) At number density η_0 for $\theta = 0.2$. Purple squares show the values obtained using Monte Carlo from reference [38]. Blue squares show the results from Langevin dynamics simulations. 28
4.1 Interaction rules. (a) (Black, solid) Lennard-Jones potential between same type particles, (Red, dashed) Weeks-Chandler-Andersen potential between opposite type particles. (b) Interaction rules: Below a critical temperature, similar particles attract and dissimilar particles do not. Each particle can instantaneously and independently change type from one type to another and back by a random process. . . . 37
4.2 Steady state phases. Simulation snapshots of (a) a phase-separated system, (b) a system dynamically self-assembled into a spherical laminar structure, (c) a system where the aggregate domain size has been stabilized, and (d) a mixed system. The system can dynamically move from demixed to mixed through these steady states by changing the switching rate. The contrast (bold or faded) of particles is used to indicate the depth of the particles in the three-dimensional box. 43

4.3 Phase diagram for the Langevin drag coefficient vs the switching probability showing four distinct phases. From left to right: (Blue) At low switching probability, the system has reached its equilibrium phase-separated configuration. (Green) At a medium-low switching probability, the perturbation due to particle switching stabilizes layered steady state structures. (Red) At medium-high switching probability, domain growth is inhibited and the domain size stabilized, but the domains are not large enough to sustain internal domains. (Cyan) At high switching probability, particles switch faster than the coarsening due to spinodal decomposition, so the system resembles a mixed system. 45

4.4 (a-l) Evolution of the radial distribution function (RDF), calculated between particles of the same type, A-A, (blue, solid) and particles of the opposite type, A-B, (green, dashed) for systems in the (a-c) phase-separated, (d-f) layered structures, (g-i) spinodal decomposition intermediate structures, and (j-l) homogeneous mixture phases. RDF snapshots taken at time = (a, d, g, j) $10^3\tau$, (b, e, h, k) $10^5\tau$, and (c, f, i, l) $10^8\tau$. 48

4.5 Average domain size as a function of time for multiple switching probabilities. At low switching probabilities, the domains grow following a power law until the system completely phase separates. As the probability of a particle being switched increases, domain growth is inhibited, restricting the maximum domain size. The solid and dashed line have slopes of 1/3 and 1/5 respectively. Error bars have roughly the size of the symbols. Marker styles and colors match the phases described in Figure 4.3 50

4.6 Steady state domain size as a function of switching probability (p_{switch}). The steady state domain size can be tuned by controlling the probability of switching particles. Marker styles and colors match the phases described in Figure 4.3 51

4.7 Aggregate evolution dynamics: (a) "Nucleation", where multiple particles that switched inside an aggregate merge, slowing down their diffusion and "nucleating" a new layer inside the aggregate; (b) coagulation, where two aggregates with the same outer layer come into contact; (c) re-solution, where particles switched while inside an aggregate diffuse to the closest layer of the same type as the new type of the switched particle or to the boundary of the aggregate to later be ejected; and (d) coarsening, where particles that are not part of any aggregate absorb into the outer layer of the same type. 53

4.8 Average time required for a switched particle to exit an aggregate of the opposite type as a function of (a) number of particles in the aggregate, and (b) aggregate radius. The solid lines represent (a) linear, and (b) cubic fits. 54

4.9 Distribution of the amount of energy introduced every time a particle type is switched for several choices of p_{switch}. The solid vertical bar represent the number average. 56
4.10 Steady-state potential energy. Marker styles and colors match the phases described in Figure 4.3. Error bars have roughly the size of the symbols. 57
4.11 Langevin thermostat energy dissipation rate as a function of switching probability (p_{switch}). Marker styles and colors match the phases described in Figure 4.3. Error bars have roughly the size of the symbols. 59
4.12 Measured steady state temperature as a function of switching probability (p_{switch}). Marker styles and colors match the phases described in Figure 4.3. Error bars have roughly the size of the symbols. . . . 59
5.1 Interaction Switching Details. Particles are switched repeatedly between two states. In the on state, particles are attracted to each other and aggregate. In the off state, attractive interactions are turned off and particles interact solely through excluded volume. 63
5.2 Comparison between reference and active systems. Images of the aggregates at a given time t for (a) a reference, inactive system, and (b) an active system. From the images, it is evident that the active system has larger aggregates than the reference system. 66
5.3 Assembly speed enhancement. Aggregate size at the end of the aggregation stage at multiple cycles vs. off/on ratio. This plot shows that for off/on ratios smaller than 0.15 the weight average aggregate size is larger than for an inactive system. 67
5.4 Aggregate size evolution. Aggregate size at the end of the aggregation stage at multiple cycles vs. off/on ratio. This log-log plot shows the aggregate sizes at the end of the aggregation stage to show how the aggregates are growing as a function of time for multiple off/on ratios. 68
5.5 Radial distribution function characterizing the internal structure of the aggregates of the same size for multiple off/on ratios. Peaks correspond to FCC ordering. 69
5.6 Probability distribution of the q_6 order parameter characterizing the internal structure of the aggregates of the same size for multiple off/on ratios. Peak at 0.57 corresponds to FCC ordering. 70
5.7 Histogram showing the distributions of aggregate sizes for multiple on/off ratios at Mw = 2500 and corresponding simulation snapshots. 71
5.8 Histogram showing the distributions of aggregate sizes for multiple on/off ratios at Cycle = 100, and corresponding simulation snapshots. 72

5.9 Light switching in dense systems. Snapshot of the final configuration of a dense system with multiple off/on ratios at the end of 100 cycles. (a) Ratio = 0.00, Interactions are always-on, the system phase separates through spinodal decomposition resulting in percolating domains that coarsen following a power law. (b) Ratio = 0.02, Short disaggregation times increase the phase separation speed resulting in a single aggregate without the percolating domains. (c) Ratio = 0.13, Larger disaggregation times produce a coexistence of percolating porous domain with small aggregates. (d) Ratio = 0.25, Much larger disaggregation times cause the system to lose all memory of the aggregation phase, and result in percolated networks with smaller domains than in a that only depend on a single aggregation phase. 74

LIST OF APPENDICES

Appendix

A. Key HOOMD scripts – Immiscible Switchable Colloids Simulation . . 81

B. Key HOOMD scripts – Photo-Switchable Colloids Simulation 87

ABSTRACT

Colloidal Structures Through Dynamic Self-Assembly

by

Antonio Francisco Osorio Vivanco

Chair: Sharon C. Glotzer

Self-assembly is one of the most promising routes for manufacturing materials and devices with nanoscale features. While static self-assembly, where structures do not require energy to maintain order, has been the focus of a large body of research over the past decade, self-assembly in driven systems and dynamic self-assembly is still in its infancy. With recent developments in experimental techniques, we can begin to consider the synthesis and fabrication of switchable building blocks that can dynamically switch between two or more states introducing dissipative dynamics into the self-assembly process, thus enabling a new generation of non-equilibrium materials and devices.

In this thesis, we use coarse-grained molecular dynamics simulations with a Langevin thermostat to explore some of the new possibilities that arise from introducing switchability and non-equilibrium dynamics into the self-assembly process of colloidal and nanoparticle systems. These possibilities include the stabilization of novel steady-state structures not available in equilibrium systems, the enhancement of self-assembly speed and increase of self-assembly propensity, the ability to capture, or dynamically arrest, a pattern that was previously only available as a transient structure

as the system evolved towards equilibrium, and the ability to dynamically tune the phase and length scale of the self-assembled systems by adjusting an external non-thermodynamic control signal, such as light. We use the radial distribution function and the local bond order parameter to characterize the systems to see how the non-equilibrium dynamics affect the resulting structures, and we use the Langevin thermostat to study the energy dissipation in the driven systems to understand the requirement for maintaining far-from-equilibrium structures.

CHAPTER I

Introduction

1.1 Motivation

Nanotechnology, the ability to manipulate and design materials and devices with features at length scales from a 10th to a 1000th of the width of a human hair, has revolutionized industries from cosmetics, food products and coatings to biotechnology and electronics, and has the potential to fundamentally change how we engineer the world around us. A lot of efforts have gone into developing the knowledge and tools required to work at this scale since Richard Feynman's famous talk "There's Plenty of Room at the Bottom", where he introduced the concept of synthesizing materials by directly manipulating atoms. Some of those efforts have focused on "top-down" approaches, where scientists and engineers attempt to make smaller devices using larger ones. These approaches, which have found great success with two dimensional devices in the electronics industry, and tools such as photolithography and atomic layer deposition techniques, have severe scaling problems as well as problems extending into the third dimension. Manufacturing three dimensional materials or devices with nanoscale features would require us to be able to place trillions of atoms, or nanoparticles, with incredible accuracy. If we were to place these particles one at a time, like Lego® blocks, the amount of time that it would take to build anything of meaningful size would make this enterprise unfeasible. Even if we were

able to parallelize this task so that millions of particles are placed every second, the resources and time required to manufacture such material would make it impractical. To address these problems, "bottom-up" approaches, where the smallest components are engineered to autonomously form larger structures, have been developed. Self-assembly is a "bottom-up" approach and it is the process where collections of building blocks come together to spontaneously form – assemble – organized structures and patterns [20, 28, 40, 41].

Self-assembly is nature's tool of creation. From individual proteins [42] and DNA [43] to bacteria [44, 45], viruses [46, 47] and the human body, self-assembly is ubiquitous in nature. Controlling the resulting structures and patterns entails designing the building blocks with specific shapes, surface properties, inter-particle interactions, charge and other properties [20] (Figure 1.1) as well as controlling the assembly environment: temperature, density, pH, etc. Mastering self-assembly would enable us to develop new materials and devices of arbitrarily large sizes with properties unlike those available today and applications in various fields such as medicine, electronics, robotics, and consumer products while being able to manufacture them in a scalable, efficient and cost-effective manner.

Self-assembly can be divided into two main types: Static and Dynamic [28]. Static self-assembly deals with systems in equilibrium, where neither the environment nor the building block change as a function of time, and the system does not dissipate energy. In static self-assembly, the equilibrium or metastable structures are characterized by the global or local free energy minimum of the system [28]. Over the last decades, much work has been dedicated to understanding static self-assembly in order to be able to predict the final equilibrium structure as well as to understand the assembly pathways that the system goes through during the process. Based on advances in statistical dynamics and work done by Clausius [48], Gibbs [49], Maxwell [50], Boltzmann [51, 52], and many others, a thermodynamic framework has been developed

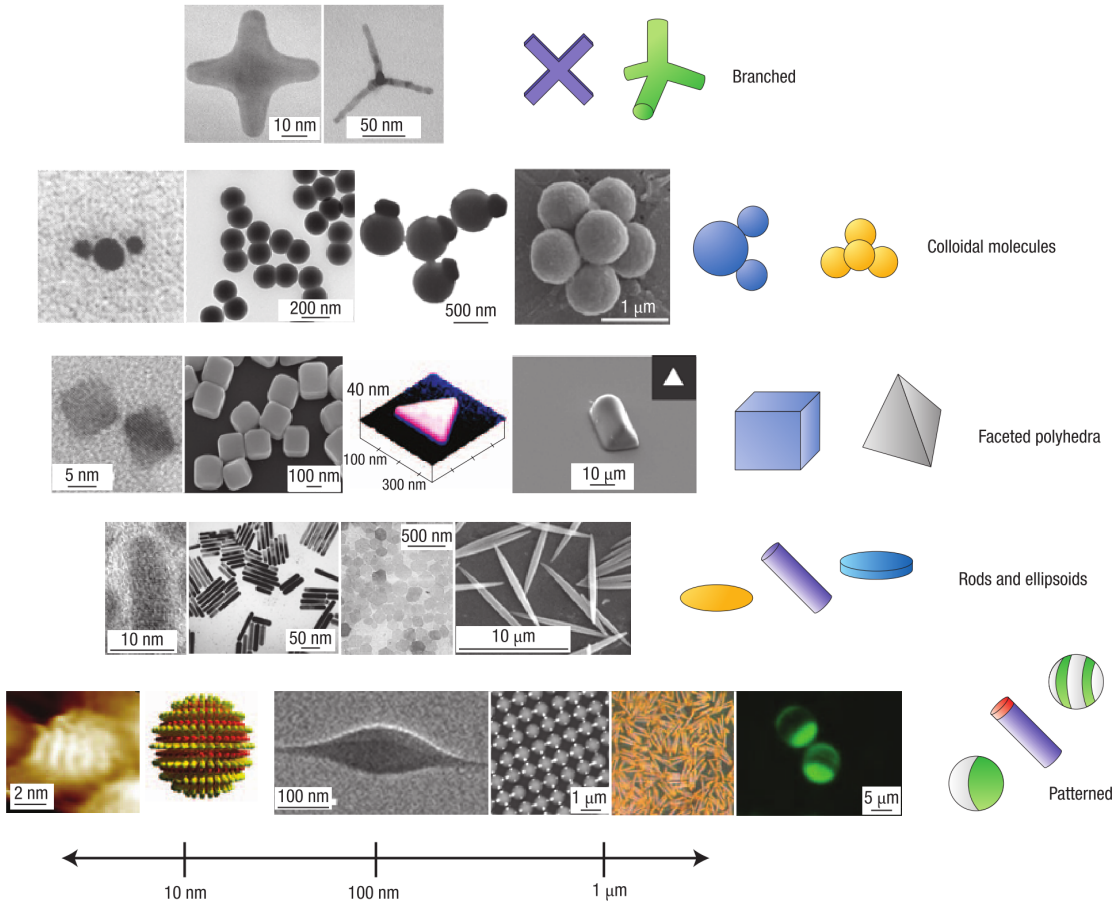

Figure 1.1: Representative examples of recently synthesized anisotropic particle building blocks. The particles are classified in rows by anisotropy type and increase in size from left to right according to the approximate scale at the bottom. From left to right, top to bottom: branched particles include gold[1] and CdTe[2] tetrapods. DNA-linked gold nanocrystals[3] (the small and large nanocrystals are 5nm and 10nm respectively), silica dumb-bells[4], asymmetric dimers[5] and fused clusters[6] form colloidal molecules. PbSe[7] and silver cubes[8] as well as gold[9] and polymer triangular prisms[10] are examples of faceted particles. Rods and ellipsoids of composition CdSe[11], gold[12], gibbsite[13] and polymer latex[14] are shown. Examples of patterned particles include striped spheres[15], biphasic rods[16], patchy spheres with valence[17] , AuPt nanorods[18] (the rod diameters are of the order of 200–300 nm) and Janus spheres[19]. Reproduced from reference [20].

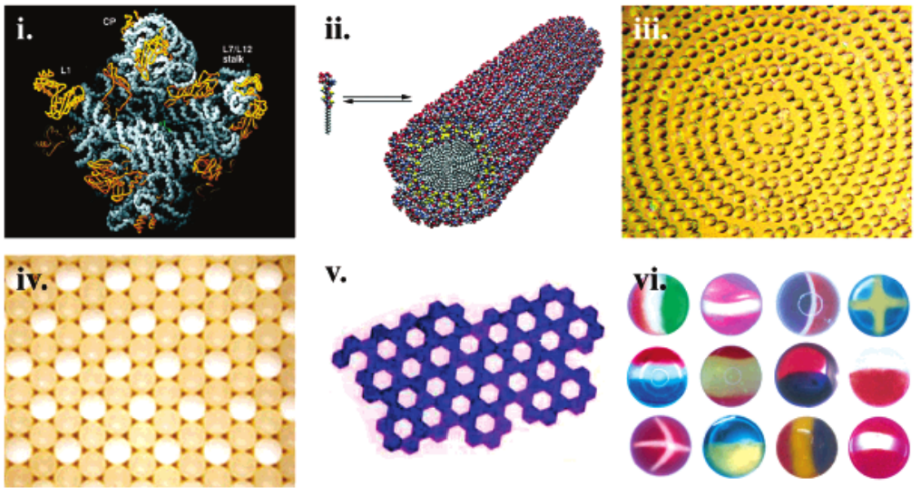

Figure 1.2: Examples of static self-assembly. (i) Crystal structure of a ribosome [21]. (ii) Self- assembled peptide-amphiphile nanofibers [22]. (iii) Electrostatic self-assembly (ESA) of polymeric microspheres on a charge-exchanging substrate modified by wet stamping [23]. (iv) ESA of macroscopic 2D crystals whose formation is mediated by charges developed by contact electrification [24]. (v) Capillary SA of polymeric plates at an interface between two liquids [25]. (vi) Self-assembled polymeric microspheres of complex internal structures [26]. Reproduced from reference [27].

that allows us to try to predict the equilibrium structure by knowing the individual building block and the thermodynamic conditions of the system. Multiple developments in our ability to synthesize increasingly complex building blocks, nanoparticles and colloids [20], have resulted in the ability to stabilize a multitude of interesting and technologically relevant structures. Micelles, self-assembled aggregates of surfactant molecules in a solvent, with applications from detergents to drug delivery, are an example of an industrial, commercially available self-assembled system[53].

Dynamic self-assembly entails systems that are driven away from equilibrium conditions, where the structure's stability depends on energy being constantly introduced into the system. The structures are formed by a competition of dynamic mechanisms, such as phase separation of an immiscible mixture, or remixing due to particle switching or chemical reactions, driving the system towards different configurations. The Belousov-Zhabotinsky reaction [54] and Rayleigh-Bérnard convection [55] are exam-

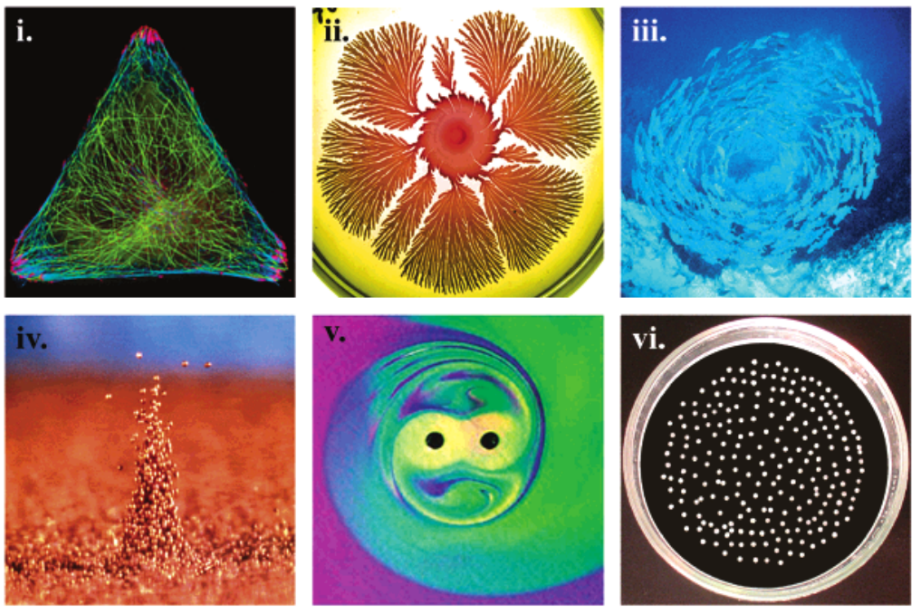

Figure 1.3: Examples of dynamic self-assembly in living (i-iii) and artificial systems (iv-vii). (i) Fluorescently labeled microtubules in a cell confined to a 40 m triangle on a SAM-patterned surface of gold (staining scheme: green = microtubules, red = focal adhesions, blue = actin filaments). (ii) Bacterial colony growth. (iii) School of fish [28]. (iv) Oscillon of vibrating metal beads. (v) Vortex-vortex interaction via magnetohydrodynamic dynamic self-assembly [29]. (vi) Surfactant-mediated dynamic self-assembly of gel particles floating at a liquid/air interface. Leaking of a surface-active compound the particles carry onto the interface gives rise to dynamic (repulsive) capillary forces acting between the objects. Reproduced from reference [27].

ples of inert systems undergoing dynamic self-assembly or self-organization. In biological systems, complex structures (i.e. lipid membranes, protein aggregates, structured proteins, etc.) central to the survival of cells are formed almost exclusively through dynamic self-assembly [56, 57]. Imagine a cell and all of the biological processes within it. As long as energy in the form of atp is present within the cell, all the internal processes continue, the cell is alive, and is able to automatically respond to changes in its environment. When the energy supply is exhausted, the cell dies devolving into its equilibrium configuration. Dynamic self-assembly examples abound in nature – school of fish, bird flocks, and bacterial colonies are all instances where the individual building blocks (fish, bird, bacteria) aggregate and behave as groups without any controlling entity, where the group behavior is controlled by local interaction rules among the individual building blocks and their environment, yet as soon as the energy supply (i.e. food) is removed these structures disappear. Similarly, materials that assemble through dynamic self-assembly require a driving mechanism that is constantly introducing energy into the system to maintain their structure and properties. To better understand how to predict pattern and structure formation as well as response and dynamics in dynamic self-assembly, a few artificial systems have been developed using rotating magnetic fields, self-propelled particles, mechanically vibrated systems, and fluid flows where the parameters can be carefully controlled. Mastering dynamic self-assembly would enable us to better understand the processes underlying living organisms, and to engineer materials and devices that are responsive and adapt to their environments, opening the doors for a host of new applications.

1.2 Overview

This work focuses on understanding dynamic self-assembly and engineering dynamically self-assembling systems to produce novel structures, stabilize structures that were only previously available as transient configurations, and to enhance or

inhibit the assembly speed of equilibrium structures.

This thesis is structured as follows:

Chapter I introduces key concepts and describes the motivation, objectives and structure of this thesis.

Chapter II presents a literature review of the current state of static and dynamic self-assembly in colloidal systems as well as of the previous research that inspired this work.

Chapter III describes the details of the simulation method, Langevin Dynamics, with emphasis on the modifications made to introduce non-equilibrium mechanisms and compare simulation results with results available in the literature to validate this method. We introduce the analysis tools used to characterize the resulting systems.

Chapter IV describes the behavior of an immiscible mixture of two species of nanocolloids driven far-from-equilibrium by dynamically switching between species. In this chapter, we present simulation results of a colloidal system, where colloids can switch between two species, that show that novel steady state structures dynamically self-assemble for judicious choices of thermodynamic and model parameters. We describe the dynamics that stabilize these dissipative structures, and present a phase diagram of predicted stable phases as a function of the relevant thermodynamic variables. We explore energy dissipation in this driven system, and demonstrate the requirements for maintaining far-from-equilibrium structures.

In Chapter V, based on previous experimental and theoretical work done with nanocolloids, whose interaction can be switched on/off with light, we drive a system of nanocolloids to self-assemble into a non-equilibrium structure by switching interparticle potentials and show that the process can enhance the assembly speed of the equilibrium thermodynamic structure by an order of magnitude, as well as produce non-equilibrium states comprised of multiple coexisting phases not available via static self-assembly. We characterize the internal structure of the aggregates as well as

the distribution of aggregate sizes, and study how these two properties change as a function of how far the system has been driven away from equilibrium.

Chapter VI summarizes key aspects of this work, describes how this work contributes to the field, and presents directions in which this research can be continued in the future.

CHAPTER II

Background

In this chapter, we present previous experimental an computational studies on the current state of knowledge about dynamic self-assembly, as well as reactive binary mixtures and photo-switchable colloid, two topics that inspired this work.

2.1 Dynamic self-assembly

Dynamic self-assembly refers to systems that are driven away from equilibrium conditions, where the structure's stability depends on energy being constantly introduced into the system. The structures are formed by a competition of dynamic mechanisms, such as phase separation of an immiscible mixture, or remixing due to particle switching or chemical reactions, driving the system towards different configurations. As we mentioned in Section 1.1, mastering dynamic self-assembly would enable us to better understand the processes underlying living organisms, and to engineer materials and devices that are responsive and adapt to their environments, opening the doors for a host of new applications.

Since dynamic self-assembling systems in nature are extremely complex, intertwined with other processes, and difficult to control, over the last few years, there has been a growing interest in designing artificial systems with accessible experimental and computational parameters to be better able to study dynamic self-assembly.

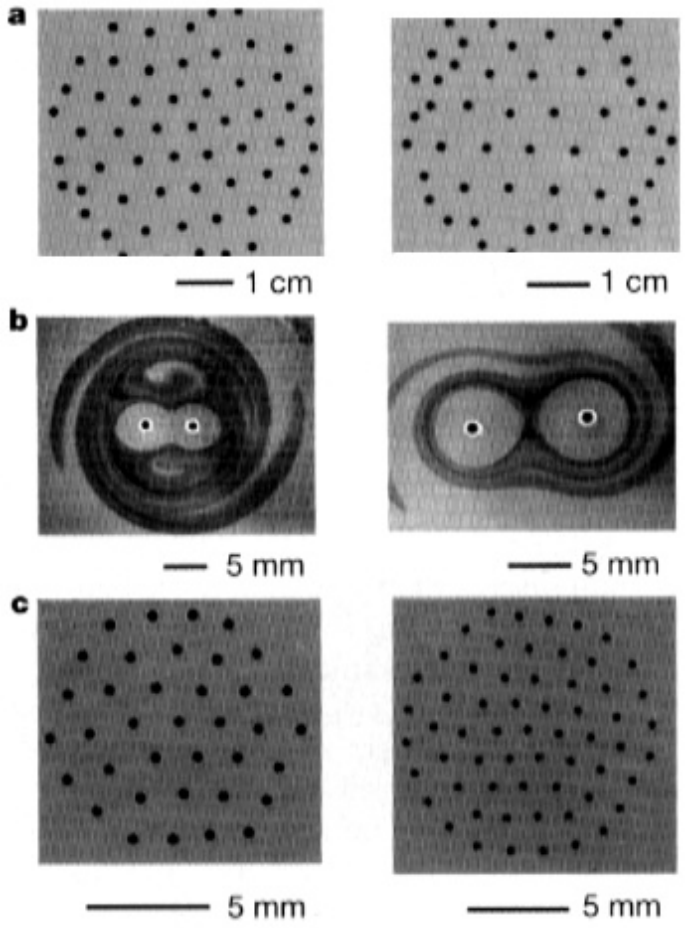

Figure 2.1: Illustrations of various effects controlling the dimensions and the stability of patterns. In a, the lattices were formed by 0.86-mm disks; the lattice spacing increased with the rotational speed (800 r.p.m. in the picture on the left, 1,100 r.p.m. in the picture on the right). The pictures in b illustrate the effect of ω on the stability of aggregates. Two 1.27-mm disks were spinning on the ethylene glycol-water interface. The streamlines were visualized by placing drops of rhodamine/water solution onto the interface. In the picture on the left, the disks were rotating at $\omega = 700$ r.p.m. No dye entered a high-pressure '8-shaped' region connecting the rotating disks, and the separation between the disks did not change with time. When ω was increased to 1,100 r.p.m., the high-pressure regions produced by the disks became disjoint, as indicated by the crossing of the streamlines in the midpoint between the disks (right). Disks moved independently of each other, and the separation between them varied with time. Optical micrographs in c show hexagonally ordered aggregates formed by 570-μm PDMS disks doped with 5% magnetite, and rotating at $\omega = 1,100$ r.p.m. on a liquid-air interface 2.5 cm above the top face of the magnet. In this experiment, the liquid was a solution of 75% ethylene glycol: 25% water. Reproduced from reference [30].

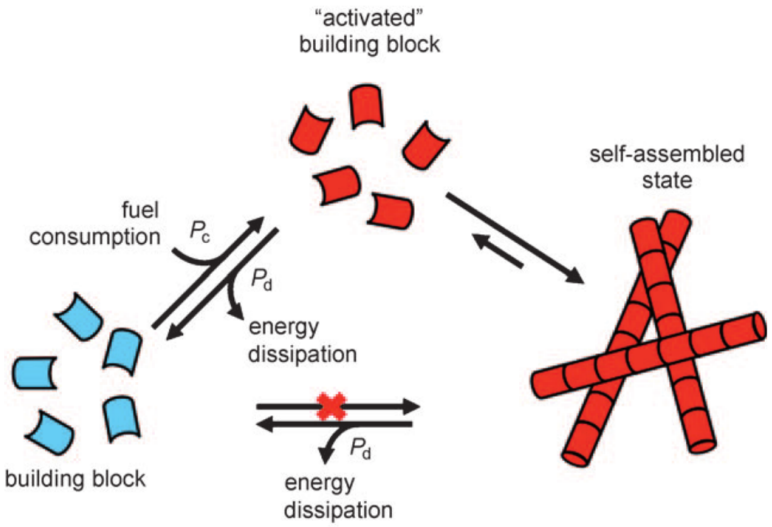

Figure 2.2: Dissipative self-assembly: a monomeric building block (blue) is activated by fuel consumption and is able to assemble (forming red fibers). In the assembled state it can dissipate its energy and revert to its monomeric state (blue). Energy is both consumed and dissipated in one cycle; self-assembly can occur only if sufficient energy is available. Reproduced from reference [31].

Here, we present some of the dynamically self-assembling systems that have been artificially engineered as test-beds for related theories.

Grzybowski *et al.* developed systems of rotating millimeter-sized magnetic disks at a liquid air interface, subject to a magnetic field from a rotating permanent magnet that self-assembles into the two dimensional patterns shown in Figure 2.1 [30], and and proceeded to extend the system into three dimensions in reference [29]. The disks in this system are attracted to to the axis of rotation of the permanent magnet, but, due to the hydrodynamic forces generated by the disks themselves spinning, they repel each other. The competition between these two mechanism stabilize the structures shown.

In 2010, Boekhoven *et al.* engineered an energy-dissipating self-assembling system that resembles system found in nature, specifically cytoskeleton tubules whose dynamic self-assembly give shape to cells [31]. Their system consisted of gelator

precursors that were converted into gelators by a reaction with chemical fuel, thus resulting in self-assembly. Hydrolysis of the gelators resulted in disassembly of the formed structures and in energy dissipation. Boekhoven *et al.* have recently shown that by controlling the catalytic process, they can tune the gel formation, therefore the mechanical properties and appearance of the resulting material [58], while using the same building block, the gelator.

A large amount of effort has been devoted to understanding self-propelled particles [59–79], while the details of the research performed in this area are beyond the scope of this thesis, it is worth noting that new experimental and theoretical systems are constantly being developed to advance our understanding of how this category of active particles assemble and their collective motion and dynamics. The developments in this area are greatly advancing our ability to understand systems driven far-from-equilibrium.

Das *et al.* developed doubly-responsive nanoparticles, to light and magnetic field, using azobenzene groups and catechol anchors for nanoparticles [80]. By controlling both stimuli, Das *et al.* controlled the optical properties of the resulting solution.

Klotsa *et al.* computationally studied a system that self-assembles into particles chains when oscillatory fluid flows are present [32, 81]. The chains form perpendicular to the direction of the oscillation and are only stable as long as energy is introduced in the form of oscillations. As soon as the oscillations stop, the structure decays into a disordered system. Figure 2.3 shows the time evolution and final structures of the experimental and computational systems.

Klajn *et al.* designed nanoparticles decorated with ligands combining photoswitchable dipoles and covalent cross-linkers. Using light, these nanoparticles can be reversibly or irreversibly assembled into three-dimensional suprastructures [82]. This system was studied by Jha *et al.* in reference [38] and it serves as the inspiration and basis for the system presented in Chapter V.

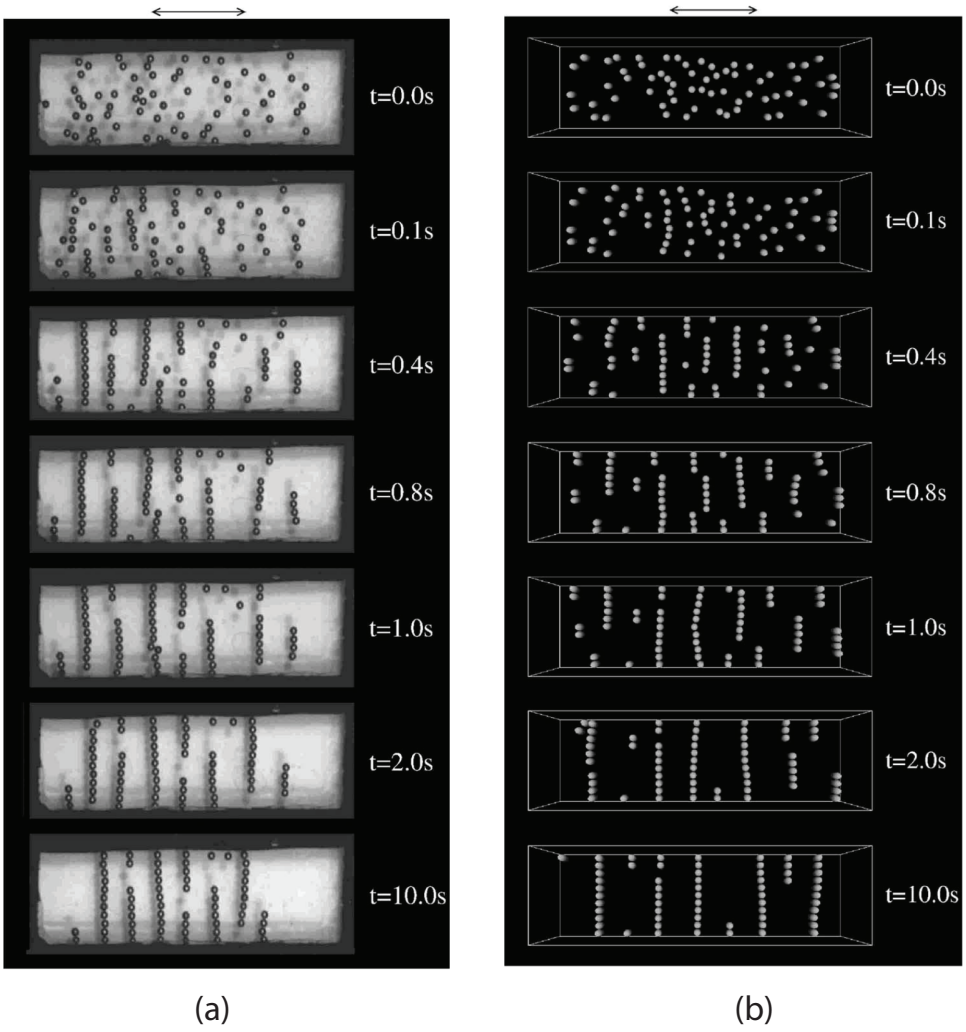

Figure 2.3: Series of snapshots, taken from (a) experiment and (b) simulation, showing the evolution of 64 spheres from an initial dispersed configuration at $t = 0$, to an ordered state after 10.0 s, under horizontal vibration. By 0.1 s, the nearest spheres have interacted with each other; pairs have started to form, aligning perpendicular to the direction of oscillation. Between 0.1 and 0.4 s, short chains form; there is also a tendency for particles and chains to attach to the side walls. Between 0.4 and 1.0 s, short chains evolve to form longer ones by attaching at the ends of the nearest chain; or they attach to the sidewalls; any free particles move toward the sidewalls or attach at the ends of the nearest chain. After 2.0 s, most particles are either part of a chain or attached to the wall; there are no free particles. Thereafter the arrangement appears to be more or less stable. Reproduced from reference [32].

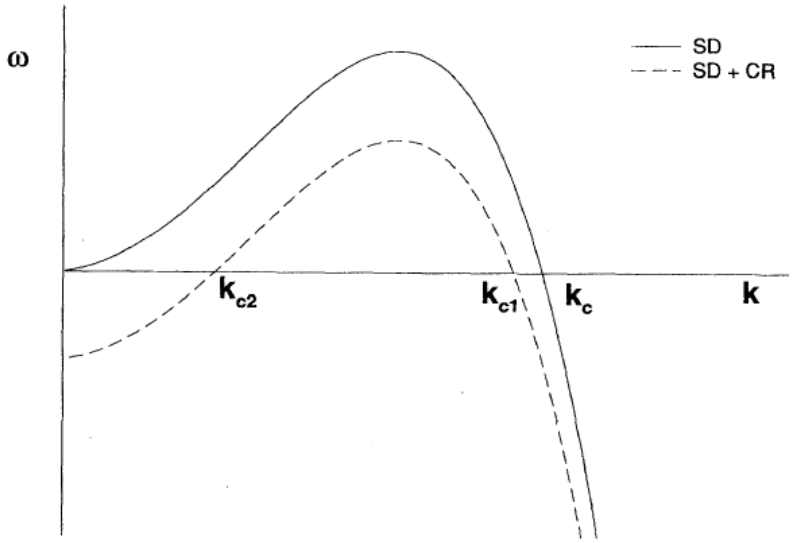

Figure 2.4: Early-time growth factor $\omega(k)$ vs wave vector k, both with (dotted line) and without (solid line) chemistry. In the absence of chemical reactions, concentration fluctuations at all wave vectors $k < k_c$ grow. Chemical reactions introduce cutoffs both at large k and small k, so that growth occurs only for intermediate-wavelength fluctuations. Reproduced from reference [33].

2.2 Reactive binary mixtures

Reactive binary mixtures are solutions of two phase-separating chemical species that undergo reactions from one type to the other. The idea of using these reactions to stabilize patterns was originally introduced by Glotzer, Di Marzio and Muthukumar (GDM) in reference [33]. They considered a two component system undergoing the following reaction:

$$A \overset{\Gamma}{\rightleftharpoons} B \tag{2.1}$$

where Γ is the reaction rate.

GDM used Cahn's linear theory to predict the growth factor (ω) at a given wave vector (k) for the case where $\Gamma = 0$. Then extend it to non-zero values of Γ. Figure 2.4 shows both regimes (zero and non-zero Γ). The solid line in the plot represents the

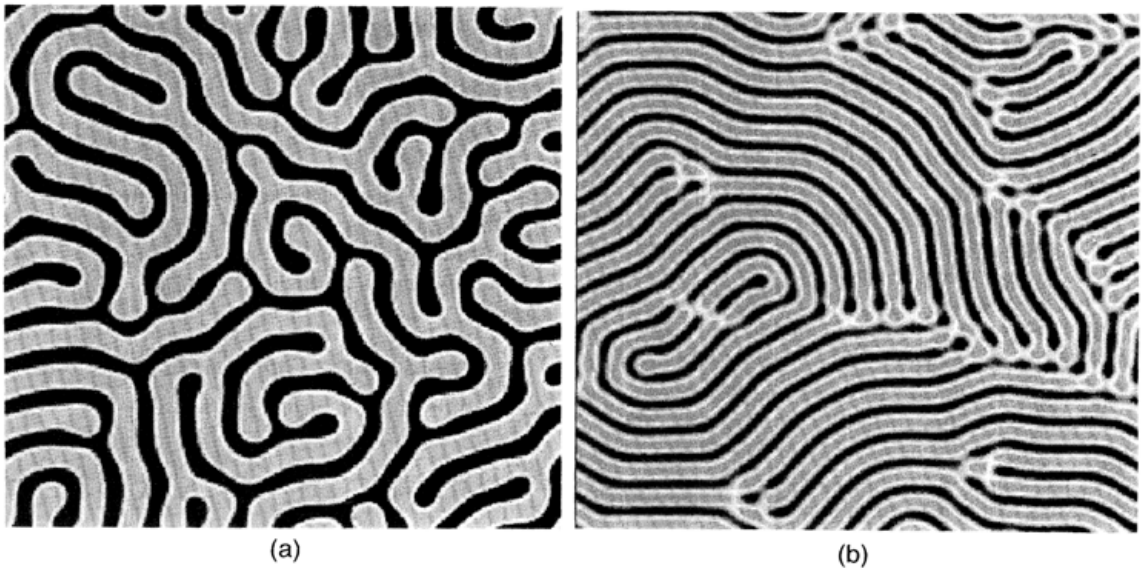

Figure 2.5: Concentration field for 256 lattice at a time $\tau = 2048$ following a quench to the unstable region, with reaction rates (a) $\Gamma = 0.05$ and (b) $\Gamma = 0.20$. A-rich regions are shown black and 8-rich regions are shown grey. Further evolution of the system tends to align domains, but the steady state domain width has already been selected. Reproduced from reference [33].

case when only Spinodal Decomposition occurs ($\Gamma = 0$), one can see that for large wave vectors (large k) (since this is reciprocal space, it refers to small aggregates) the growth rate is negative. This mean that below a certain size the system tends to disaggregate. Then, for aggregates larger than k_c, smaller wave vectors, the growth rate is always positive (above the line). This means that the aggregates from that size on will always grow. On the other hand, for the non-zero Γ case (dashed line), aggregation starts at k_{c1} but as the aggregate size increases it crosses into the disaggregation regime at k_{c2}. Domains of wave vectors smaller than k_{c2} will tend to decay. These two dynamics stabilize patterns with domains of wave vector $k = k_{c2}$. Figure 2.5 shows the resulting steady state morphologies. A study by Glotzer, Stauffer and Jan using Monte Carlo (MC) corroborated these results [83].

Toxvaerd attempts to recreate the results presented in reference [83] using Molecular Dynamics instead of Monte Carlo [84]. He does not get the same labyrinthine

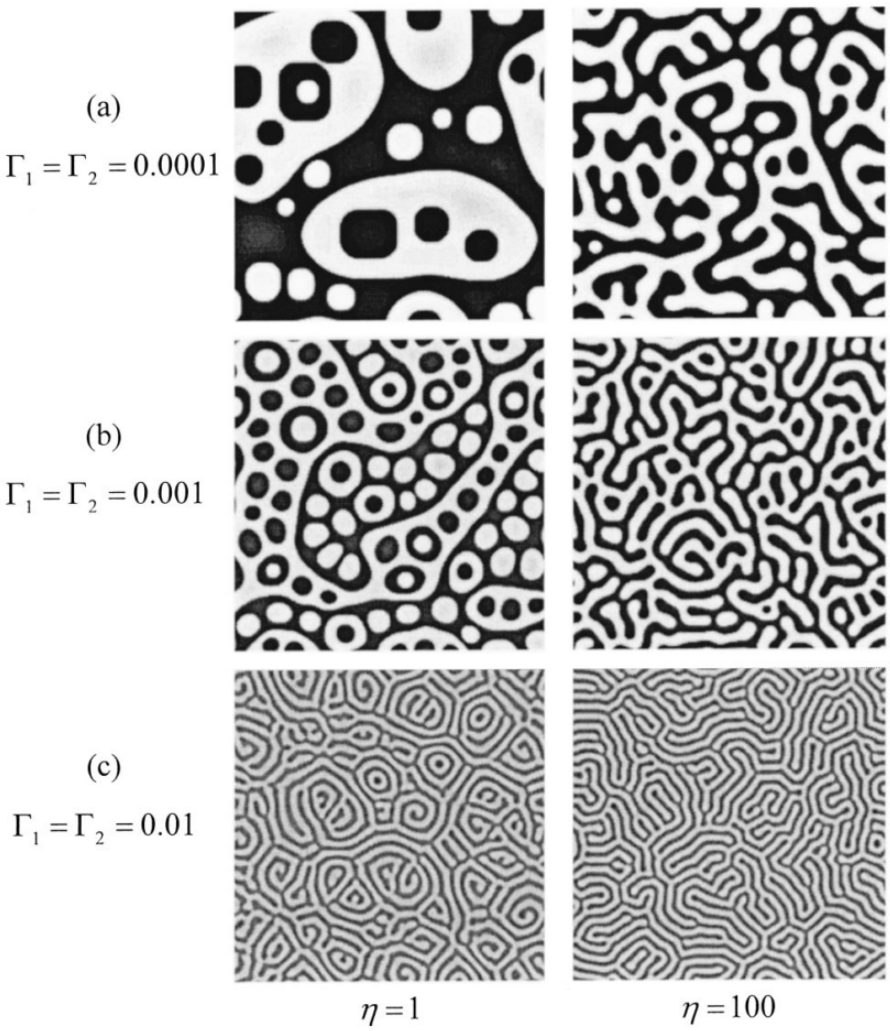

Figure 2.6: Domain patterns obtained from numerical simulations under critical quench at $t = 10,000$ with and without hydrodynamic effects. The initial order parameter $\phi_{ini} = 0$, and the order parameter in equilibrium $\overline{\phi} = 0$. A-rich regions and B-rich regions are represented by white and black, respectively Reproduced from reference [34].

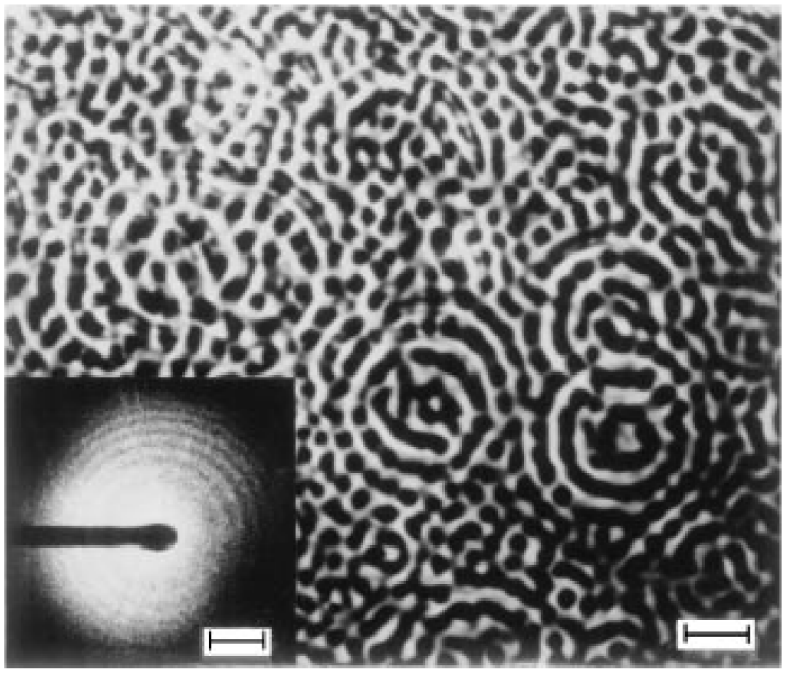

Figure 2.7: Morphology and the corresponding light scattering pattern of a P(S-*stat*-CMS) / PVME (50 / 50) blend irradiated at 90°C in 600 min. The scales are 10 μm and $1 \times 10^4 cm^{-1}$, respectively. Reproduced from reference [35].

patterns, and states that the main differences arise from the fact that the MC simulations were done in a lattice and that stochastic dynamics such as Langevin Dynamics (Brownian Dynamics included) and MC, do not capture the hydrodynamic modes that pure MD does. In this work, Toxvaerd uses NVT MD, using a Verlet integrator but does not explore the thermostat used or the effect of the coupling to the thermostat.

Using MC, Motoyama and Otha stabilize concentric rings of alternating species by judicious choice of the reaction rates and interaction strengths. They use the free energy of these structures to predict the size of each of these domain [85, 86]. In 2003, Huo *et al.* [34], studied the effect of hydrodynamics in reactive binary mixtures. The resulting morphologies also suggest concentric rings of alternating species as the steady state structures for certain parameters (Figure 2.6). These results were confirmed by Furtado and Yeomans using Lattice Boltzmann simulations[87].

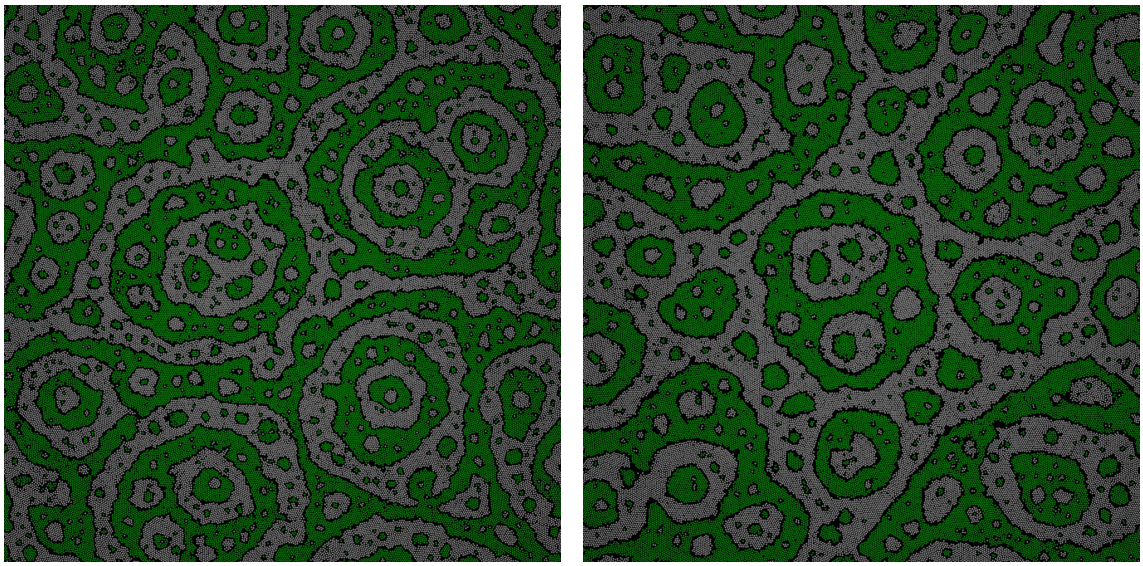

Figure 2.8: Simulation snapshots of the resulting steady state structures using Langevin dynamics at two different switching rates. Both images show concentric rings patterns similar to those shown in the literature.

Using polymer blends, poly(vinyl methyl ether) (PVME, $M_W = 9.6{\times}10^4$, $M_W/M_n = 2.6$), and a styrene-chloromethyl styrene random copolymer [P(S-*stat*-CMS), $M_W = 2.7 \times 10^5$, $M_W/M_n = 1.7$], Tran-Cong *et al.* [35, 88] performed the first experimental realization of a reactive binary mixture. Figure 2.7 shows the resulting morphology in the experimental system, where concentric rings can be observed.

We ran two dimensional simulations using Langevin dynamics at densities similar to those in the literature to validate our model. Figure 2.8 shows that the resulting morphologies qualitatively agree with previous theoretical and experimental results. These results inspired the work presented in Chapter IV. We used the same base concept of species switching types, but extended the system to three dimensions and used densities resembling nanocolloidal and nanoparticle solutions.

Recently, research on reactive mixtures has expanded into more than ternary and quaternary mixtures. While those areas are beyond the scope of this thesis, it provides a possible direction for expanding this work.

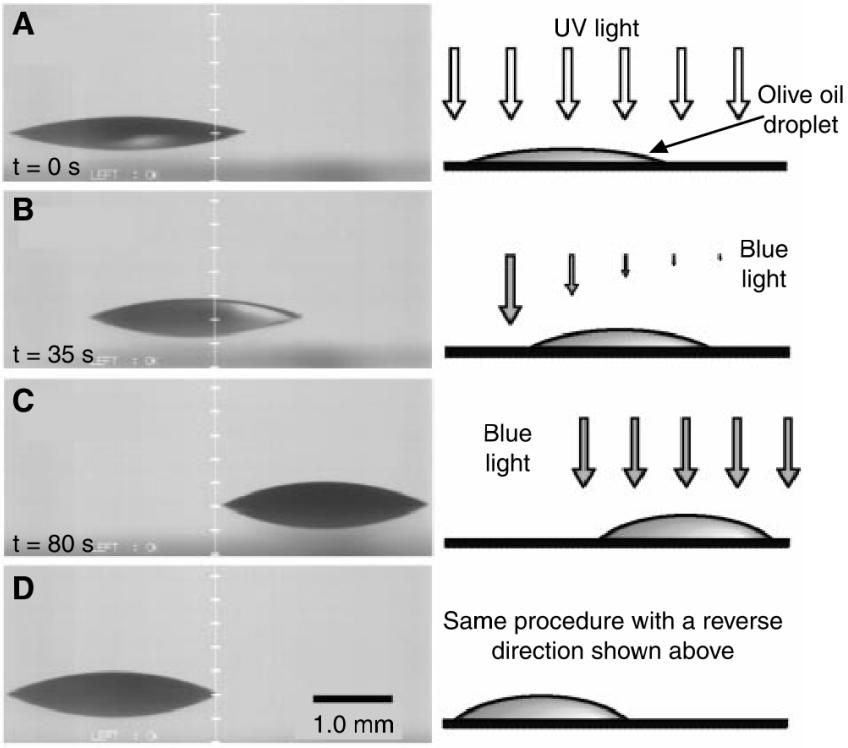

Figure 2.9: Lateral photographs of light-driven motion of an olive oil droplet on a silica plate modified with CRA-CM. The olive oil droplet on a cis-rich surface moved in a direction of higher surface energy by asymmetrical irradiation with 436-nm light perpendicular to the surface. (A to C) The sessile contact angles were changed from 18 (A) to 25 (C). (D) The moving direction of the droplet was controllable by varying the direction of the photoirradiation. Reproduced from reference [36].

2.3 Switchable colloids

In this section, we present some of the surface, colloidal, and nanoparticle synthesis development that enable us to think about self-assembly building blocks that are dynamic in time. These building blocks can change their inter-particle interactions, shape, etc. in response non-thermodynamic external stimuli.

In 2000, Ichimura developed a surface covered in a photoisomerizable monolayer whose surface free energy could be reversibly manipulated via photoirradiation [36]. Using this surface, Ichimura was able to control the movement of an olive oil droplet by asymmetrically shining blue light onto the surface, as shown in Figure 2.9.

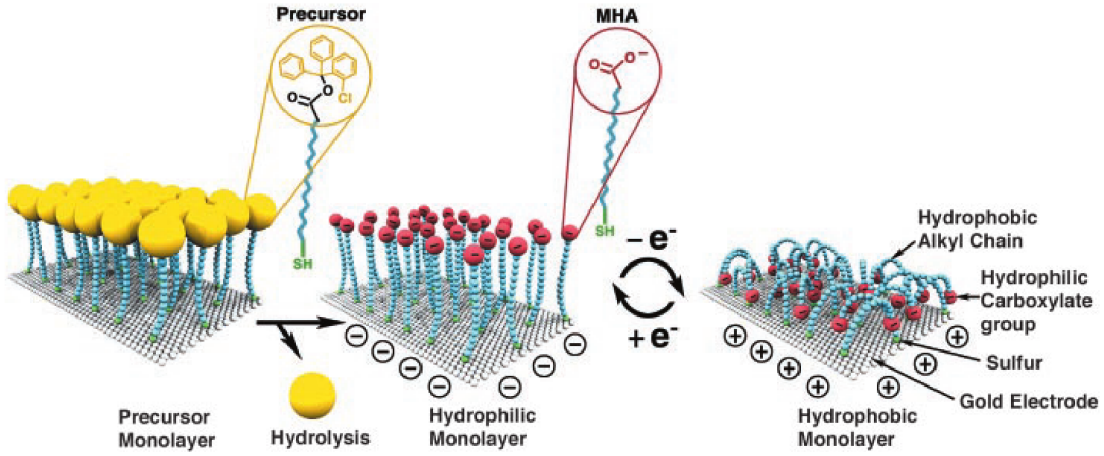

Figure 2.10: Idealized representation of the transition between straight (hydrophilic) and bent (hydrophobic) molecular conformations (ions and solvent molecules are not shown). The precursor molecule MHAE, characterized by a bulky end group and a thiol head group, was synthesized from MHA by introducing the (2-chlorophenyl)diphenylmethyl ester group. Reproduced from reference [37].

Lahan *et al.* engineered a surface that can reversibly change its interfacial properties, such as wettability, in response to an electric potential[37]. A monolayer of molecular tethers on the surface was able to undergo a conformational transition between a hydrophilic and a hydrophobic state. Figure 2.10 shows a cartoon of the transition.

These two surface technologies, among others [89], paved the way for dynamic surfactants on nanoparticles and nanocolloids, which resulted in particles that can dynamically and reversibly change their properties.

Early work by Makino *et al*, Okubo *et al*, Kim *et al*, and Dingenouts *et al*, focused on synthesizing particles that were able to change their properties with changes in thermodynamic properties, such as pH and temperature [90–93]. More recent work, introduced in Section 2.1, has dedicated to introducing dynamic behavior to nanoparticles using non-thermodynamic controls, such as chemical fuel [31], magnetic fields [80], and light [80, 82].

These recent developments, especially the development of photo-switchable particles that can reversibly change their inter-particle interactions between attractive and excluded volume, motivated the research presented in Chapter V.

CHAPTER III

Methods

This chapter describes the details of the simulation and analysis methods used throughout this thesis. The main method used is Langevin dynamics, a coarse grained method designed for simulating particle in a solvent, with a velocity Verlet integrator. We give the rationale for our parameter choice and explain how we introduce non-equilibrium dynamics into our simulations. Also, we describe the main methods used to characterize the resulting systems.

3.1 Simulation

3.1.1 Langevin dynamics

Langevin Dynamics (LD) is a coarse grained method used to simulate nanocolloids and nanoparticles in a solvent which incorporates the interactions between particles, the drag due to the solvent, and the thermal fluctuations that drive Brownian motion. LD is based on the Langevin equation, a stochastic differential equation, of the form:

$$m_i \ddot{x}_i = F_i^C + F_i^D + F_i^R \tag{3.1}$$

where F_i^C is the conservative force due to inter-particle interactions, F_i^D is the force due to drag that a particle experiences when traveling through a solvent, and F_i^R is

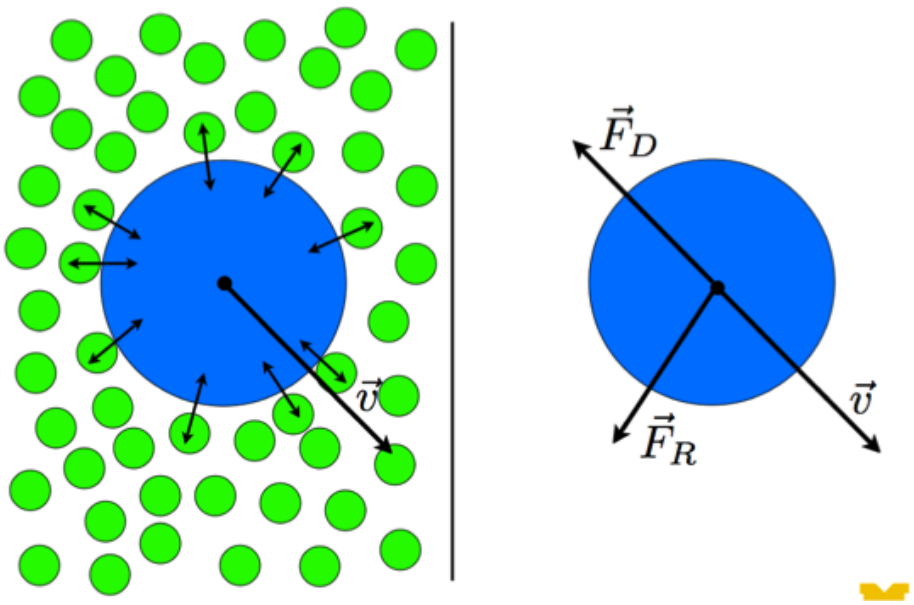

Figure 3.1: Langevin dynamics. Coarse grained F_i^D, drag force, due to a particle's movement through a solvent and F_i^R, random force, due to thermal motion of the solvent. [Credit: Dr. Joshua Anderson]

the random force due to thermal motions in the solvent. Here, m_i and x_i are the particle mass and position, respectively.

The conservative force F_i^C is determined by the gradient of the pairwise Lennard-Jones (LJ) and Weeks-Chandler-Andersen (WCA) potentials between a particle and its neighbors. The drag force F_i^D is proportional to the particle's velocity but on the opposite direction:

$$F_i^D = -\gamma m \vec{v}_i \tag{3.2}$$

The random force F_i^R satisfies the fluctuation-dissipation theorem:

$$\left\langle F_i^R \right\rangle = 0 \tag{3.3}$$

$$\left\langle F_i^R(t) F_j^R(t') \right\rangle = 6\gamma m k_B T \delta_{ij} \delta(t - t')) \tag{3.4}$$

where k_B is Boltzmann's constant, δ_{ij} is the Kronecker delta, $\delta(t - t')$ is the Dirac

delta function, γ is the Langevin drag coefficient, m is the particle mass, and T is the absolute solvent temperature.

The drag force exerted on a spherical particle in an environment with very low Reynolds numbers as it moves in a viscous fluid, such as nanocolloids in a solvent, is given by Stokes' law:

$$F^D_{Stokes} = -6\pi\eta r v$$

where η is the solvent viscosity, r is the particle radius, and v is the particle velocity. By equating F^D_{Stokes} to F^D_i (Equation 3.2), we calculate the proper γ for our system [94].

3.1.2 Integration method

We use a velocity Verlet method [95] to integrate Newton's equations of motion using the forces calculated using Langevin dynamics to calculate the new position and velocity for each particle. The velocity Verlet algorithm is described by the relationships:

$$\vec{x}(t + \Delta t) = \vec{x}(t) + \vec{v}(t)\Delta t + \frac{1}{2}\frac{\vec{f}(t)}{m}\Delta t^2 \tag{3.5}$$

$$\vec{v}(t + \Delta t) = \vec{v}(t) + \frac{1}{2}\left(\frac{\vec{f}(t)}{m} + \frac{\vec{f}(t + \Delta t)}{m}\right)\Delta t \tag{3.6}$$

where $\vec{x}$ is the particle position, $\vec{v}$ is the particle velocity, and $\vec{f}$ is the force experienced by a particle from the Langevin dynamics calculation.

During the execution of this algorithm, every time step, first Equation 3.5 is solved, then $\vec{f}(t+\Delta t)$ is calculated using the new particle positions, and finally Equation 3.6 is solved and the resulting velocities are stored for the next time step.

The error on the Velocity Verlet method is in the same order as the original Verlet algorithm. The particle positions are accurate to the order of Δt^4, and the particle velocities are accurate to the order of Δt^2.

3.1.3 Inter-particle potentials

We use two types of potentials to model the interactions between particles:

Attractive interactions are modeled using a 12-6 Lennard-Jones (LJ) potential of the form:

$$V_{LJ}(r) = \begin{cases} 4\epsilon\left[\left(\frac{\sigma}{r}\right)^{12} - \left(\frac{\sigma}{r}\right)^{6}\right] + 4\epsilon\left[\left(\frac{\sigma}{r_c}\right)^{12} - \left(\frac{\sigma}{r_c}\right)^{6}\right] & r < r_c \\ 0 & r \geq r_c \end{cases} \tag{3.7}$$

where σ is the particle diameter, ϵ the interaction strength, and r is the center-to-center distance between two particles. For computational efficiency the pair potential is truncated at $r_c = 2.5\sigma$ and then shifted to zero at r_c to avoid the discontinuity at the cut-off distance.

Excluded volume interactions are modeled using the Weeks-Chandler-Andersen (WCA) [96] inter-particle potential.The form of the WCA pair potential is similar to the LJ potential (Equation 3.7) with the cutoff set to $r_c = 2^{1/6}\sigma$.

These two potentials are used throughout the literature to model attractive and close to hard sphere colloids and nanoparticles.

3.1.4 Validation

To verify that the particle diffusion, controlled by the Langevin drag coefficient (γ), matched the expected diffusion of a nanoparticle solution. We calculated γ using the experimental values given at ref [38]. Then, we ran a simulation of 10,000 particles with only excluded volume interactions (WCA) at low density ($\rho = 0.01$) using the calculated γ. Measured the mean squared displacement (MSD) of the particles and

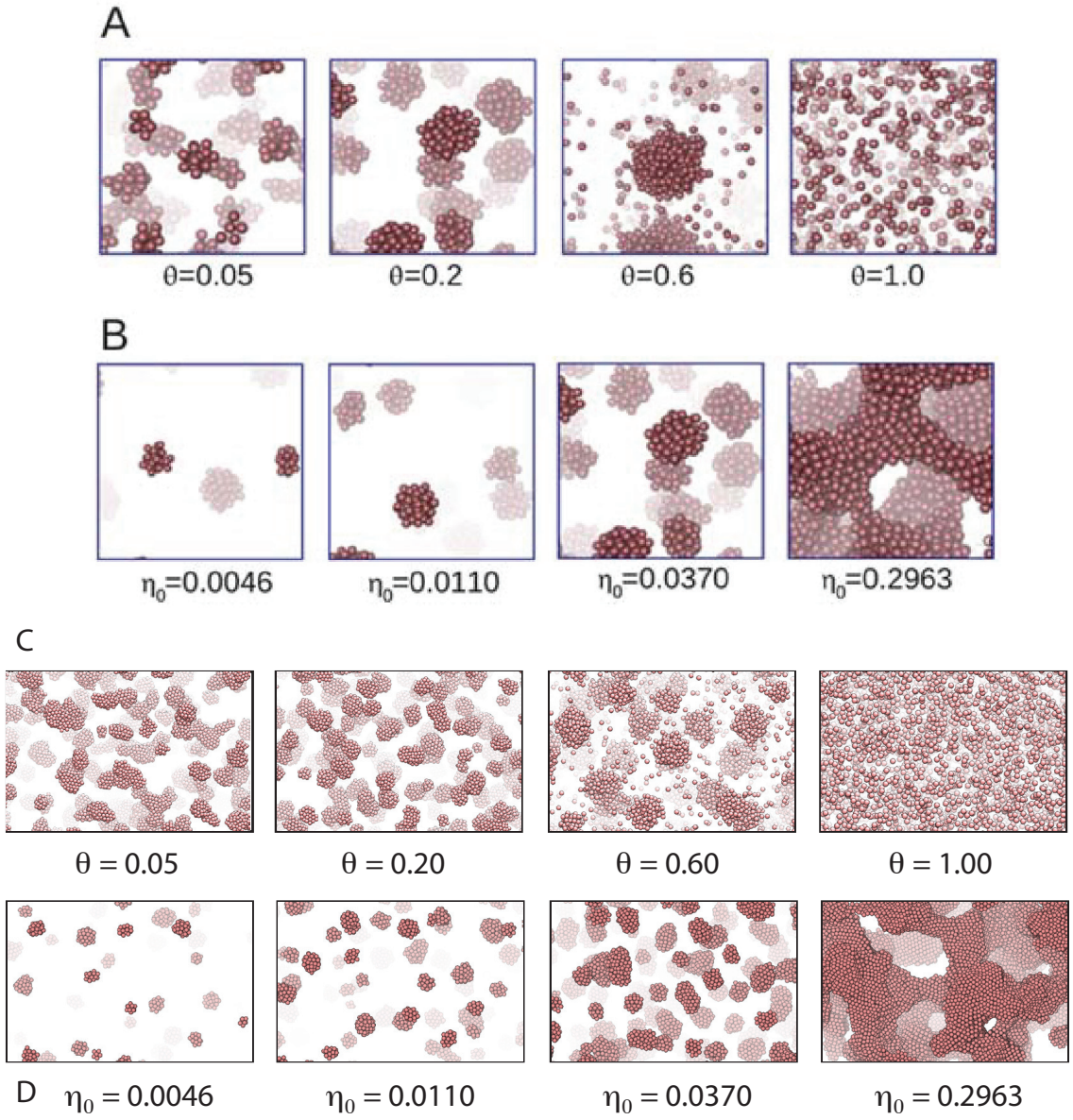

Figure 3.2: Typical simulation snapshots at the end of aggregation phase after one cycle of light exposure. (A,B) Monte Carlo results from reference [38]. (C,D) Langevin dynamics results. (A,C) For a range of θ with $\eta_0 = 0.037$. (B,D) For a range of η_0 with $\theta = 0.2$. Snapshots are zoomed in to show individual aggregates in detail and do not show the entire simulation box. The contrast (bold or faded) of particles is used to indicate the depth of particles from the top plane (close or farther).

calculated the diffusion coefficient from the slope of the MSD. The resulting diffusion coefficient was within 10% of the experimental diffusion coefficient.

To verify that the aggregation dynamics in our system are correct, we recreated the Monte Carlo results published in ref [38] using Langevin dynamics. Figures 3.2(A,B) show typical simulation snapshot for multiple temperatures (θ) and densities (η_0) using Monte Carlo. Figures 3.2(C,D) show the corresponding simulation snapshots using Langevin dynamics. Both results agree qualitatively. Figure 3.3 show number average aggregate size (M_n) and polydispersity (PD) of the aggregates at the end of one cycle for the systems simulated using Monte Carlo and Langevin dynamics. Here, we can see that both methods are in quantitative agreement. The differences at low θ are due to unphysical kinetic traps in Monte Carlo simulations not allowing cluster moves, which have been documented in reference [97].

3.1.5 Particle type switching

To simulate particles switching from one type to another and vice versa as described in Section 4.2.1, we created a HOOMD-Blue plugin that accessed the particle data in the simulation every $X = 100$ time steps and attempted to switch particles according to a given probability. We defined Lennard-Jones (LJ) interactions for pairs of particles of type A-A and B-B, and Weeks-Chandler-Andersen (WCA) interactions for A-B.

When the plugin was activated, a script looped over all particles in the system sequentially drawing a random number. If the random number is greater than the given probability the particle type was switched, otherwise it was left unchanged. Particle switches were entirely stochastic and did not depend on the local configuration of the system.

The potential energy of the system was calculated before and after the switch and stored for later analysis.

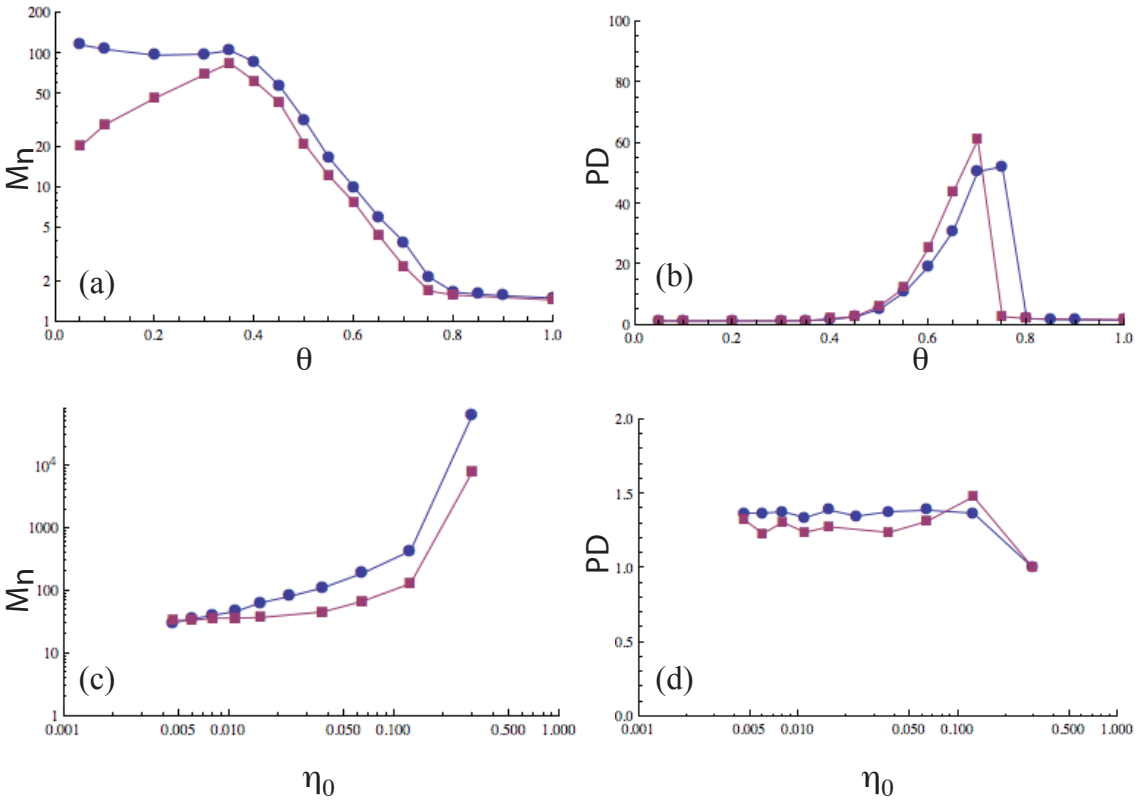

Figure 3.3: (a,c) Number average aggregate size (M_n) and (b,c) polydispersity(PD) of the aggregates at the end of the aggregation phase after one cycle of light exposure. (a,b) At temperature θ for $\eta_0 = 0.037$. (c,d) At number density η_0 for $\theta = 0.2$. Purple squares show the values obtained using Monte Carlo from reference [38]. Blue squares show the results from Langevin dynamics simulations.

3.1.6 Particle on/off switching

To simulate all particles in a system switching on and off, two inter-particles potentials were defined for particle pair A-A. A LJ potential for the on phase, and a WCA potential for the off phase. The simulation script looped over all the desired number of cycles enabling and disabling the appropriate potential for the current phase. All particles were turned on/off simultaneously.

3.2 Analysis

3.2.1 Radial distribution function

The radial distribution function (RDF), also called pair correlation function $g(r)$, is a function used to characterize the local structure of the system, and describes how density varies, in average, as a function of distance to a particle. The RDF is the average number density of $\rho(r)$ at distance r from any particle, normalized by the density at distance r from an atom in an ideal gas at the same density. In a random system, $g(r) = 1$ for all values of r, any deviation from this value indicates correlations between the particles. Additional details and an algorithm for calculating the RDF can be found in reference [95].

In this work, we use two kinds of RDF. The first kind is calculated between particles of the same type. At small r values, this RDF gives us information about the internal ordering of the aggregates. At large r values, it enables us to estimate the size of continuous domains. The second kind is calculated between particles of opposite type. This RDF provides information about how far apart are two domains from each other, and allows us to identify when layered structures form within aggregates.

3.2.2 Bond order parameter

To determine the structure of our aggregates, we used the bond order parameter described by Steinhardt, Nelson and Ronchetti in reference [98]. This bond order parameter tries to capture the symmetry of bond orientations regardless of bond length. In this work, we consider a bond to exist between two particles whose center-to-center distance is less than 1.3σ. This distance was obtained from the minimum between the first and second peak of the radial distribution function (RDF) [39].

The local order parameter is given by the relationship:

$$Q_{lm}(\vec{r}) \equiv Y_{lm}\left(\theta(\vec{r}), \phi(\vec{r})\right), \tag{3.8}$$

where $Y_{lm}(\theta, \phi)$ are spherical harmonics, and $\theta(\vec{r})$ and $\phi(\vec{r})$ are the polar and azimuthal angles of the bond with respect to some reference coordinate system. We do not need to associate a direction with a bond, provided we only use even-l spherical harmonics, which are invariant under inversion.

Then, the global bond order parameter can be calculated by averaging $Q_{lm}(\vec{r})$ over all bonds.

$$\overline{Q}_{lm} \equiv \langle Q_{lm}(\vec{r}) \rangle, \tag{3.9}$$

where the average is taken over all the bonds in the system. It is important to consider the order parameter rotationally invariant combinations:

$$q_l \equiv \left(\frac{4\pi}{2l+1} \sum_{m=-l}^{l} \left| \overline{Q}_{lm} \right|^2 \right)^{1/2} \tag{3.10}$$

and

$$W_l \equiv \sum_{\substack{m_1,m_2,m_3 \\ m_1+m_2+m_3=0}} \begin{pmatrix} l & l & l \\ m_1 & m_2 & m_3 \end{pmatrix} \overline{Q}_{lm_1} \overline{Q}_{lm_2} \overline{Q}_{lm_3} \tag{3.11}$$

where the coefficients:

$$\begin{pmatrix} l & l & l \\ m_1 & m_2 & m_3 \end{pmatrix}$$

are the Wigner $3j$ symbols [99]. It is standard to define a normalized quantity:

$$\hat{W}_l \equiv \frac{W_l}{\left(\sum_m |Q_{lm}|^2\right)^{3/2}} \tag{3.12}$$

Table 3.1 give the q_4, q_6, $\hat{W}_4$, and $\hat{W}_6$ values for ideal fcc, hcp, sc, and bcc structures as well as for a liquid.

Geometry	q_4	q_6	$\hat{W}_4$	$\hat{W}_6$
fcc	0.19094	0.57452	-0.15932	-0.01316
hcp	0.09722	0.48476	0.13410	-0.01244
sc	0.76376	0.35355	0.15932	0.01316
bcc	0.08202	0.50083	0.15932	0.01316
liquid	0	0	0	0

Table 3.1: Bond order parameters for face-centered-cubic (fcc), hexagonal close-packed (hcp), simple cubic (sc), body-centered-cubic (bcc), liquid structures. Reproduced from reference [39].

3.2.3 Aggregate size M_W

The weight averaged aggregate sizes are calculated by clustering the particles in the system into aggregates and then counting the number of aggregates n_i, with aggregation number i, where i is the number of particles in the aggregate [38]. Two particles are considered to be in the same aggregate if their center-to-center distance is less than 1.3σ.

The number of aggregates is then used to calculate the weight average aggregate size M_W:

$$M_W = \frac{\sum_i n_i i^2}{\sum_i n_i i} \tag{3.13}$$

the number average aggregate size:

$$M_n = \frac{\sum_i n_i i}{\sum_i n_i} \tag{3.14}$$

and the polydispersity (PD):

$$PD = \frac{M_W}{M_n}. \tag{3.15}$$

3.2.4 Thermostat energy dissipation

To measure the amount of energy, as heat, that the Langevin thermostat is exchanging with the system, at each time step during the force integration portion, we add the work done by the conservative, dissipative and random forces and tally them for later analysis.

The amount of energy dissipated as heat by the thermostat is given by the relationship:

$$Q = \sum_i \left(F_i^C + F_i^D + F_i^R\right) \Delta x_i$$

where Q is the heat removed by the thermostat between times t and $t+\Delta t$, and Δx_i is the change in position of particle i during the same time window. In equilibrium, this quantity oscillates around zero and it is typically used to verify energy conservation and to quantify the amount of energy drift in the system due to machine precision numerical round off and integration error. But, in driven systems, the work performed

by the Langevin thermostat measures the amount of energy that the thermostat must dissipate to maintain a constant temperature. Since there is no other dissipation mechanism, the amount of energy measured corresponds to the amount of energy input required to maintain the steady state structures.

CHAPTER IV

Steady State Structures

We consider the behavior of an immiscible mixture of two species of nanocolloids driven far-from-equilibrium by dynamically switching between species. Using Langevin Dynamics simulations on graphics processors, we show that novel steady state structures dynamically self-assemble for judicious choices of thermodynamic and model parameters. We describe the dynamics that stabilize these dissipative structures, and present a phase diagram of predicted stable phases as a function of the relevant thermodynamic variables. We explore energy dissipation in this driven system, and demonstrate the requirements for maintaining far-from-equilibrium structures.[1]

4.1 Introduction

Energy-dissipating structures that are assembled from constituent building blocks in systems driven far-from-equilibrium have shown great promise for a host of applications because they can be adaptable, self-healing and self-replicating [27, 28]. Many efforts have been directed towards understanding the behavior of systems driven far-from-equilibrium. Dynamically self-assembling systems are one class of such non-equilibrium systems, arising in various man-made and natural phenomena, including life [27, 89].

[1]This chapter is adapted from Reference [100] A. F. Osorio Vivanco, I. Szleifer, S. C. Glotzer. "Dissipative Self-Assembly of Switchable Colloids Driven Far-From-Equilibrium", *submitted.*

Developments in surface [36, 37, 101], colloidal and nanoparticle [80, 82, 102] synthesis motivate the consideration of design and fabrication of nanoscale colloids whose properties are not static but can be changed either autonomously or on command by the input of energy. Such active matter systems are interesting from the point of view of self-assembly because they go beyond traditional thermodynamic systems in which the constituent building blocks – whether atoms, molecules, nanoparticles, or colloids – have inherent properties that are unchanging and immutable. One example of nontraditional colloidal matter is the self-propelled colloid, in which particles are driven to move in ways that produce novel collective behavior [59–79]. Systems of shape-changing particles are another example of active matter, where thermodynamic assemblies can be affected by the shape change of the constituent building blocks [103–106].

In this paper, we study the behavior of another new class of active matter - switchable nanocolloids. We investigate a binary mixture of nanocolloids in which the particles can switch, or interconvert, from one species to the other according to an externally controlled rate decoupled from the thermodynamics of the system. We envision this switching to occur by using an external energy source to actuate photochromic molecular switches [101], reversibly photo-isomerizable monolayers [36], or other types of active surfactants [37, 102] on the surface of nanocolloids, effectively switching locally the inter-particle potential. This problem couples the thermodynamic process of phase separation to a dissipative reaction process that tends towards remixing, producing novel behavior as a result of the competition.

Our study is motivated by previous studies of reactive binary mixtures, where reversible reactions stabilize steady state domain sizes when coupled with spinodal decomposition [33, 34, 83–87, 107–109]. Two-dimensional studies conducted using Monte Carlo [83], Molecular Dynamics [84], modified TDGL with Navier-Stokes [34, 107], Lattice Boltzmann [87], and Cell Dynamical Systems [109] show that different

morphologies can be stabilized by judicious choice of thermodynamic parameters.

This chapter is organized as follows: In Section 4.2, we describe the simulation model and method as well as the techniques used to determine the average size of the emerging domains and the amount of energy dissipated by the system. In Section 4.3, we present the steady state structures found and the phase diagram of the system, followed by an explanation of how these structures form, and finally report measurements of how much energy is required to maintain the structures in steady state.

4.2 Model and methods

4.2.1 Model

We consider two types of particles. Interactions between nanocolloids of the same type are modeled via an isotropic Lennard-Jones (LJ) 12-6 pair potential of the form shown in Equation (4.1) and Figure 4.1(a)(black, solid), with particle diameter σ, and interaction strength $\epsilon = 2.5$, where r is the center-to-center distance between two particles. The pair potential is truncated and smoothed to zero at $r_c = 2.5\sigma$.

$$V_{LJ}(r) = \begin{cases} 4\epsilon\left[\left(\frac{\sigma}{r}\right)^{12} - \left(\frac{\sigma}{r}\right)^{6}\right] + 4\epsilon\left[\left(\frac{\sigma}{r_c}\right)^{12} - \left(\frac{\sigma}{r_c}\right)^{6}\right] & r < r_c \\ 0 & r \geq r_c \end{cases} \tag{4.1}$$

Particles of opposite type interact via a Weeks-Chandler-Andersen (WCA) pair potential [96], which is purely repulsive and has the same form and parameters as LJ, but with $r_c = 2^{1/6}\sigma$, as shown in Figure 4.1(a)(red, dashed). Particles of one type can switch to the opposite type with probability p_{switch}. Figure 4.1(b) shows the particle interaction rules.

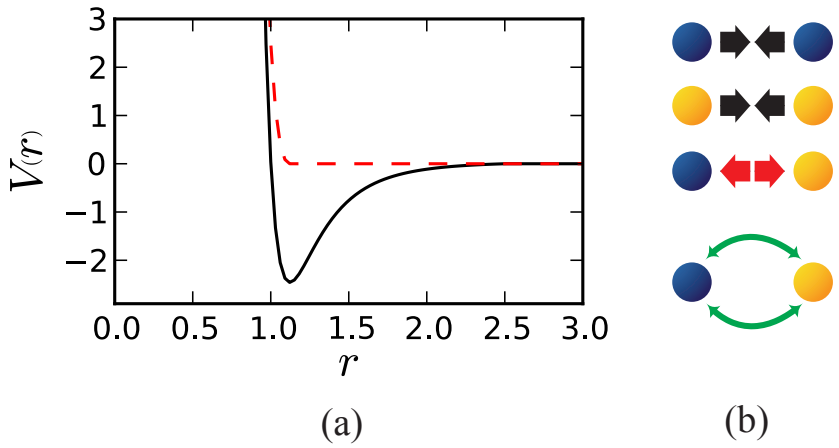

Figure 4.1: Interaction rules. (a) (Black, solid) Lennard-Jones potential between same type particles, (Red, dashed) Weeks-Chandler-Andersen potential between opposite type particles. (b) Interaction rules: Below a critical temperature, similar particles attract and dissimilar particles do not. Each particle can instantaneously and independently change type from one type to another and back by a random process.

4.2.2 Simulation Method

We use Langevin Dynamics (LD), a stochastic molecular dynamics method with a Langevin thermostat, to simulate the time evolution of an isothermal system of two types of particles in a three-dimensional box with periodic boundary conditions. In LD, each particle is subjected to conservative (F_i^C), drag (F_i^D), and random (F_i^R) forces, and its motion is governed by the Langevin equation:

$$m_i \ddot{x}_i = F_i^C + F_i^D + F_i^R$$

Here, m_i and x_i are the particle mass and position, respectively. The conservative force F_i^C is determined by the gradient of the pairwise Lennard-Jones (LJ) and Weeks-Chandler-Andersen (WCA) potentials between a particle and its neighbors. The

random force F_i^R satisfies the fluctuation-dissipation theorem:

$$\left\langle F_i^R \right\rangle = 0$$
$$\left\langle F_i^R(t) F_j^R(t') \right\rangle = 6\gamma m k_B T \delta_{ij} \delta(t - t'))$$

where k_B is Boltzmann's constant, δ_{ij} is the Kronecker delta, $\delta(t - t')$ is the Dirac delta function, γ is the Langevin drag coefficient, m is the particle mass, and T is the absolute solvent temperature. The drag force is related to the particle velocity v_i by $F_i^D = -\gamma m v_i$. More details on the simulation method may be found in ref [95]. The Langevin drag coefficient γ is carefully chosen using the method described in Section 4.2.3, so that the resulting drag force F_i^D is equivalent to the drag force experienced by a particle of a determined size in a solvent with a specific viscosity. As will be seen later, proper selection of γ is crucial for getting the correct steady state morphological results and phase diagram, and for measuring the amount of energy dissipated by the system. We perform simulations of $N = 64,000$ particles at number density $\rho = 0.125\sigma^{-3}$, in a cubic box of edge length $L = 80\sigma$ with periodic boundary conditions. The temperature of the system is maintained by the Langevin thermostat at $T = 0.4\epsilon \,/\, k_B$. The time step of the velocity Verlet algorithm used to integrate Newton's equation of motion is $\Delta t = 0.006\tau$, where $\tau = (m\sigma^2 \,/\, \epsilon)^{1/2}$ is the unit of time.

Initially, half of the particles ($N/2$) are of type A and the other half are of type B. The particles are thermalized by increasing the temperature to $T^* = 5T$ and running the system while particle switching is turned off to randomize their starting positions until a homogeneous mixture is achieved. Then the system is quenched to temperature T and particle switching is turned on. Every $X = 100$ time steps, each particle attempts to switch to the opposite type with switching probability p_{switch}. Particle switching is accomplished by sweeping through every particle in the system in a

sequential order and generating a random number; if the random number is lower than p_{switch}, the particle is switched to the opposite type. If not, the particle remains the same type.

Multiple simulations were run using different starting conditions, including phase separated and lamellar initial states as well as mixed initial conditions. We found that the steady state results do not depend on initial conditions.

For our simulations, we used locally authored code and the GPU-based HOOMD-Blue code package under development in our group, (`http://codeblue.umich.edu/hoomd-blue/index.html`) [110] which permitted rapid exploration of the phase diagram. The simulations were run on our GPU cluster at the University of Michigan on NVIDIA Tesla S2050s. Roughly 1600 independent simulations were investigated over 250,000 GPU hours.

4.2.3 Langevin drag coefficient (γ) selection

The mechanism driving the evolution and stability of our structures is the competition between the thermodynamic process of phase separation and a dissipative reaction process that tends towards remixing. In order to model this competition properly, we must ensure that the timescales are scaled appropriately. We use the Langevin drag coefficient (γ) to control the timescale of the phase separation by selecting a γ (using the method explained below) that reflects the desired experimental conditions. This γ coupled with the other simulation parameters will allow us, through dimensional analysis, to determine the length, energy and time scales of the system and will give meaning to the rate at which particles switch types, controlled by the switching probability p_{switch}. We will then explore how the relationship between these two control variables, γ and p_{switch}, determine the resulting steady state structures via a "phase" diagram.

The drag force exerted on a spherical particle in an environment with very low

Reynolds numbers as it moves in a viscous fluid, such as nanocolloids in a solvent, is given by Stokes' law:

$$F^D_{Stokes} = -6\pi\eta r v$$

where η is the solvent viscosity, r is the particle radius, and v is the particle velocity. When using a Langevin thermostat, the drag force experienced by a particle when moving through a solvent is given by:

$$F^D_{Langevin} = -\gamma m v.$$

By equating these two drag forces, we calculate the proper γ for our system [94].

4.2.4 Characterizing dynamic evolution

Understanding the time evolution of the system and the competing dynamic mechanisms is important to be able to predict the expected steady state structure.

We characterize the evolution of the system by calculating the radial distribution function (RDF) between particles of the same type and using the result to estimate the size of the domains. Then, we calculate the RDF between particles of opposite types and use the result to measure how far the domains are from each other. In a system undergoing spinodal decomposition, both RDFs, between same and opposite type particles, give similar results, but in the layered structures the RDF between opposite type particles helps us identify when new interfaces and layers are being created.

To understand the mechanism that drives the phase transition between small steady state domains and layered structures presented in Section 4.3.1, we run small simulations with similar parameters as described above that start with one aggregate of N particles. Then, a random particle within the aggregate is switched to the

opposite type and the time it takes for the particle to leave the aggregate is measured. This helps us get an intuition of how the time a switched particles stays in a domain of the opposite type scales with domain size.

4.2.5 Energy input and dissipation measurements

The stability of dynamically self-assembled, energy-dissipating structures depends on the constant energy input into the system. Once the energy source is removed, the now unstable steady state structure devolves to its equilibrium structure. To measure the amount of energy required to maintain our steady state structures, we calculate the amount of energy, as heat, that the Langevin thermostat is removing from the system by adding the work done by the conservative, dissipative and random force. This work is given by the relationship:

$$Q = \sum_i \left(F_i^C + F_i^D + F_i^R\right) \Delta x_i$$

where Q is the heat removed by the thermostat between times t and $t + \Delta t$, and Δx_i is the change in position of particle i during the same time window. In equilibrium, this quantity oscillates around zero and it is typically used to verify energy conservation and to quantify the amount of energy drift in the system due to machine precision numerical round off and integration error. But, in our driven system, the work performed by the Langevin thermostat measures the amount of energy that the thermostat must dissipate to maintain a constant temperature. Since there is no other dissipation mechanism, the amount of energy measured corresponds to the amount of energy input required to maintain the steady state structures.

We also measure the amount of energy introduced into the system when a particle switches types by histogramming the difference in the potential energy of a particle before and after a switch.

4.3 Results and discussion

In the absence of particle switching, we confirm the expected thermodynamic demixing of the system by spinodal decomposition [111] into coexisting A-rich and B-rich phases when the temperature of the system is quenched to $T = 0.4\epsilon$. In the presence of switching and, consequently, energy input and dissipation, the system is no longer thermodynamic and is instead driven to a non-equilibrium steady state. These states are described below.

4.3.1 Steady state structures

We observe the spontaneous formation of complex spherical structures with concentric layers made of alternating types of particles as shown in Figure 4.2(a) and structures where spinodal decomposition has been stopped and domains with sizes smaller than the equilibrium domain size are stable (Figure 4.2(b)) when the switching probability p_{switch} is chosen appropriately. Specifically, for $p_{switch} < 3 \times 10^{-5}$ when $\gamma = 1\tau^{-1}$, switched particles can diffuse to their corresponding domains and the system achieves its thermodynamic equilibrium configuration resulting in bulk phase separation (Figure 4.2(c)). For $p_{switch} > 2 \times 10^{-1}$ when $\gamma = 1\tau^{-1}$, particles switch faster than they can diffuse to form domains, resulting in a homogeneous mixture (Figure 4.2(d)).

The multi-layered aggregates are dynamic, constantly moving and interacting with other aggregates. New layers are continuously created as particles switch types and aggregate inside the innermost layer, and move from layer to layer. Particles in the outer layer are exchanged when two aggregates with the same outer layer come into contact. This intrinsic dynamism stabilizes the dissipative aggregates as long as energy is being input into the system. It also allows the system to be reconfigured – to adjust its layer thickness, aggregate size and overall morphology – by regulating the amount of energy supplied by adjusting p_{switch}.

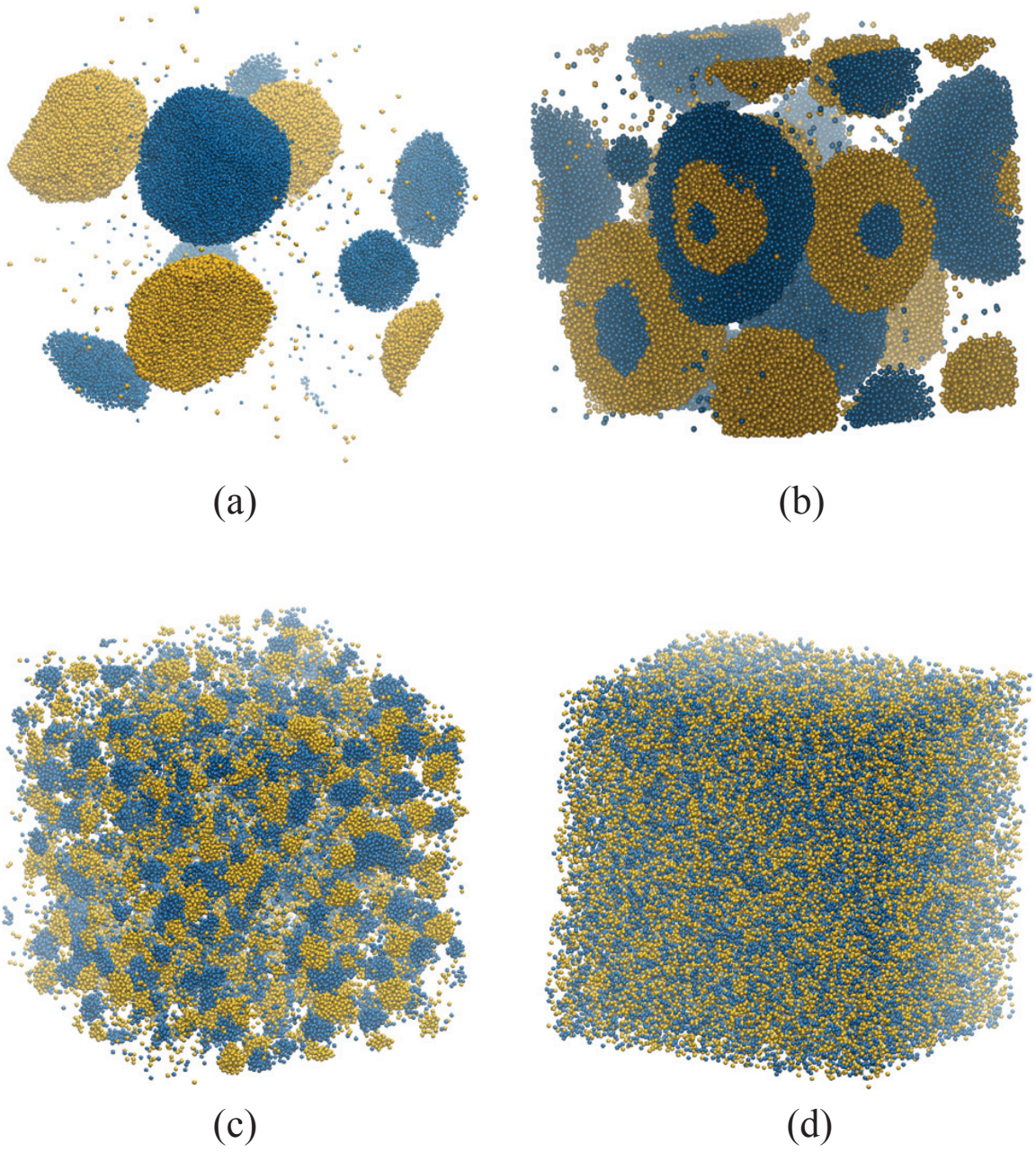

Figure 4.2: Steady state phases. Simulation snapshots of (a) a phase-separated system, (b) a system dynamically self-assembled into a spherical laminar structure, (c) a system where the aggregate domain size has been stabilized, and (d) a mixed system. The system can dynamically move from demixed to mixed through these steady states by changing the switching rate. The contrast (bold or faded) of particles is used to indicate the depth of the particles in the three-dimensional box.

4.3.2 Phase diagram

The competition between the thermodynamic process of phase separation and a dissipative reaction process that tends towards remixing stabilizes the structures shown in Figure 4.2. Figure 4.3 shows how the interplay of these two processes affects the resulting steady state of the system. The Langevin friction coefficient γ controls how fast the particles can diffuse, and therefore the speed of the demixing, by regulating the friction force experienced by the particles as they move through a solvent. The switching probability controls the rate at which particles tend to remix by, in general, switching a particle located in an energetically favorable configuration surrounded by particles of the same type, to an unfavorable configuration surrounded by particles of the opposite type.

The phase diagram has four distinct steady state phases. In one phase, (blue in Figure 4.3) the perturbations due to particle switching are not large enough to prevent the system from reaching its equilibrium configuration of bulk phase separation. In three other phases, the system is dynamically stabilized into different classes of steady state structures: (green) spherical structures made of concentric layers of alternating types of particles, (red) spinodal decomposition (SD) intermediate structures and a (cyan) well-mixed, homogeneous, system.

Unlike in equilibrium systems, the value of γ, and therefore the timescale of phase separation via spinodal decomposition, shifts the value of p_{switch} where phase transitions occur. This γ dependence illustrates an important distinction when simulating systems in equilibrium vs far-from-equilibrium, and the reason why it is so crucial to understand the role of this parameter when simulating far-from-equilibrium systems. Barring kinetic arrest in a metastable state, equilibrium simulations should have no dependence on thermostat coupling parameters such as γ. Far-from-equilibrium simulations, as well as equilibrium simulations concerned with dynamics, are sensitive to the time evolution of the system and how the energy is exchanged with the thermo-

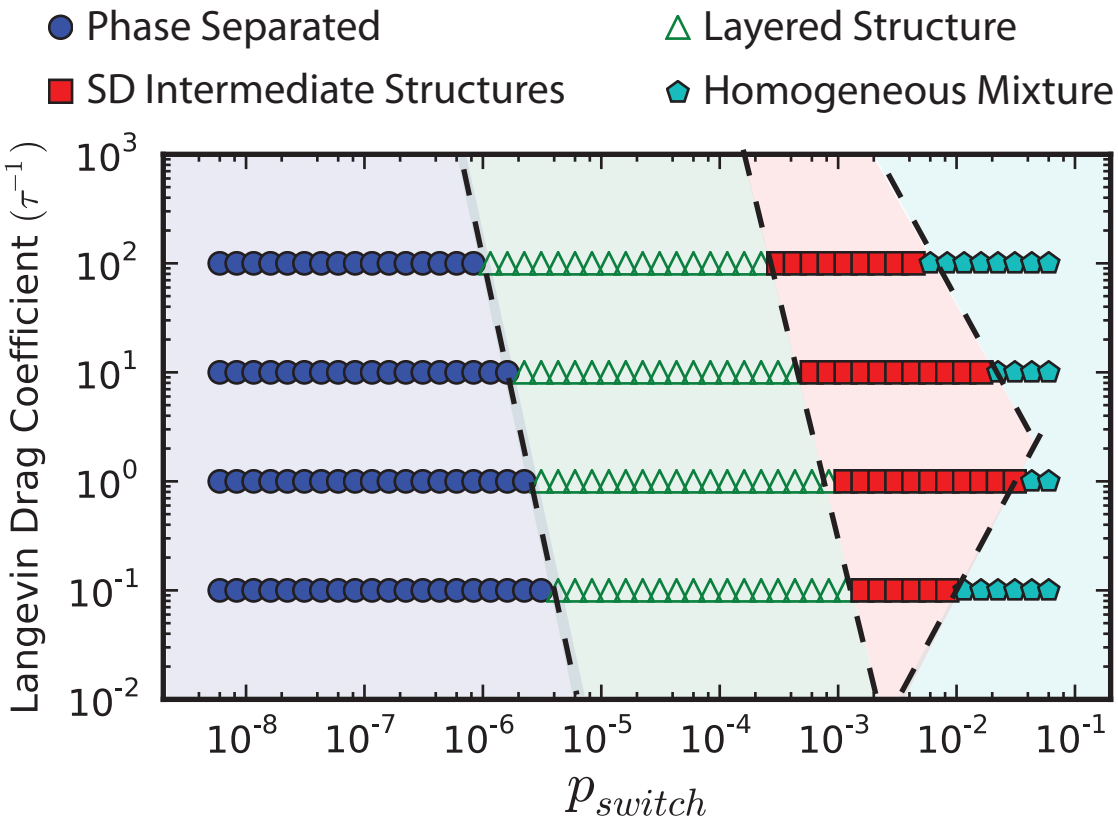

Figure 4.3: Phase diagram for the Langevin drag coefficient vs the switching probability showing four distinct phases. From left to right: (Blue) At low switching probability, the system has reached its equilibrium phase-separated configuration. (Green) At a medium-low switching probability, the perturbation due to particle switching stabilizes layered steady state structures. (Red) At medium-high switching probability, domain growth is inhibited and the domain size stabilized, but the domains are not large enough to sustain internal domains. (Cyan) At high switching probability, particles switch faster than the coarsening due to spinodal decomposition, so the system resembles a mixed system.

stat, controlled via a thermostat coupling parameter.

As we will see in the following sections, the transitions between phase separated and layered structures, and between layered structures and SD intermediate structures depends strongly on the time it takes for a switched particle to leave an aggregate of the opposite type. As γ increases, particle diffusion slows down and it takes longer for a particle to be ejected from an aggregate, allowing for the nucleation of new layers within aggregates at lower values of p_{switch}. Similarly, as the aggregation dynamics slow for higher values of γ, lower values of p_{switch} are needed to let aggregates grow large enough to be able to sustain inner layers.

The transition between spinodal decomposition intermediate structures and a homogeneous mixture shows an interesting re-entrant behavior. The transition point does not just depend on the time it takes for the particles to decompose into domains, which dominates the behavior at $\gamma = 10\tau^{-1}$ and above, but also, we believe, in the amount of energy that the thermostats must dissipate to maintain a constant temperature. As we will see in Section 4.3.5, the energy introduced in the system due to particle switching increases with increasing p_{switch}. The Langevin friction coefficient γ controls the coupling between the thermostat and the particles and hence the thermostat's ability to remove energy from the system. At $\gamma = 1\tau^{-1}$ and lower, and such high switching rates, the thermostat is not able to effectively remove enough energy to maintain the temperature to keep the system at the desired temperature, inhibiting phase separation. As we increase γ, the coupling between thermostat and the particles is stronger, enabling the thermostat to maintain the desired temperature by being able to remove energy from the system at higher rates. For this reason, we see the transition occurring sooner (at higher p_{switch} values) for increasing γ.

4.3.3 Structure evolution

To elucidate the formation of the different phases, we examine the radial distribution function (RDF), calculated between particles of opposite types, and between particles of the same type during early (time = $10^3\tau$), mid ($10^5\tau$), and late times ($10^8\tau$) following a quench to the two-phase region of the phase diagram determined in the absence of switching. Figure 4.4 shows the evolution of both (A-A and A-B) RDFs for systems with steady state of (a-c) phase separation, (d-f) layered structures, (g-i) SD intermediate structures, and (j-l) homogeneous mixtures.

During early times, all systems, except the homogeneous mixture as the steady state, undergo phase separation via spinodal decomposition. The domain sizes have not grown to a size large enough for the remixing due to particle switching to considerably affect domain growth or the microstructure. When p_{switch} is large enough to completely inhibit phase separation, the system remains mixed.

At intermediate times, domains continue to grow. The system with SD intermediate structures reaches a maximum domain size (h) with smaller domains than those in the phase separated and layered structures systems. Examination of the A-B RDF shows that domains in the phase separated system (b) and SD intermediate structures (h) are almost completely devoid of particles of the opposite type. However, in the system with the layered structures, a new plateau appears at distances between 5 and 10 particle diameters, hinting at the emergence of new layers within the domains.

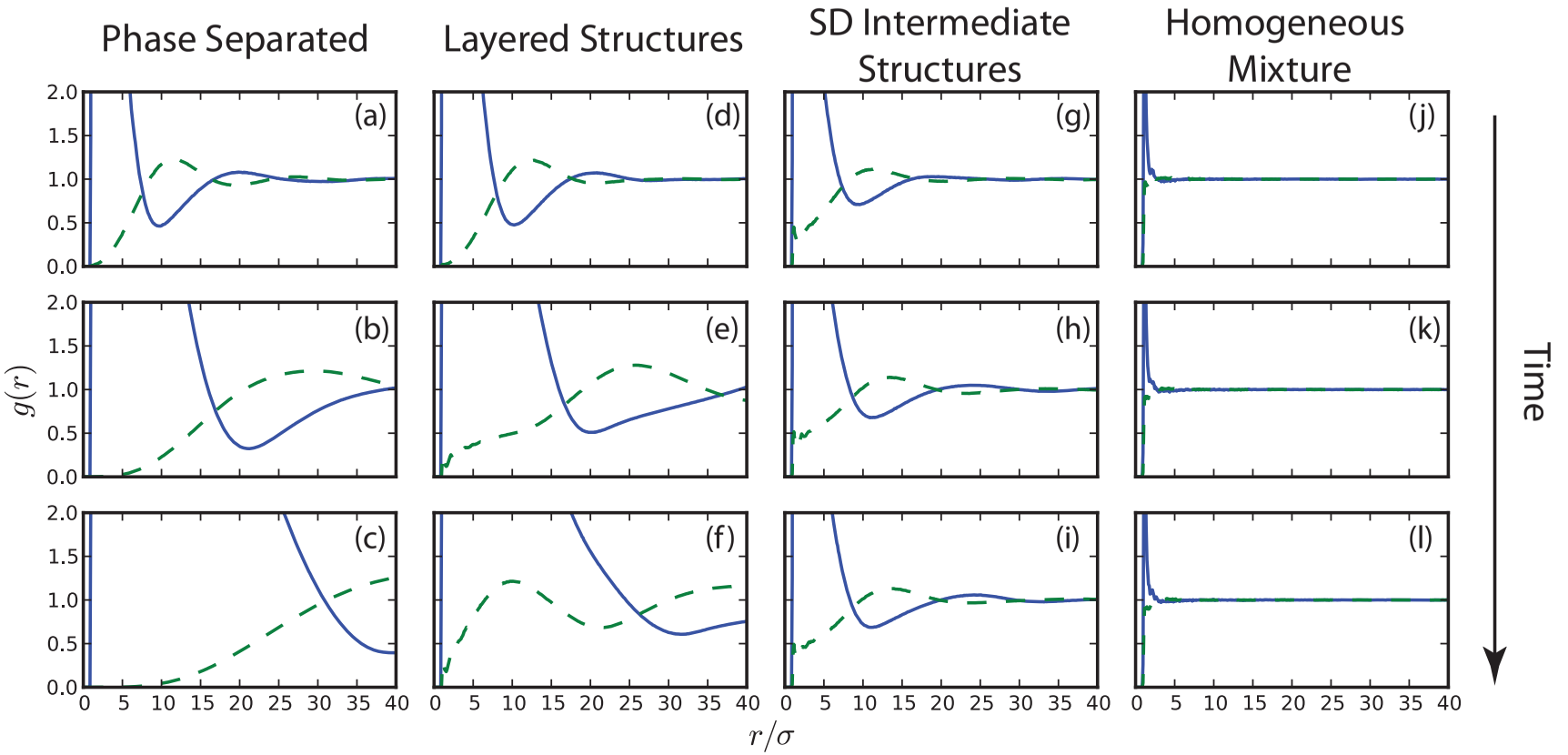

Figure 4.4: (a-l) Evolution of the radial distribution function (RDF), calculated between particles of the same type, A-A, (blue, solid) and particles of the opposite type, A-B, (green, dashed) for systems in the (a-c) phase-separated, (d-f) layered structures, (g-i) spinodal decomposition intermediate structures, and (j-l) homogeneous mixture phases. RDF snapshots taken at time = (a, d, g, j) $10^3\tau$, (b, e, h, k) $10^5\tau$, and (c, f, i, l) $10^8\tau$.

At late times, we can clearly see the structural differences between these phases at steady state. The system in (c) has completely phase separated as evident from the various RDFs, which have reached the maximum domain sizes allowed in our system (limited by system size). Layers are stabilized inside same type domains in the Layered Structures system (f) as indicated by the A-B RDF peak at r = 10, inside the large domains indicated by the same A-A and A-B RDF. In the system of SD intermediate structures, the RDFs at late times (i) are identical to those at intermediate times, illustrating the fact that phase separation has ceased. The absence of peaks in the A-A or B-B RDFs inside the domains indicates the absence of layers.

It is generally accepted that, in spinodal decomposition, the evolution of domains follows a simple power law $R(t) \propto t^{\beta}$, where β is the growth exponent [112]. Figure 4.5 shows the time evolution of the domain size, calculated from the same-type RDF. At $p_{switch} = 10^{-7}$, the system phase separates via spinodal decomposition and follows a power law with a growth exponent $\beta = 0.33$ during early times. At later times the domains grow at a slower rate ($\beta = 0.20$) due to particle switching disturbing domain growth until the domain reaches the maximum size permitted by the system. As switching is increased to $p_{switch} = 2 \times 10^{-4}$, where the steady state corresponds to layered structures, the domain grows in a similar fashion to the previous case, but once it reaches a critical size where remixing due to particle switching becomes dominant, domain growth ceases and new layers begin forming inside existing aggregates. Further increasing $p_{switch} = 2 \times 10^{-3}$ decreases the critical domain size to a regime where domains are too small to support inner layers, stabilizing SD intermediate structures. It is evident from the figure that steady state domain sizes have been achieved and that any further growth is inhibited.

Figure 4.6 shows the steady state domain size as a function of p_{switch}. We can see that for p_{switch} below 2×10^{-6} the system is able to attain domain sizes of $\sim 32\sigma$, the maximum size allowed in our system, but as p_{switch} increases the domain size

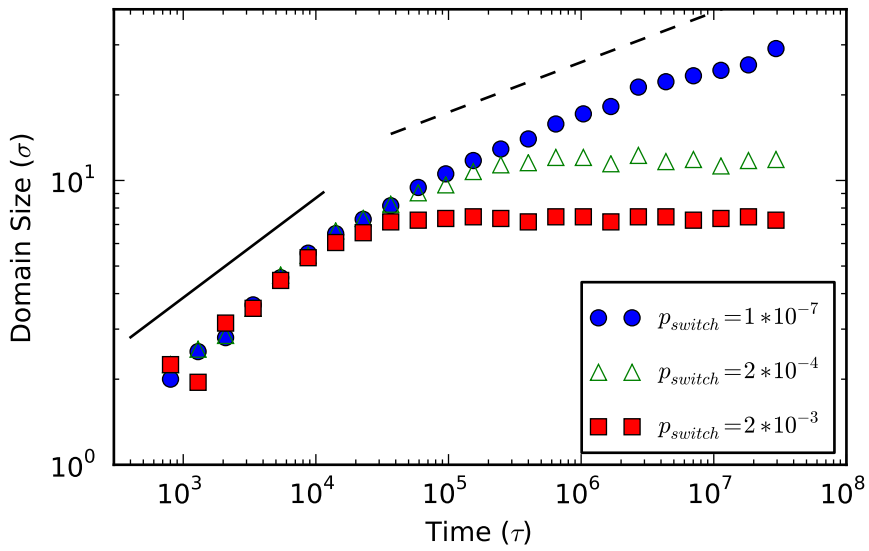

Figure 4.5: Average domain size as a function of time for multiple switching probabilities. At low switching probabilities, the domains grow following a power law until the system completely phase separates. As the probability of a particle being switched increases, domain growth is inhibited, restricting the maximum domain size. The solid and dashed line have slopes of 1/3 and 1/5 respectively. Error bars have roughly the size of the symbols. Marker styles and colors match the phases described in Figure 4.3

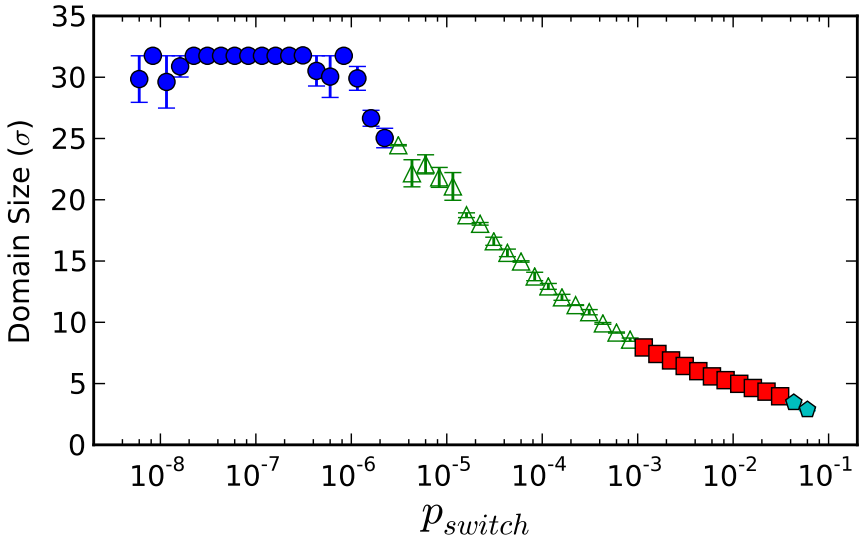

Figure 4.6: Steady state domain size as a function of switching probability (p_{switch}). The steady state domain size can be tuned by controlling the probability of switching particles. Marker styles and colors match the phases described in Figure 4.3

decreases correspondingly. The figure shows a clear dependence of domain size on switching rate, demonstrating that not only the microstructure, but also the length scales, domains and layer thickness are controllable by an external parameter. Because these steady state domain sizes do not depend on initial conditions and p_{switch} is controlled externally by introducing energy into the system, one could envision designing materials using mechanisms similar to the ones described in this paper that act more like responsive devices that adjust their properties in response to external stimuli than inert materials that remain in a single configuration through their useful life.

4.3.4 Dynamics that stabilize layered structures

To better understand how steady state layered structures stabilize, we have identified four different dynamical processes, by visual inspection using the visual molecular

dynamics (VMD) package [113], that guide the evolution of the system (Figure 4.7): (a) new layer nucleation, (b) aggregate coagulation, (c) particle re-solution, and (d) aggregate coarsening, which will be explained below.

As aggregates or layers grow, particles inside them switch from type A to B or vice versa. This switching leaves the particle in a thermodynamically unfavorable local environment, surrounded by particles of the opposite type. To minimize its energy, the particle diffuses through the aggregate until it finds a layer of particles of like type or gets ejected into the solvent. Figure 4.8 shows the time it takes for a particle to exit an aggregate of the opposite type to reach a more energetically favorable configuration after being switched (simulation and analysis details are provided in Section 4.2.5). This time increases linearly with the mass of the aggregate (number of particles) and cubically with increasing aggregate radius. When this time becomes large enough for a second particle within a domain to switch and for these two particles to aggregate (Figure 4.7(a)), the particles stick together, lowering their diffusion rate through the layer, and increasing the probability that additional switched particles within the same domain will encounter them, effectively giving rise to ("nucleating") a new layer inside of the domain they were originally in. From these relationships, the probability of nucleating a new layer p_{NL} is given by:

$$p_{NL} \propto N_{Ag} \propto R_{Ag}^3$$

$$p_{NL} \propto p_{switch}$$

where N_{Ag} is the number of particles in an aggregate and R_{Ag} is the aggregate radius. This new inner layer becomes increasingly spherical in order to minimize its interface with the outer layer.

As these multi-layered aggregates diffuse in the solvent, they come in contact with other aggregates. When two aggregates with the opposite type of outer layer come

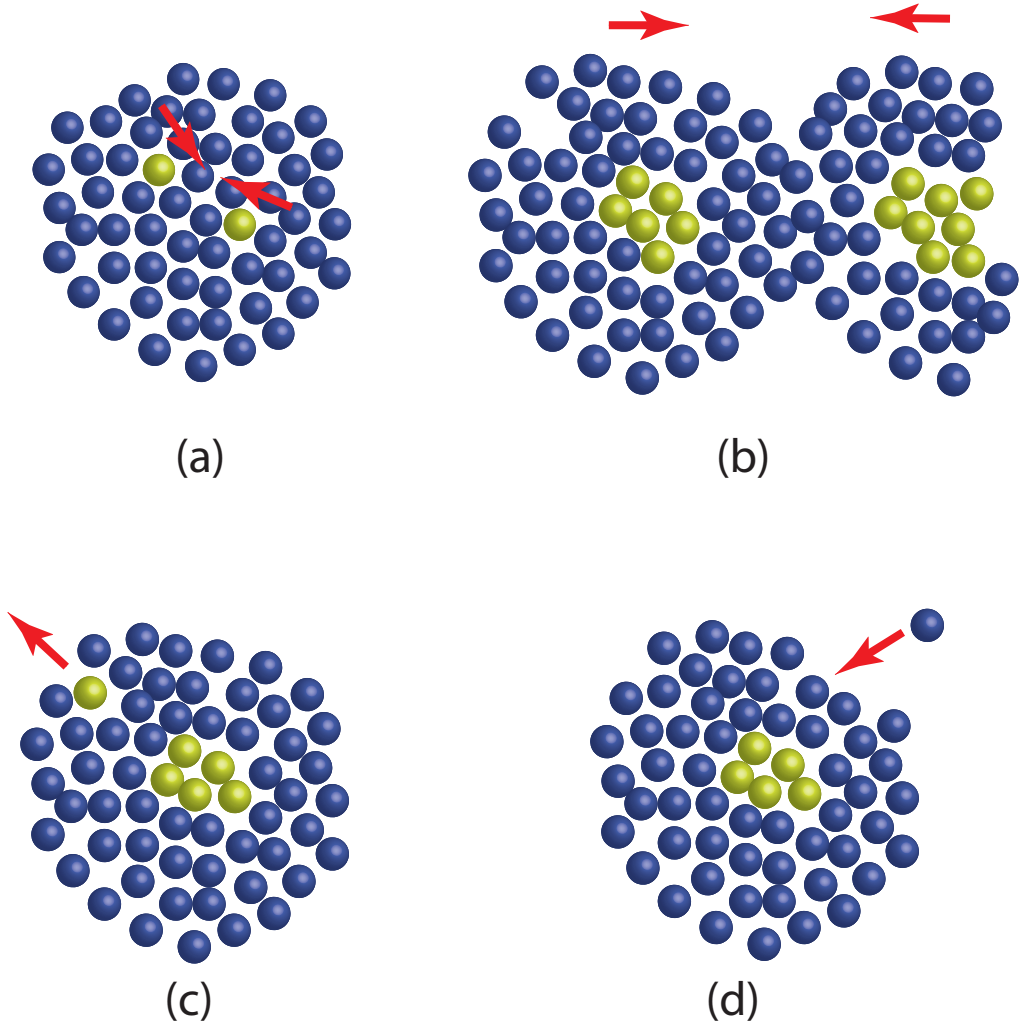

Figure 4.7: Aggregate evolution dynamics: (a) "Nucleation", where multiple particles that switched inside an aggregate merge, slowing down their diffusion and "nucleating" a new layer inside the aggregate; (b) coagulation, where two aggregates with the same outer layer come into contact; (c) re-solution, where particles switched while inside an aggregate diffuse to the closest layer of the same type as the new type of the switched particle or to the boundary of the aggregate to later be ejected; and (d) coarsening, where particles that are not part of any aggregate absorb into the outer layer of the same type.

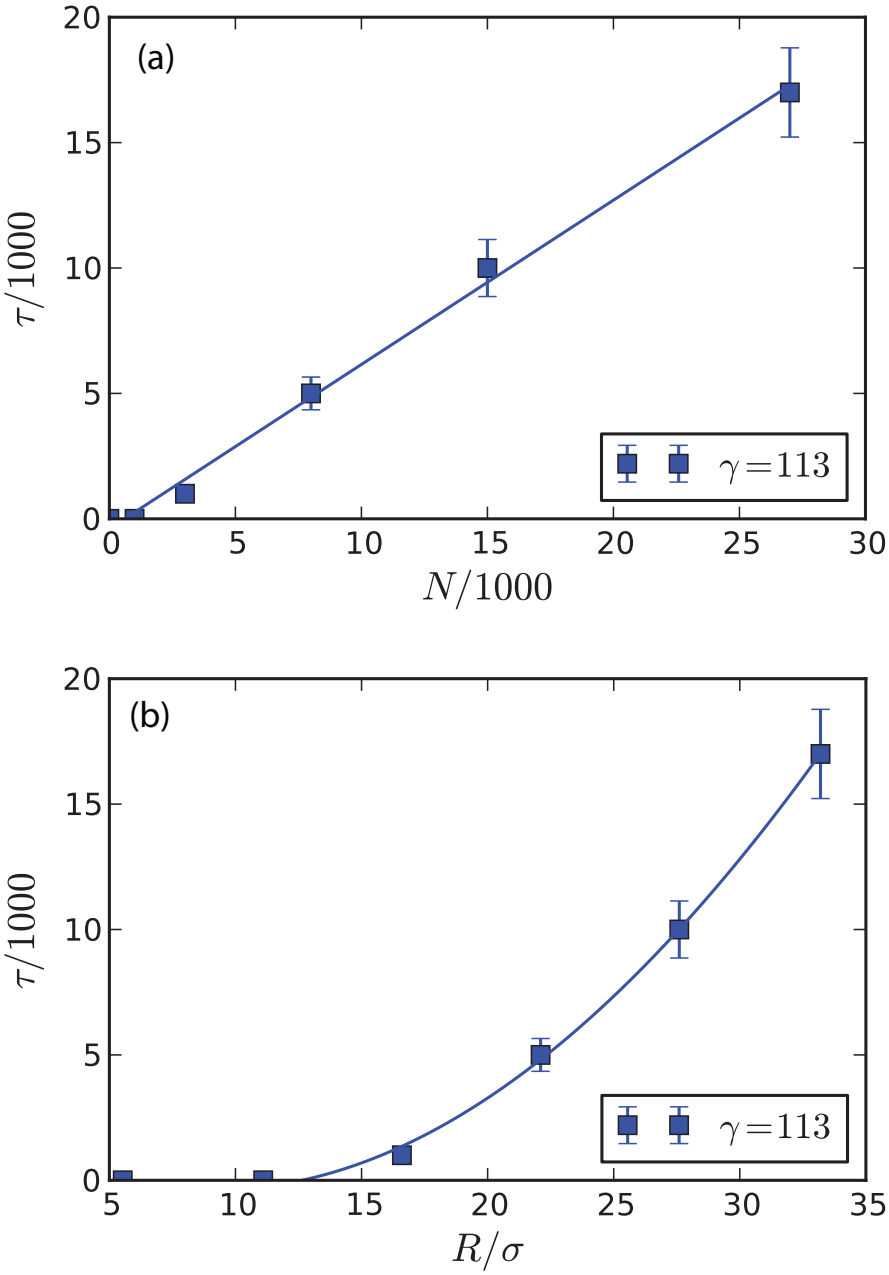

Figure 4.8: Average time required for a switched particle to exit an aggregate of the opposite type as a function of (a) number of particles in the aggregate, and (b) aggregate radius. The solid lines represent (a) linear, and (b) cubic fits.

close they repel each other, but, when aggregates with the same type of outer layer come in contact (Figure 4.7(b)), particles transfer from one aggregate to the other in an attempt to minimize their energy, leaving behind two aggregates with outer layers of opposite types. This dynamic process maintains the diversity of the outer layer type observed in Figure 4.2(b).

Switched particles also diffuse between layers to minimize their energy, and when they are in the outer layer, they can be ejected into the solvent (Figure 4.7(c)) to later be absorbed into another aggregate. Particles that are not part of any aggregate or that have been re-soluted into the solvent diffuse around the system until finding an aggregate with an outer layer of the same type, coarsening the aggregate, as shown in Figure 4.7(d).

The interplay of these mechanisms limits the size of the resulting aggregates and layers, and stabilizes the morphology of the layered structures.

4.3.5 Energy input and dissipation

The dynamic self-assembly of energy-dissipating structures requires a constant supply of energy, and therefore requires a thermostat to remove the energy being continuously added into the system to maintain a constant temperature. As illustrated in Section 4.3.2, having a physical intuition about how the thermostat dissipates the energy introduced into the system and how the thermostat coupling affects the system dynamics is of crucial importance when simulating far-from-equilibrium systems. The Langevin thermostat, in addition to providing a dissipation mechanism that we can physically relate to our system, also provides a mechanism for calculating the amount of energy that the thermostat exchanges with the system, described in Section 4.2.5. This measure can be used to set bounds and checks on our simulation results, and to determine under what conditions these simulations represent realizable experimental systems.

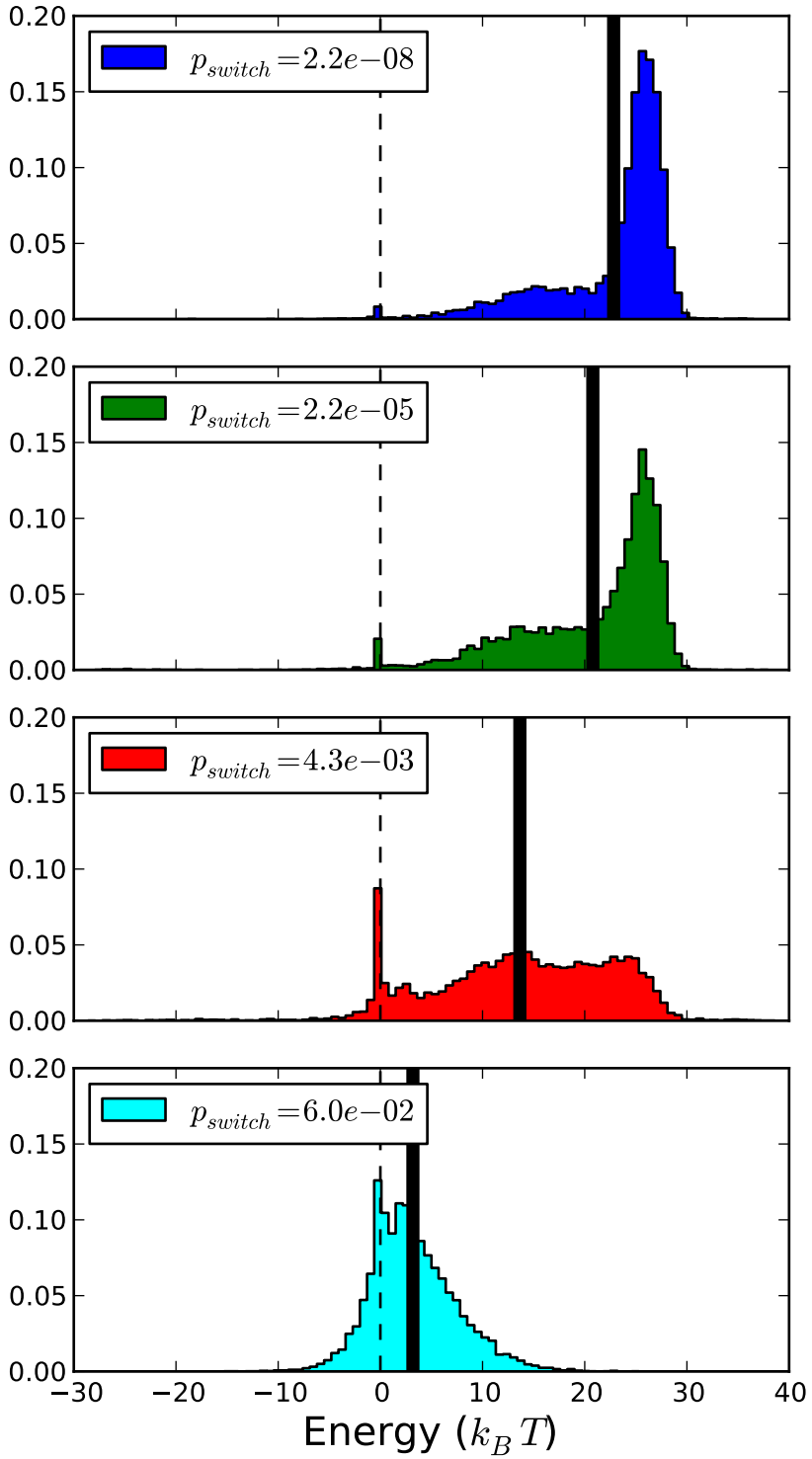

Figure 4.9: Distribution of the amount of energy introduced every time a particle type is switched for several choices of p_{switch}. The solid vertical bar represent the number average.

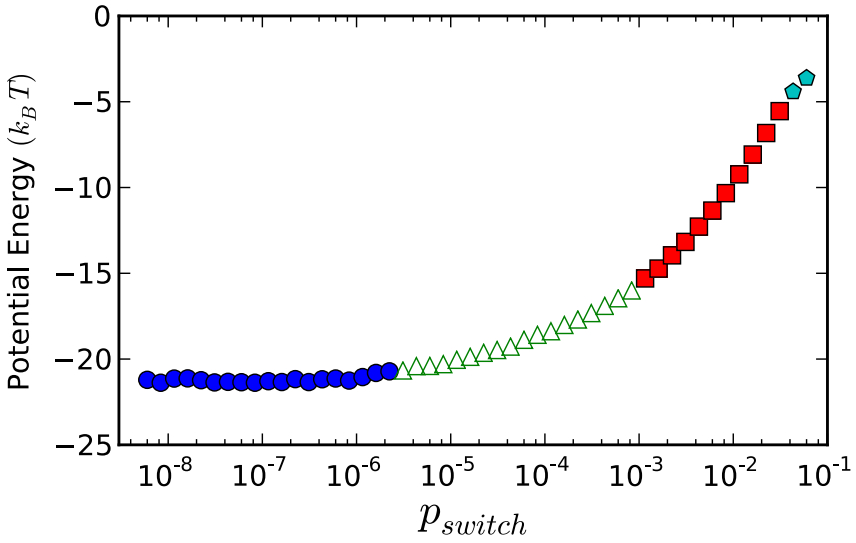

Figure 4.10: Steady-state potential energy. Marker styles and colors match the phases described in Figure 4.3. Error bars have roughly the size of the symbols.

Figure 4.9 shows the distribution of the amount of energy introduced at every particle switch for values of p_{switch} that correspond to each of the four steady state phases. We can see that for all phases, particle switches tend to introduce energy into the system, usually switching a particle from an energetically favorable configuration to a higher energy configuration. This result agrees with Figure 4.10, which shows that the average steady state potential energy for the system negative. As p_{switch} increases the potential energy of each particle increases, reducing the energy introduced per particle switch.

Figure 4.11 shows the energy required to maintain the structures previously described as a function of p_{switch}. We can see that for systems where the perturbation due to particle switching is not large enough to drive the system away from its equilibrium configurations (blue, filled circles) the energy required to maintain the structures is orders of magnitude less than elsewhere. The energy dissipation rate at these values of p_{switch} is due, mainly, to round off error due to machine precision and due to error introduced by the velocity Verlet integrator. As p_{switch} increases, steady state

structures different from the equilibrium structure of phase separation are dynamically stabilized: (green, triangles) layered structures, (red, squares) SD intermediate structures, and (cyan, pentagons) homogeneous mixture); and energy introduced by particle switches has to constantly be removed by the thermostat. Since particle switches usually introduce energy into the system when domains are of any significant size, the energy dissipation rate increases monotonically with increasing p_{switch} until it reaches a maximum. The maximum energy dissipation is reached when the system is not able to phase separate at all and the system remains a homogeneous mixture, so the energy before and after a switch is roughly the same on average.

At low values of p_{switch} every particle switch introduces a large amount of energy into the system, but switches seldom occur so the energy introduced on average is low. As p_{switch} increases the energy introduced per switch decreases, but the number of switching events increases greatly, which leads to the straight segment in Figure 4.11. As p_{switch} increases further, each switch introduces diminishing amounts of energy, reaching a maximum dissipation rate when the system is homogeneously mixed. These three ranges give rise to the S-shaped curve for the energy dissipation rate.

It is worth noting that through most of the range of p_{switch} values studied, the thermostat is able to maintain the temperature of the system at the desired temperature. But for low γ values, it is possible for the thermostat to not be able to remove enough energy to maintain the desired temperature and the system heats up to a constant, steady state temperature that is higher than the desired temperature. Figure 4.12 shows the temperature as a function of p_{switch} when $\gamma = 1$. For large values of p_{switch}, the temperature of the system has increased by about 7% due to the thermostat's inability to remove enough energy from the system. This effect is not present in higher values of γ for the range of p_{switch} under this study but it is expected to affect higher values of γ as the amount of energy introduced into the system is increased.

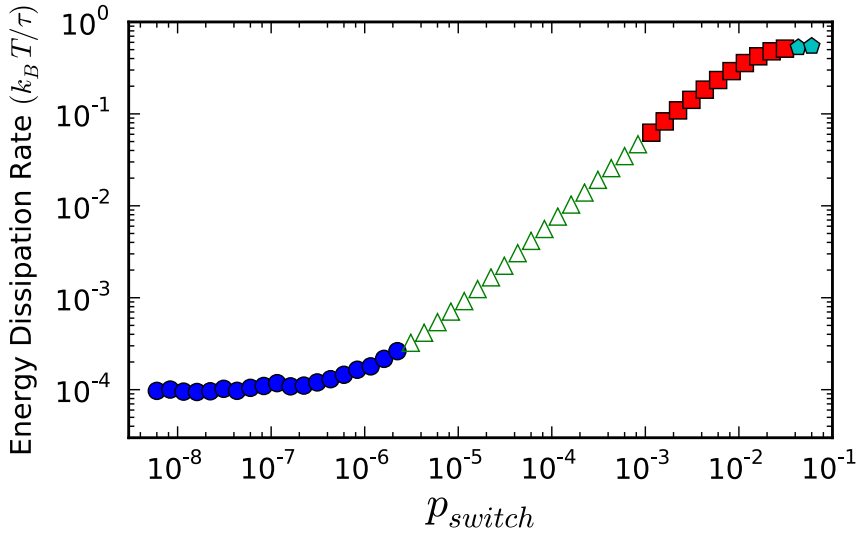

Figure 4.11: Langevin thermostat energy dissipation rate as a function of switching probability (p_{switch}). Marker styles and colors match the phases described in Figure 4.3. Error bars have roughly the size of the symbols.

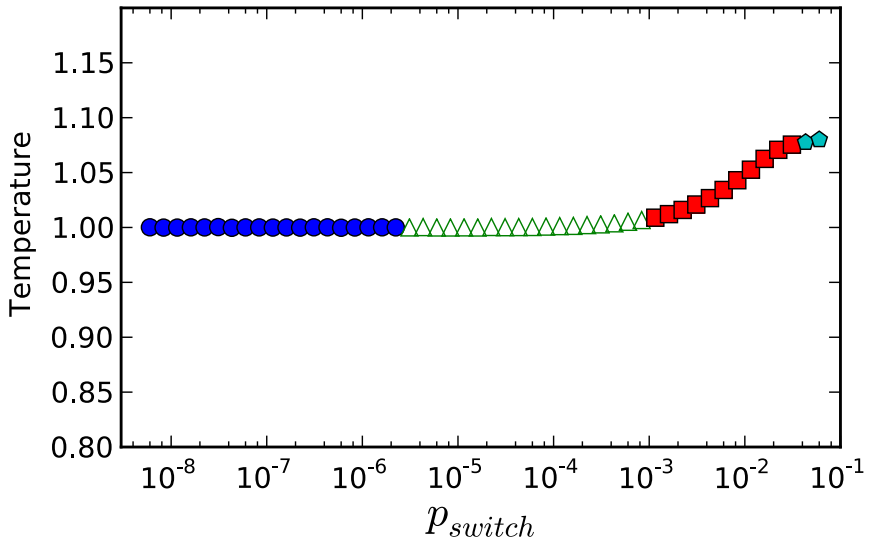

Figure 4.12: Measured steady state temperature as a function of switching probability (p_{switch}). Marker styles and colors match the phases described in Figure 4.3. Error bars have roughly the size of the symbols.

4.4 Conclusions

By combining thermodynamic phase separation and time dependent interactions, we have engineered a colloidal system with switchable, competing interactions that can dynamically not only stabilize a structure that was previously only available transiently in this system – namely, spinodal decomposition intermediate structures – but also self-assemble into novel steady state ordered layered structures whose length scales can be tuned by adjusting an external, non-thermodynamic, stimuli.

By introducing a non-equilibrium, dissipative mechanism into the colloidal building block we have created a material that could, in principle, dynamically change its mechanical, optical, electrical, etc. properties, as a response of an external control, thereby behaving more like a device than an equilibrium material.

We have also described a procedure that can be used in computer experiments to quantify the amount of energy that a system dissipates in steady state, and which is independent of the energy input mechanism.

The domain size stabilization is consistent with previously reported results from studies concerning 2D binary fluid mixtures where reaction rates were able to capture specific domain sizes. Spinodal decomposition intermediate structures and circular structures were predicted in 2D incompressible liquids. Based on those results, we extended the system to three dimensions and lower densities corresponding to nanocolloidal self-assembly.

CHAPTER V

Assembly Speed Enhancement and Transient Structures

Nanoscale and colloidal particles are important in many areas of science and technology from biological and pharmaceutical industries to paints and body armor. The controlled assembly of these particles into extended structures, via the synthesis of building blocks designed with specific shape and inter-particle interactions, enables the fabrication of materials with unique structures and properties [20, 114, 115]. Photo-switchable nanoparticles, [116] e.g., introduce the possibility to control the structure of the material in time with light and electric fields. Novel devices such as liquid crystal displays [117] and e-ink displays [118] use materials whose structure is controlled by an external field, and their performance is in part determined by the materials ability to switch between two or more equilibrium structures reliably and speedily. Here, we drive a system of nanocolloids to self-assemble into a non-equilibrium structure by switching inter-particle potentials and show that the process can enhance the assembly speed of the equilibrium thermodynamic structure by an order of magnitude, as well as produce non-equilibrium states comprised of multiple coexisting phases not available via static self-assembly.[1]

[1]This chapter is adapted from Reference [119] A. F. Osorio Vivanco, M. Olvera de la Cruz, S. C. Glotzer. "Optimized Assembly Speed in Dynamic Systems of Photo-Switchable Colloids", *in preparation.*

5.1 Introduction

A large body of work has been dedicated to understanding the properties of equilibrium colloidal suspensions and to exploring the different equilibrium structures that result from modifying the assembling building block [20, 28, 114, 120–123]. Yet, active, non-equilibrium, colloidal research is still in its early exploratory phase [124]. Recent work focused on increasing self-assembly speed uses microwave annealing for diblock copolymers [125], and magnetic interactions [126], flows [127], and evaporation [128] for aggregating colloids. As an alternative to modifying the colloidal environment (e.g. modify the environment the colloid is exposed to, temperature, pressure, magnetic field, etc.), to enhance the assembly speed, recent developments in surface [36, 37, 101] and colloidal synthesis [37, 116] enable the modification of the colloidal particle itself. This approach, as explored e.g., in Jha et al. [38], could yield faster assembly processes, novel structures, and dynamic control of steady state structures.

5.2 Model and methods

5.2.1 Model

Here, we study a system of strongly attractive colloidal nanoparticles. Under the usual conditions particles diffuse until they encounter other particles and irreversibly aggregate. Aggregates coarsen by merging with other aggregates. This slow process is called Diffusion Limited Cluster Aggregation (DLCA) [129–131] and has been thoroughly studied over the past decades. Instead of employing the usual conditions, however, we repeatedly disrupt this process by turning off and on the attractive interaction between all particles simultaneously. As shown in Figure 5.1, we cycle the system through two stages: an aggregation stage, where the interactions between particles are switched on and particles aggregate, and a disaggregation stage, where

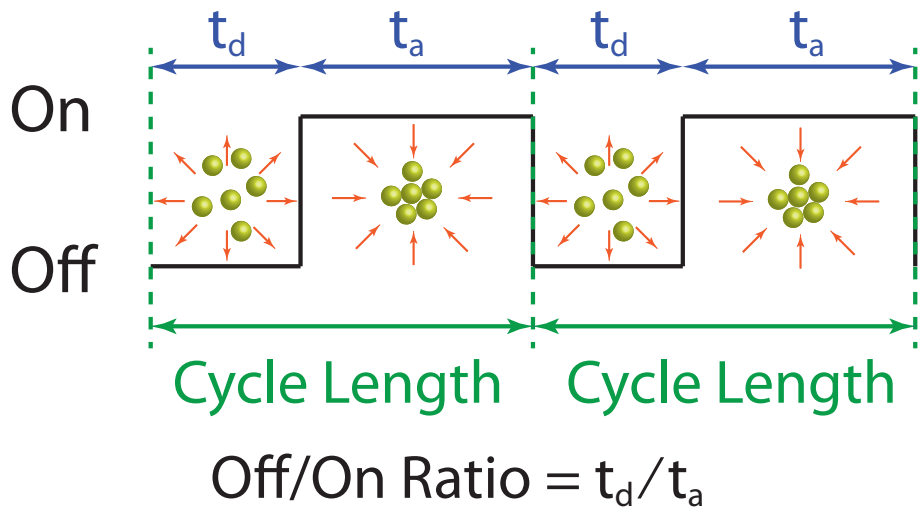

Figure 5.1: Interaction Switching Details. Particles are switched repeatedly between two states. In the on state, particles are attracted to each other and aggregate. In the off state, attractive interactions are turned off and particles interact solely through excluded volume.

the inter-particle interactions are switched off and particles diffuse away from each other in search of a more entropically favorable configuration. The length of these stages are defined as t_a and t_d respectively, and the system is subjected to repeated cycles.

Interactions between particles during the on phase are modeled via an isotropic Lennard-Jones (LJ) 12-6 pair potential of the form shown in Equation (3.7) with particle diameter $\sigma = 1$, and interaction strength $\epsilon = 2.5$, where r is the center-to-center distance between two particles. Interactions between particles during the off phase are modeled using the Weeks-Chandler-Andersen (WCA) pair potential described in Section 3.1.3.

To simulate all particles in a system switching on and off simultaneously, two inter-particles potentials were defined for particle pair A-A. A LJ potential for the on phase, and a WCA potential for the off phase. Only one of the two inter-particle potentials is enable at any given time.

5.2.2 Simulation method

We use Langevin Dynamics (LD), a stochastic molecular dynamics method with a Langevin thermostat, to simulate the time evolution of an isothermal system in a three-dimensional box with periodic boundary conditions. Section 3.1.1 describes the details of the LD method.

The Langevin drag coefficient $\gamma = 113$ is carefully chosen so that the resulting drag force F_i^D is equivalent to the drag force experienced by a particle of a determined size in a solvent with a specific viscosity.

We perform simulations of $N = 64,000$ particles at number density $\rho = 0.125\sigma^{-3}$ and $\rho = 0.296\sigma^{-3}$, in a cubic box of edge length $L = 80\sigma$ with periodic boundary conditions. The temperature of the system is maintained by the Langevin thermostat at $T = 0.4\epsilon \,/\, k_B$. The time step of the velocity Verlet algorithm used to integrate Newton's equation of motion is $\Delta t = 0.006\tau$, where $\tau = \left(m\sigma^2 \,/\, \epsilon\right)^{1/2}$ is the unit of time.

The particles are thermalized by turning off the interactions, enabling the WCA potential and disabling the LJ potential, to randomize their starting positions.

For our simulations, we used locally authored code and the GPU-based HOOMD-Blue code package under development in our group, (`http://codeblue.umich.edu/hoomd-blue/index.html`) [110]. The simulations were run on our GPU cluster at the University of Michigan on NVIDIA Tesla S2050s. Roughly 1000 independent simulations were investigated over 98,000 GPU hours.

5.2.3 q_6 order parameter

Section 3.2.2 describes in detail the algorithm used to calculate bond order parameters. In this chapter, we use the maximum of the probability distribution of the q_6 order parameter to identify the internal structure of the aggregate and the intensity of the same to quantify the degree of order in the aggregate.

5.2.4 Aggregate size distribution

Section 3.2.3 details the algorithm used to cluster particles into aggregates and how the aggregate size and size distribution are calculated. In this chapter, the weight average aggregate size M_W is used to characterize the system.

5.3 Results and discussion

5.3.1 Aggregation speed enhancement

Figure 5.2 a,b show the snapshots of two aggregating systems at a similar time after aggregation has started following a quench from high to low temperature. In the reference systems Figure 5.2(a), the inter-particle interactions are always on. In the active system Figure 5.2(b), the interactions are cycled on and off as described above. It is evident from the images that the aggregates in the active system are much larger than those in the reference system when the systems are compared at equal times.

The weighted aggregate size (M_W) normalized by the aggregate size in the reference system (M_{W0}) is plotted in Figure 5.3 for several off/on ratios and after several number of cycles. The figure shows that for certain off/on ratios aggregates grow up to four times larger than when the interactions are always on, after the same amount of time. We also observe that the average aggregate size in the active system compared to that in the inactive system increases with increasing number of cycles.

For $t_d/t_a \leq 0.17$, we instead inhibit growth and the relative mean aggregate size decreases significantly. For $t_d/t_a \leq 0.20$, aggregates fully disassemble and reassemble during each cycle, resulting in a system that simply oscillates between fully disaggregated and fully aggregated.

Figure 5.4 shows the time evolution of the aggregate size in the different active systems and in the inactive reference system. Here, it is evident as well that when

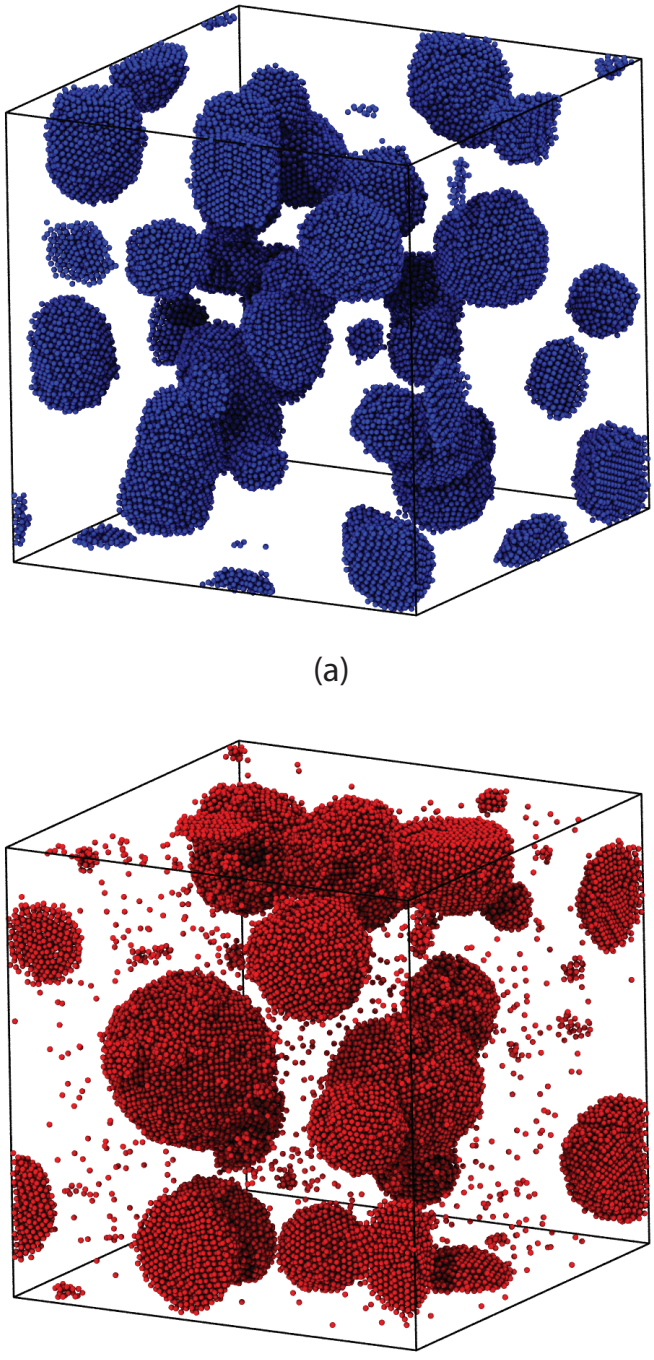

Figure 5.2: Comparison between reference and active systems. Images of the aggregates at a given time t for (a) a reference, inactive system, and (b) an active system. From the images, it is evident that the active system has larger aggregates than the reference system.

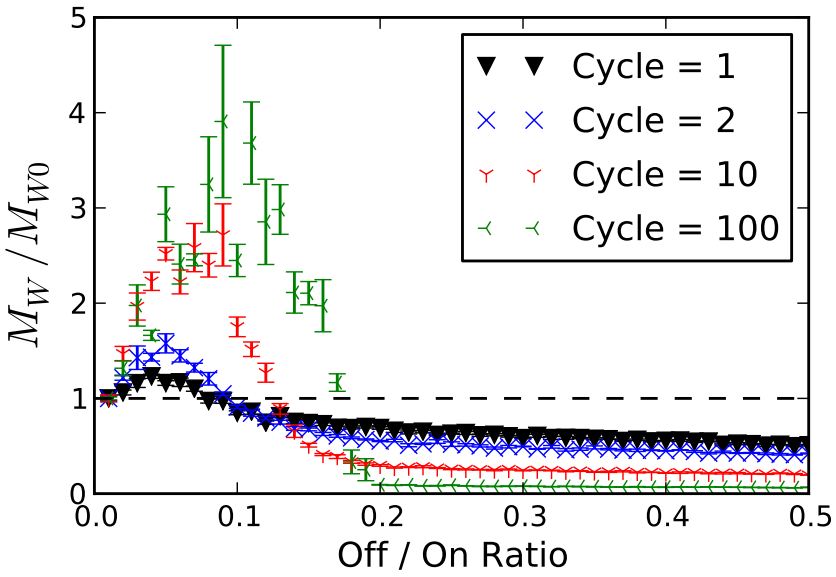

Figure 5.3: Assembly speed enhancement. Aggregate size at the end of the aggregation stage at multiple cycles vs. off/on ratio. This plot shows that for off/on ratios smaller than 0.15 the weight average aggregate size is larger than for an inactive system.

interactions are switched on/off periodically (e.g. off/on ratios 0.03 and 0.05) the aggregates grow faster than when interactions are left always on. It is interesting that for off/on ratio 0.11, the initial aggregation speed is slower than for always on, but aggregates are still growing, the disaggregation time is not long enough for the system to completely lose memory of the On stage configuration. But at some aggregate value $\sim$ 600 particles, the growth rate considerably changes, suggesting that the length of the disaggregation time affects aggregates of different sizes differently, and while aggregate growth below a critical nucleus size is hindered, above a nucleus size is enhanced. This result also suggests the possibility of an aggregate size dependent optimal off/on ratio or t_d duration, which would be an interesting tuning parameter to control the aggregation process and which warrants further study. It is notable that the systems with off/on ratio = 0.05 reached the same aggregate size as the final size for the inactive reference system about an order of magnitude earlier in time.

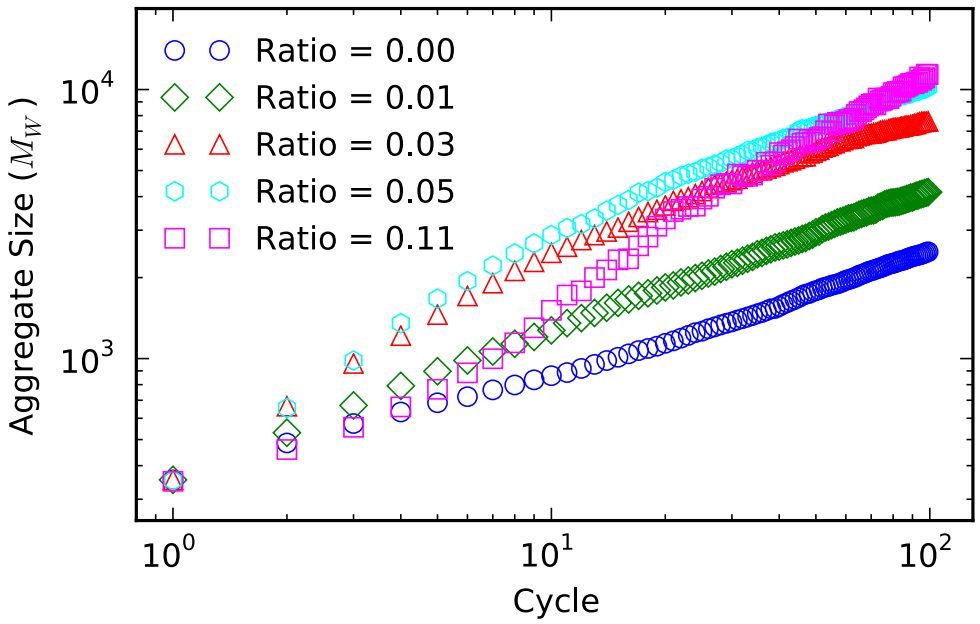

Figure 5.4: Aggregate size evolution. Aggregate size at the end of the aggregation stage at multiple cycles vs. off/on ratio. This log-log plot shows the aggregate sizes at the end of the aggregation stage to show how the aggregates are growing as a function of time for multiple off/on ratios.

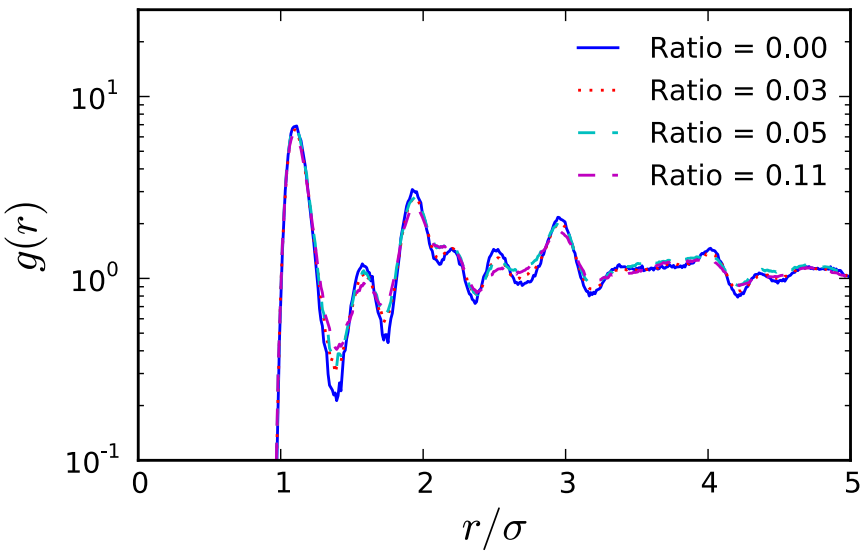

Figure 5.5: Radial distribution function characterizing the internal structure of the aggregates of the same size for multiple off/on ratios. Peaks correspond to FCC ordering.

5.3.2 Aggregate characterization

To verify that the non-equilibrium dynamics are not changing the final structures to be assembled, we characterize the individual aggregates using the radial distribution function (RDF) and the q_6 order parameter [98], as well as characterizing the system as a whole by looking at the distribution of aggregate sizes.

The RDF and q_6 order parameter are shown in Figure 5.5 and Figure 5.6 respectively. The RDF shows that the key features are independent of off/on ratio, suggesting that the internal structure of the aggregates for all cases is similar. The peaks in the RDF correspond to an FCC crystal structure [132]. At significantly large off/on ratios, the peaks soften, suggesting that the switching activity introduces disorder to the system, a logical consequence of extended disaggregation. The q_6 order parameter probability distribution supports these results with the main peak corresponding to FCC at $q_6 = 0.57$ [133] and the lower peaks for increasing switching activity suggesting increased disorder. If the switching activity is stopped, the

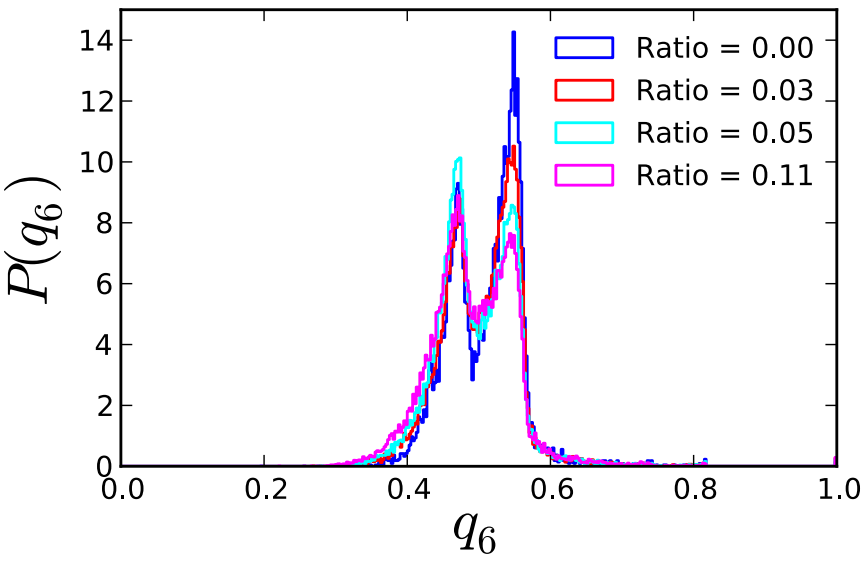

Figure 5.6: Probability distribution of the q_6 order parameter characterizing the internal structure of the aggregates of the same size for multiple off/on ratios. Peak at 0.57 corresponds to FCC ordering.

RDF and q_6 order parameter probability distribution evolve to resemble the inactive reference case.

5.3.3 Aggregate size distribution

Figure 5.7 shows the distribution of aggregate sizes for multiple ratios when the average aggregate size $M_W = 2500$ particles and the corresponding simulation snapshots. While the average size is equal for all these distributions we can see that the shape of the distribution changes for different off/on ratios. In the inactive reference case, we can see a Gaussian distribution of aggregate sizes as would be expected. Since particles effectively permanently join aggregates, the snapshot shows very few single particles or small aggregates. As we raise the off/on ratio to 0.03, we can see that the distribution broadens and in the corresponding snapshot a small number of single particles and small aggregates appear. Further increasing the off/on ratio further drives the system into a bimodal distribution where large aggregates coex-

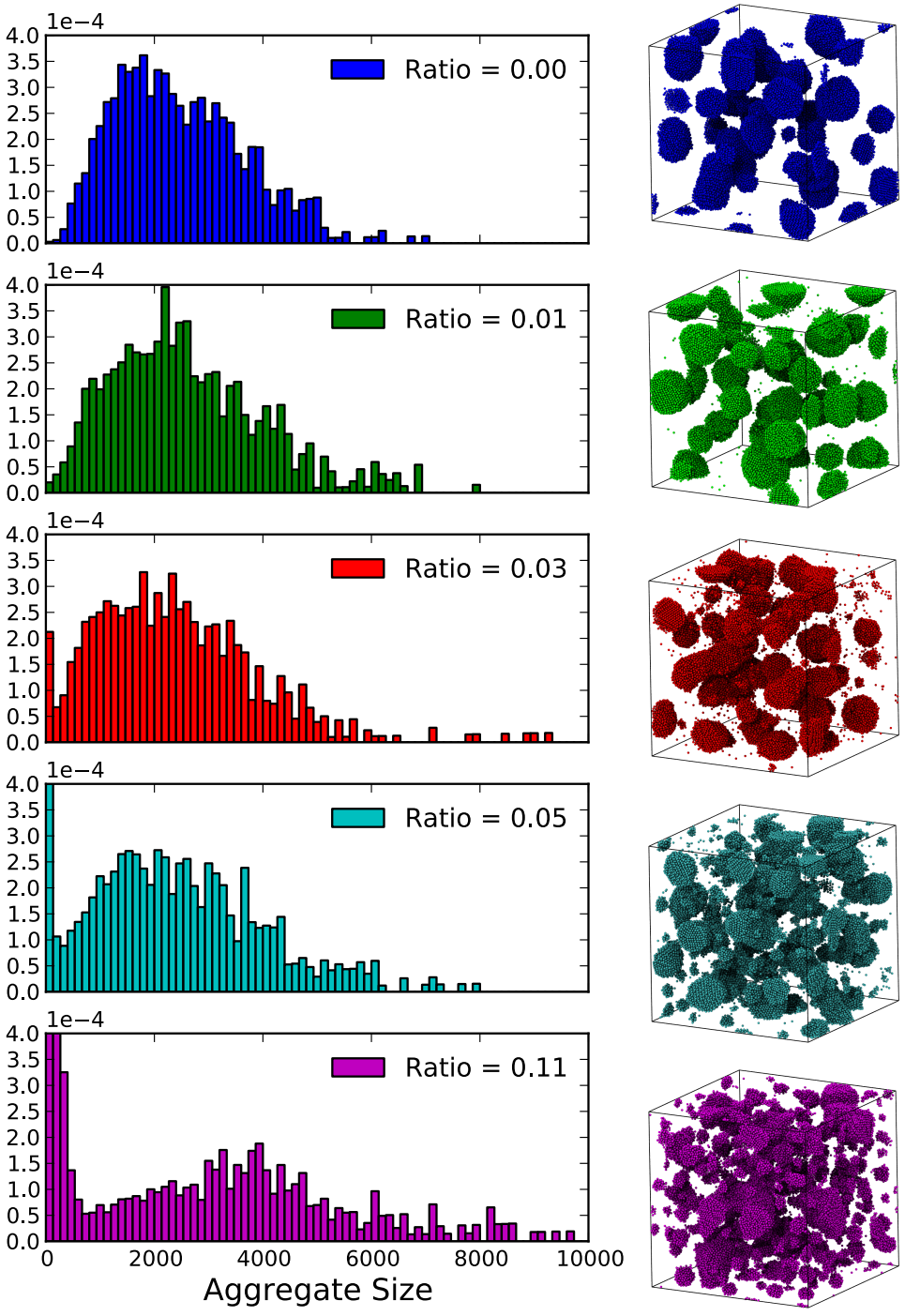

Figure 5.7: Histogram showing the distributions of aggregate sizes for multiple on/off ratios at Mw = 2500 and corresponding simulation snapshots.

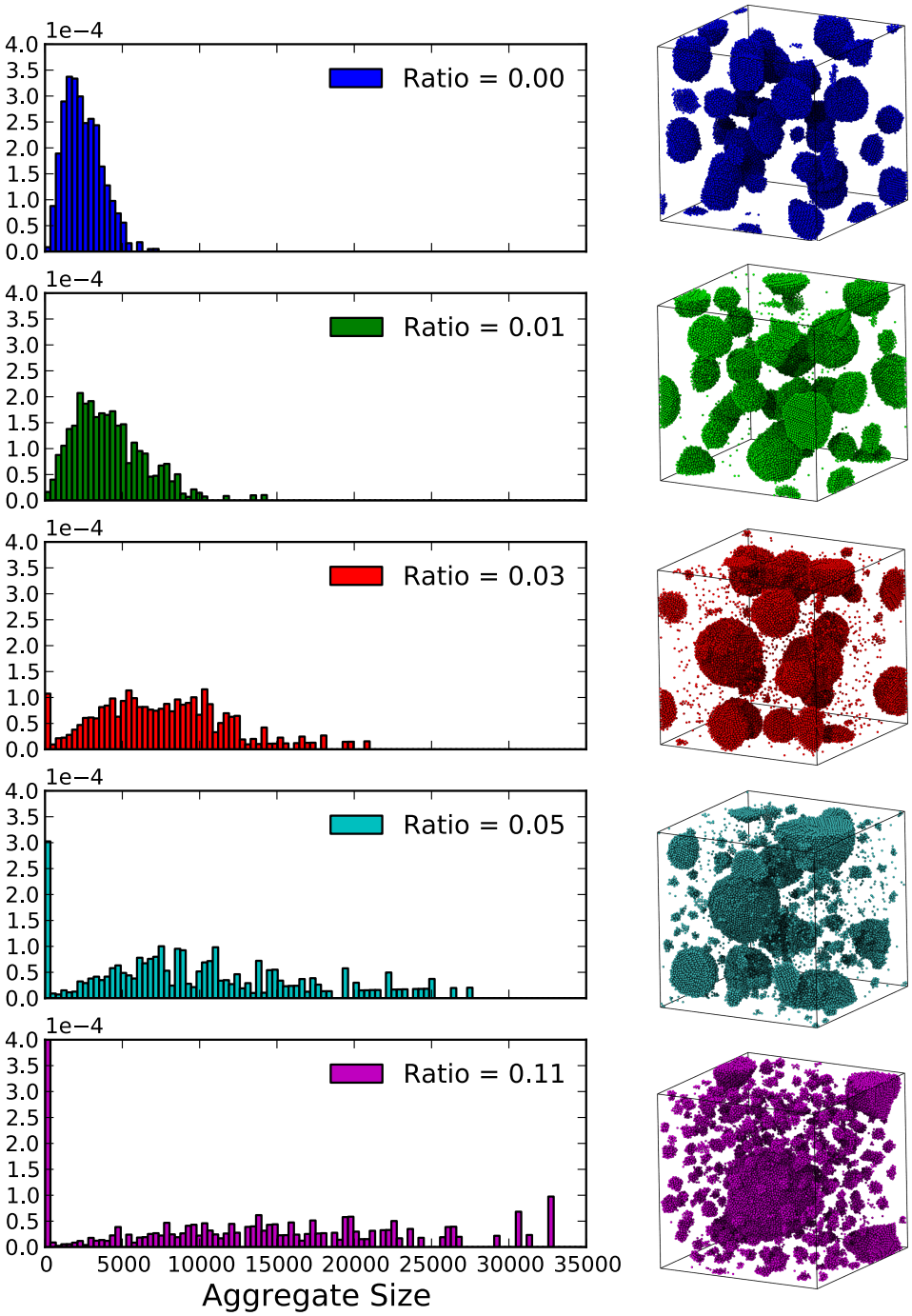

Figure 5.8: Histogram showing the distributions of aggregate sizes for multiple on/off ratios at Cycle = 100, and corresponding simulation snapshots.

ist with small aggregates. This distribution is only present as long as the switching continues, as soon as the switching stops the peak representing the small aggregates starts to decrease. Figure 5.8 show the aggregate size distribution and simulation snapshots for several off/on ratios after 100 cycles. The distributions show that for a given amount of time, or number of cycles, the aggregates grow much larger when the system is active, driven. As the system is driven further away from equilibrium, small aggregates coexist with larger aggregates.

5.3.4 Transient structures in dense systems

We introduced switching interactions into a denser system that generally phase separates first into percolating domains that coarsen over time [112](Figure 5.9(a)) instead of clustering into aggregates. For low off/on ratios (= 0.02), the phase separation process was sped up; and, given a similar amount of time, larger domain that are no longer percolating (Figure 5.9(b)) are observed. These domains are expected to be spherical aggregates, but at these high densities the periodic boundary conditions stabilize the cylindrical structures. As we increase the disaggregation time (off/on ratio = 0.13), we observe a new phase emerge where porous percolating domains coexist with small aggregates (Figure 5.9(c)). This is comparable to the regime in the less dense system where small aggregates coexist with large aggregates. If the disaggregation time is increased to the point where the system loses all memory of the configuration at the end of the previous aggregation stage, the system oscillates between a well-dispersed system and small percolating domains (Figure 5.9(d)) resembling early stage spinodal decomposition.

The coexistence of small aggregates with larger aggregates in the low density system as well as the coexistence of small aggregates with percolating domains in the high density system hint at the possibility that by adjusting the different switching parameters specific aggregate sizes could be stabilized. While we were unable to

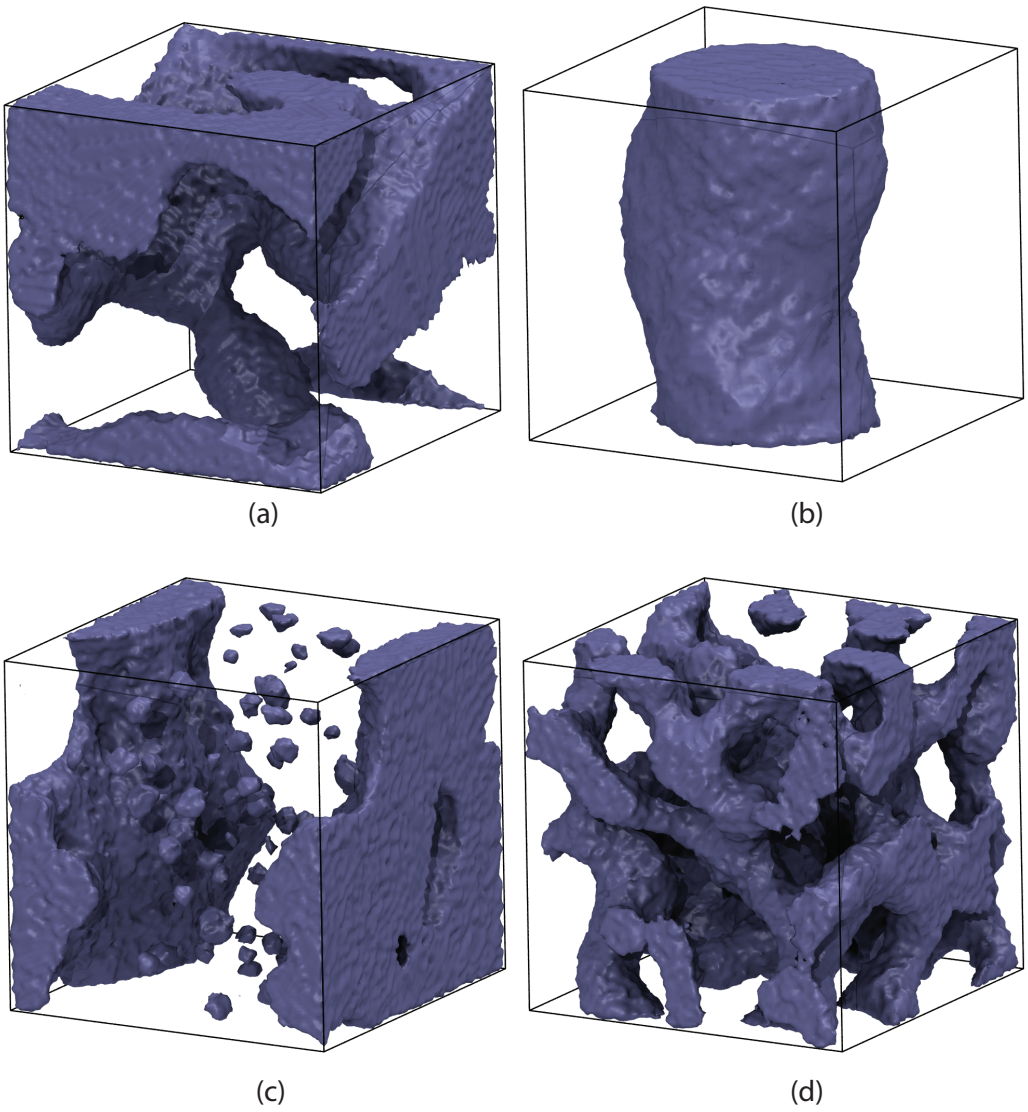

Figure 5.9: Light switching in dense systems. Snapshot of the final configuration of a dense system with multiple off/on ratios at the end of 100 cycles. (a) Ratio = 0.00, Interactions are always-on, the system phase separates through spinodal decomposition resulting in percolating domains that coarsen following a power law. (b) Ratio = 0.02, Short disaggregation times increase the phase separation speed resulting in a single aggregate without the percolating domains. (c) Ratio = 0.13, Larger disaggregation times produce a coexistence of percolating porous domain with small aggregates. (d) Ratio = 0.25, Much larger disaggregation times cause the system to lose all memory of the aggregation phase, and result in percolated networks with smaller domains than in a that only depend on a single aggregation phase.

produce any structures with stable, steady-state aggregate size, we believe that it is possible to create materials where light can be used to dynamically control the aggregate sizes, and hence the properties of the material.

5.4 Conclusions

By introducing a non-equilibrium dynamic, switching inter-particle interactions or and off we have enhance the assembly speed of aggregating colloids where the resulting structures at the end the aggregation times are structurally similar to those obtained from equilibrium, produced structures with coexistence of phases that were not previously available, and hinted at the possibility of dynamically stabilizing steady state length scales in the available structures. In the future, by judiciously adding these type of switchable interactions to specific areas of the colloidal building block, we could envision developing materials that can quickly and efficiently switch between multiple stable structures, changing the materials optical, mechanical, etc. properties as response to different external controls.

CHAPTER VI

Conclusions

6.1 Summary

Self-assembly is one of the most promising routes for manufacturing materials and devices with nanoscale features. While static self-assembly, where structures do not require energy to maintain order, has been the focus of a large body of research over the past decade, dynamic self-assembly is still in its infancy. The intention of this dissertation was to advance the field of dynamic self-assembly by introducing two computational systems where dynamic self-assembly can be observed, and using these systems to produce supporting evidence for some of the benefits that dynamic self-assembly can bring over static self-assembly, and to motivate the further development of these kind of systems. Using computer simulations, we developed two far-from-equilibrium – driven – systems by modifying well understood systems, i.e. phase separation and colloidal aggregation, and showed that we can stabilize steady state structures not available in equilibrium, stabilize patterns and structures that were only available as transients during the system's evolution to equilibrium, generate transient structures with coexisting phases, and enhance or inhibit the speed at which a system assembles by introducing non-equilibrium dynamics.

In Chapter IV, using concepts from reactive binary mixtures, we extended a phase separating colloidal solution by letting colloids reversibly and randomly switch be-

tween two species. By combining phase separation and time dependent interactions, we stabilized steady state ordered layered spherical structures whose length scales can be tuned by adjusting an external, non-thermodynamic control. We were also able to, with judicious choice of parameters, stabilize steady state patterns that resemble early spinodal decomposition, which were previously only available as transient structures during the process of phase separation. By careful selection of the thermostating mechanism, we have also presented a procedure that can be used in computer experiments to quantify the amount of energy that a system dissipates in steady state. This measurement is independent of the energy input mechanism. In the future, this system could lead to materials whose internal structure and length scale, therefore mechanical, optical, electrical, etc. properties, can be tuned by an external non-thermodynamic control parameter, resulting in materials that behave more like devices than passive equilibrium materials.

In Chapter V, based on recent developments in the synthesis of photo-switchable colloids, we extended an aggregating attractive nanoparticle solution to switch between two states: an "on" state, where particles are attracted to each other and aggregate; and an "off" state, where particles interact via excluded volume. By introducing a non-equilibrium dynamic, we enhanced the assembly speed of aggregating colloids where the resulting structures are structurally similar to those obtained from equilibrium, reducing the assembly time for active systems by an order of magnitude. We were also able to generate transient structures with a bimodal distribution of aggregate sizes for low density systems, and where percolating domains coexisted with small aggregates for high density systems. In the future, by judiciously adding this type of switchable interactions to colloidal building blocks, we could envision developing materials that can quickly and efficiently switch between multiple stable structures, enabling a new generation of devices.

Both of the systems studied in Chapter IV and V provide a basic framework

and test-bed to further study dynamic self-assembly and to test theories regarding non-equilibrium systems.

6.2 Outlook

As discussed in Chapter IV, the choice of thermostat and thermostat coupling parameters is crucial for arriving at the correct steady state structure. Additional theoretical, computational, and experimental research is needed to understand how to dissipate heat from driven system in order not to affect – damage – the dynamics of the simulated system. Many research works regarding far-from-equilibrium systems published in the literature were performed using thermostats that unphysically rescale velocities, instantly dissipating any energy introduced and damaging the system's dynamics. A large amount of work is needed to better understand how to extend current tools to properly model and simulate dynamically self-assembling systems in a computationally efficient manner.

In Chapter V, we studied how turning interactions on and off repeatedly affected the assembly speed. If the length of the "off" phase was small the assembly speed was enhanced. But for a range of off/on ratios a steady state aggregate size was stabilized. It would be interesting to explore the concept of controlling the steady state aggregate size by turning interactions on and off, and to adjust the off/on ratio to dynamically tune the aggregate size. Since the optical properties of the nanoparticle solution depends on the aggregate size, these could be controlled using an external light by adjusting switching parameters.

Recent work with system that assemble via hierarchical pathways have shown that the yield of the resulting structures can be increased by adjusting the relative interaction strengths that come into play at each of the hierarchical steps. We could introduce the concept of turning interactions on and off described in Chapter V to selectively switch interactions that are preventing higher yields. By selectively turning

interactions on and off, we could reshape the energy landscape of the hierachical assembly pathway to increase the crystallization yield.

Finally, with new developments in colloidal and nanoparticle synthesis techniques, we can think of a multitude of ways to create increasingly complex building blocks whose shape is time dependent or those that are decorated with multiple patches with independent specific interactions. These interactions can be used to introduce dynamic mechanisms and behaviors into the system. The parameter space for these building blocks would be immense and would offer a new domain of possibilities for new structures and new functionalities.

APPENDICES

APPENDIX A

Key HOOMD scripts – Immiscible Switchable Colloids Simulation

```
##############################################################################
# Project: 01 - Self-Assembly of Switchable Colloids
# Subproject: 013 - Switching Rate vs. Domain Size
# Hoomd Version: 0.11.2
# Description: Trying to figure out how does the domain size
#    scale as a function of the switching rate
#
##############################################################################
from hoomd_script import *
from hoomd_plugins import random_switch
import random
import os
import numpy

#to be used with the PBS Array feature
```

```
def get_array_id():
    pbs_arrayid = os.getenv('PBS_ARRAYID');
    if pbs_arrayid is None:
        return 0
    else:
        return int(pbs_arrayid) - 1;


# Setting up simulation group conditions

#  ID
id = get_array_id()

# Common simulation parameters
timesteps = 2e8    # [1] Number of time steps to perform
temp = 1.0    # [Eu]
deltaT = 0.006 # [Tu] Time to be advanced every time step
density = 0.125 # [Lu^-3] Number density
a = (1.0/density)**(1.0/3.0) # [Lu] Lattice parameter for
    initial configuration
m = 40 # [1] m^3 Number of particles
switch_period = 100 # [1] Number of time steps between
    switching attempts
bdgamma = 113
random_seed_generator = 12345

# ID dependent value arrays
```

```
switch_rate_array = numpy.logspace(-4,3,50)

# Setting the initial conditions that depend on the id
switch_rate = switch_rate_array[id%50]
switch_prob = switch_rate * deltaT / switch_period

random_seed = random_seed_generator * (int(id/50) + 1)

print ("\nID Dependent Parameters:")
print ("SP = %.2e" % switch_prob)
print ("SR = %.2e" % switch_rate)
print ("RandomSeed = %d" % random_seed)
print ("")

# Logging
#xml_period = int(timesteps/20)
logger_period = int(timesteps/1000)

# Initializing the system
system = init.create_empty(N=m*m*m, box=(m*a,m*a,m*a),
    n_particle_types=2)

# Moving the particles to their starting location
lo = -m*a / 2.0;
for p in system.particles:
    (i,j,k) = (p.tag % m, p.tag/m % m, p.tag/m**2 % m)
    p.position = (lo + i*a+a/2, lo+j*a+a/2, lo+k*a+a/2)
```

```
# Setting up the starting velocities to match the temperature
random.seed(1234);
for p in system.particles:
    mass = p.mass;
    vx = random.gauss(0, temp / mass)
    vy = random.gauss(0, temp / mass)
    vz = random.gauss(0, temp / mass)
    p.velocity = (vx, vy, vz)

# Setting up the different starting conditions
for p in system.particles:
    (i,j,k) = (p.tag % m, p.tag/m % m, p.tag/m**2 % m)
    if (i+j+k) % 2 == 1:
        p.type = "B"

# Setting up the interaction potentials
lj = pair.lj(r_cut=2.5)
#  Smooth and shifted
lj.set_params(mode="shift")
lj.pair_coeff.set('A', 'A', epsilon=2.0, sigma=1.0, alpha
   =1.0)
lj.pair_coeff.set('B', 'B', epsilon=2.0, sigma=1.0, alpha
   =1.0)
lj.pair_coeff.set('A', 'B', epsilon=2.0, sigma=1.0, alpha
   =1.0, r_cut=2.0**(1.0/6.0))
```

```
# Setting up the integrator
all = group.all()
integrate.mode_standard(dt=deltaT)

bd = integrate.bdnvt(group=all,T=temp,seed=12345)
bd.set_gamma('A', gamma=bdgamma)
bd.set_gamma('B', gamma=bdgamma)
bd.set_params(tally=True);

# Initial thermalization
bd.set_params(T=temp*10)
run(5000)
bd.set_params(T=temp)

# Setting up switching
random_switch.update.switchAB(p=switch_prob, period=
    switch_period, seed=1234)

# Setting up logging parameters
# 4.81 -> gives 40 logarithmics numbers with the lastone
    right before the final timestep.
xml = dump.xml(filename='outID' + str(id+1), period = lambda
    n: 10**(n/4.82) )
xml.set_params(position=True,type=True,velocity=True,mass=
    True)

logger = analyze.log(filename='outID' + str(id+1) + '.log',
```

```
    period=logger_period, quantities=['pair_lj_energy', '
    volume', 'temperature', 'pressure', 'kinetic_energy', '
    potential_energy', 'momentum', 'time','
    bdnvt_reservoir_energy_all'])

# Running the simulation
run(timesteps+1)
```

APPENDIX B

Key HOOMD scripts – Photo-Switchable Colloids Simulation

```
##################################################################
#
# Project: 02 - Photo-Switchable Colloids
# Subproject: 008 - Assembly Speed Enhancement vs. Off/On
    ratio
# Hoomd Version: v0.11.2
# Description: Running system with multiple cycle lengths and
#    multiple On/Off ratios to see how large aggregates get.
#
##################################################################

from hoomd_script import *
import random
import os
import numpy as np
```

```
#to be used with the PBS Array feature
def get_array_id():
    pbs_arrayid = os.getenv('PBS_ARRAYID');
    if pbs_arrayid is None:
        return 0
    else:
        return int(pbs_arrayid) - 1;

# Setting up simulation group conditions

#  ID
idx = get_array_id();



# Common simulation parameters
total_ts = 1e8    # [1] Number of total time steps to perform
temp = 1.0    # [Eu]
deltaT = 0.006 # [Tu] Time to be advanced every time step
density = 0.125 # [Lu^-3] Number density
a = (1.0/density)**(1.0/3.0) # [Lu] Lattice parameter for
    initial configuration
m = 40 # m^3 Number of particles
bdgamma = 113    # [1/Tu] Langevin Coefficient
ep = 2.5 # [Eu] LJ \epsilon
random_gen = 23451 # [1] Random number generator seed
cycle_ts = 1e6
```

```
# Id dependent value array
cycle_ratio_array = [0.0, 0.01, 0.03, 0.05, 0.11]

# Setting up initial conditions that depend on the id
cycle_ratio = cycle_ratio_array[idx % len(cycle_ratio_array)]

off_ts = cycle_ts * cycle_ratio
on_ts = cycle_ts * (1.0 - cycle_ratio)
n_cycles = int( total_ts / cycle_ts)
random_seed = random_gen * (idx + 1)

print ("\nID Dependent Parameters:")
print ("Cycle Length = %.2e" % cycle_ts)
print ("On Length = %.2e" % on_ts)
print ("Off Length = %.2e" % off_ts)
print ("Number of cycles = %d" % n_cycles)
print ("Random seed = %d" % random_seed)
print ("")

# Logging parameters
logger_period = cycle_ts/10
dcd_period = cycle_ts

# Initializing the system
system = init.create_empty(N=m*m*m, box=(a*m, a*m, a*m),
    n_particle_types=1)
```

```
# Moving the particles to their starting location
lo = -m*a / 2.0;
for p in system.particles:
    (i,j,k) = (p.tag % m, p.tag/m % m, p.tag/m**2 % m)
    p.position = (lo + i*a+a/2, lo+j*a+a/2, lo+k*a+a/2)

# Setting up the starting velocities to match the temperature
random.seed(random_seed);
for p in system.particles:
    mass = p.mass;
    vx = random.gauss(0, temp / mass)
    vy = random.gauss(0, temp / mass)
    vz = random.gauss(0, temp / mass)
    p.velocity = (vx, vy, vz)
    p.type = "A"

# Setting up the interaction potentials
lj_on = pair.lj(r_cut=2.5)
#  Attractive
lj_on.set_params(mode="shift")
lj_on.pair_coeff.set('A', 'A', epsilon=ep, sigma=1.0, alpha
   =1.0)

#  Repulsive
lj_off = pair.lj(r_cut=2.0**(1.0/6.0))
lj_off.set_params(mode="shift")
```

```
lj_off.pair_coeff.set('A', 'A', epsilon=ep, sigma=1.0, alpha
    =1.0)

# Setting up the integrator
all = group.all()
integrate.mode_standard(dt=deltaT)

# Continue with the integrator
bd = integrate.bdnvt(group=all,T=temp,seed=random_seed)
bd.set_gamma('A', gamma=bdgamma)
bd.set_params(tally=True);

# Randomizing initial position
lj_on.disable()
lj_off.enable()
run(1e3)

# Setting up logging
logger = analyze.log(filename='outID-%d.log'%idx,
                     period=logger_period,
                     quantities=['pair_lj_energy',
                                 'temperature',
                                 'kinetic_energy',
                                 'momentum',
                                 'bdnvt_reservoir_energy_all'
                                    ])
xml = dump.xml(filename='out' + 'ID-%d.xml'%idx, vis=True)
```

```
dcd = dump.dcd(filename='out' + 'ID-%d.dcd'%idx, period=
    dcd_period)

# Running the simulation
for cycle in range(1, n_cycles+1):
    print ("\n\nCurrently on cycle: %d / %d\n\n" % (cycle,
        n_cycles))

    # Disassembling Phase
    lj_on.disable(log=True)
    lj_off.enable()
    run(off_ts)

    # Assembling Phase
    lj_on.enable()
    lj_off.disable()
    run(on_ts)
```

BIBLIOGRAPHY

BIBLIOGRAPHY

[1] Sihai Chen, Zhong Lin Wang, John Ballato, Stephen H. Foulger, and David L. Carroll. Monopod, bipod, tripod, and tetrapod gold nanocrystals. *Journal of the American Chemical Society*, 125(52):16186–7, December 2003. ISSN 0002-7863. doi: 10.1021/ja038927x. URL http://pubs.acs.org/doi/abs/10.1021/ja038927xhttp://www.ncbi.nlm.nih.gov/pubmed/14692749.

[2] Liberato Manna, Delia J. Milliron, Andreas Meisel, Erik C. Scher, and A. Paul Alivisatos. Controlled growth of tetrapod-branched inorganic nanocrystals. *Nature Materials*, 2(6):382–5, June 2003. ISSN 1476-1122. doi: 10.1038/nmat902. URL http://www.ncbi.nlm.nih.gov/pubmed/12764357.

[3] Colin J. Loweth, W. Brett Caldwell, Xiaogang Peng, A. Paul Alivisatos, and Peter G. Schultz. DNA-Based Assembly of Gold Nanocrystals. *Angewandte Chemie International Edition*, 38(12):1808–1812, June 1999. ISSN 1433-7851. doi: 10.1002/(SICI)1521-3773(19990614)38:12⟨1808::AID-ANIE1808⟩3.0.CO;2-C. URL http://doi.wiley.com/10.1002/%28SICI%291521-3773%2819990614%2938%3A12%3C1808%3A%3AAID-ANIE1808%3E3.0.CO%3B2-C.

[4] Patrick M. Johnson, Carlos M. van Kats, and Alfons van Blaaderen. Synthesis of colloidal silica dumbbells. *Langmuir : the ACS journal of surfaces and colloids*, 21(24):11510–7, November 2005. ISSN 0743-7463. doi: 10.1021/la0518750. URL http://www.ncbi.nlm.nih.gov/pubmed/16285834.

[5] Yu Lu, Hui Xiong, Xuchuan Jiang, Younan Xia, Mara Prentiss, and George M. Whitesides. Asymmetric dimers can be formed by dewetting half-shells of gold deposited on the surfaces of spherical oxide colloids. *Journal of the American Chemical Society*, 125(42):12724–5, October 2003. ISSN 0002-7863. doi: 10.1021/ja0373014. URL http://www.ncbi.nlm.nih.gov/pubmed/14558817.

[6] Vinothan N. Manoharan, Mark T. Elsesser, and David J. Pine. Dense packing and symmetry in small clusters of microspheres. *Science*, 301 (5632):483–7, July 2003. ISSN 1095-9203. doi: 10.1126/science.1086189. URL http://doi.wiley.com/10.1029/2003GL016875http://www.ncbi.nlm.nih.gov/pubmed/12881563.

[7] Kyung-Sang Cho, Dmitri V. Talapin, Wolfgang Gaschler, and Christopher B. Murray. Designing PbSe nanowires and nanorings through oriented attachment of nanoparticles. *Journal of the American Chemical*

Society, 127(19):7140–7, May 2005. ISSN 0002-7863. doi: 10.1021/ja050107s. URL http://www.ncbi.nlm.nih.gov/pubmed/23180451http://www.ncbi.nlm.nih.gov/pubmed/15884956.

[8] Yugang Sun and Younan Xia. Shape-controlled synthesis of gold and silver nanoparticles. *Science*, 298(5601):2176–9, December 2002. ISSN 1095-9203. doi: 10.1126/science.1077229. URL http://www.ncbi.nlm.nih.gov/pubmed/12481134.

[9] Natalie Malikova, Isabel Pastoriza-Santos, Martin Schierhorn, Nicholas A. Kotov, and Luis M. Liz-Marzán. Layer-by-Layer Assembled Mixed Spherical and Planar Gold Nanoparticles: Control of Interparticle Interactions. *Langmuir*, 18(9):3694–3697, April 2002. ISSN 0743-7463. doi: 10.1021/la025563y. URL http://pubs.acs.org/doi/abs/10.1021/la025563y.

[10] Dhananjay Dendukuri, Daniel C. Pregibon, Jesse Collins, T. Alan Hatton, and Patrick S. Doyle. Continuous-flow lithography for high-throughput microparticle synthesis. *Nature Materials*, 5(5):365–9, May 2006. ISSN 1476-1122. doi: 10.1038/nmat1617. URL http://www.ncbi.nlm.nih.gov/pubmed/16604080.

[11] X Peng, L Manna, W Yang, J Wickham, E Scher, A Kadavanich, and Ap Alivisatos. Shape control of CdSe nanocrystals. *Nature*, 404(6773):59–61, March 2000. ISSN 1476-4687. doi: 10.1038/35003535. URL http://www.ncbi.nlm.nih.gov/pubmed/10716439.

[12] Ser-Sing Chang, Chien-Liang Lee, and C. R. Chris Wang. Gold Nanorods: Electrochemical Synthesis and Optical Properties. *The Journal of Physical Chemistry B*, 101(34):6661–6664, August 1997. ISSN 1520-6106. doi: 10.1021/jp971656q. URL http://pubs.acs.org/doi/abs/10.1021/jp971656q.

[13] F. M. van der Kooij, Katerina Kassapidou, and Henk N. W. Lekkerkerker. Liquid crystal phase transitions in suspensions of polydisperse plate-like particles. *Nature*, 406(6798):868–71, August 2000. ISSN 1476-4687. doi: 10.1038/35022535. URL http://www.ncbi.nlm.nih.gov/pubmed/10972283.

[14] Ali Mohraz and Michael J. Solomon. Direct visualization of colloidal rod assembly by confocal microscopy. *Langmuir : the ACS journal of surfaces and colloids*, 21(12):5298–306, June 2005. ISSN 0743-7463. doi: 10.1021/la046908a. URL http://www.ncbi.nlm.nih.gov/pubmed/15924453.

[15] Alicia M. Jackson, Ying Hu, Paulo Jacob Silva, and Francesco Stellacci. From homoligand- to mixed-ligand- monolayer-protected metal nanoparticles: a scanning tunneling microscopy investigation. *Journal of the American Chemical Society*, 128(34):11135–49, August 2006. ISSN 0002-7863. doi: 10.1021/ja061545h. URL http://www.ncbi.nlm.nih.gov/pubmed/16925432.

[16] Kyung-ho Roh, David C. Martin, and Joerg Lahann. Biphasic Janus particles with nanoscale anisotropy. *Nature Materials*, 4(10):759–63, October 2005. ISSN

1476-1122. doi: 10.1038/nmat1486. URL http://www.ncbi.nlm.nih.gov/pubmed/16184172.

[17] Gang Zhang, Dayang Wang, and Helmuth Möhwald. Decoration of microspheres with gold nanodots–giving colloidal spheres valences. *Angewandte Chemie (International ed. in English)*, 44(47):7767–70, December 2005. ISSN 1433-7851. doi: 10.1002/anie.200502117. URL http://www.ncbi.nlm.nih.gov/pubmed/16276544.

[18] Benjamin R. Martin, Daniel J. Dermody, Brian D. Reiss, Mingming Fang, L. Andrew Lyon, Michael J. Natan, and Thomas E. Mallouk. Orthogonal Self-Assembly on Colloidal Gold-Platinum Nanorods. *Advanced Materials*, 11(12):1021–1025, August 1999. ISSN 0935-9648. doi: 10.1002/(SICI)1521-4095(199908)11:12⟨1021::AID-ADMA1021⟩3.0.CO;2-S. URL http://doi.wiley.com/10.1002/%28SICI%291521-4095%28199908%2911%3A12%3C1021%3A%3AAID-ADMA1021%3E3.0.CO%3B2-S.

[19] Olivier Cayre, Vesselin N. Paunov, and Orlin D. Velev. Fabrication of asymmetrically coated colloid particles by microcontact printing techniques. *Journal of Materials Chemistry*, 13(10):2445, 2003. ISSN 0959-9428. doi: 10.1039/b308817k. URL http://xlink.rsc.org/?DOI=b308817k.

[20] Sharon C. Glotzer and Michael J. Solomon. Anisotropy of building blocks and their assembly into complex structures. *Nature Materials*, 6(8):557–62, August 2007. ISSN 1476-1122. doi: 10.1038/nmat1949. URL http://www.ncbi.nlm.nih.gov/pubmed/17667968.

[21] N. Ban. The Complete Atomic Structure of the Large Ribosomal Subunit at 2.4 A Resolution. *Science*, 289(5481):905–920, August 2000. ISSN 00368075. doi: 10.1126/science.289.5481.905. URL http://www.sciencemag.org/cgi/doi/10.1126/science.289.5481.905.

[22] J. D. Hartgerink, E. Beniash, and S. I. Stupp. Self-assembly and mineralization of peptide-amphiphile nanofibers. *Science*, 294(5547):1684–8, November 2001. ISSN 0036-8075. doi: 10.1126/science.1063187. URL http://www.ncbi.nlm.nih.gov/pubmed/11721046.

[23] Christopher J. Campbell, Stoyan K. Smoukov, Kyle J. M. Bishop, and Bartosz A. Grzybowski. Reactive surface micropatterning by wet stamping. *Langmuir : the ACS journal of surfaces and colloids*, 21(7):2637–40, March 2005. ISSN 0743-7463. doi: 10.1021/la046942p. URL http://www.ncbi.nlm.nih.gov/pubmed/15779924.

[24] Bartosz A. Grzybowski, Adam Winkleman, Jason A. Wiles, Yisroel Brumer, and George M. Whitesides. Electrostatic self-assembly of macroscopic crystals using contact electrification. *Nature Materials*, 2(4):241–5, April 2003. ISSN 1476-1122. doi: 10.1038/nmat860. URL http://www.ncbi.nlm.nih.gov/pubmed/12690397.

[25] Thomas D. Clark, Rosaria Ferrigno, Joe Tien, Kateri E. Paul, and George M. Whitesides. Template-directed self-assembly of 10-microm-sized hexagonal plates. *Journal of the American Chemical Society*, 124(19):5419–26, May 2002. ISSN 0002-7863. URL http://www.ncbi.nlm.nih.gov/pubmed/11996582.

[26] Marcin Fialkowski, Agnieszka Bitner, and Bartosz A. Grzybowski. Self-assembly of polymeric microspheres of complex internal structures. *Nature Materials*, 4(1):93–97, December 2004. ISSN 1476-1122. doi: 10.1038/nmat1267. URL http://www.nature.com/doifinder/10.1038/nmat1267.

[27] Marcin Fialkowski, Kyle J. M. Bishop, Rafal Klajn, Stoyan K. Smoukov, Christopher J. Campbell, and Bartosz A. Grzybowski. Principles and implementations of dissipative (dynamic) self-assembly. *The Journal of Physical Chemistry B*, 110(6):2482–96, March 2006. ISSN 1520-6106. doi: 10.1021/jp054153q. URL http://www.ncbi.nlm.nih.gov/pubmed/16471845.

[28] George M. Whitesides and Bartosz A. Grzybowski. Self-assembly at all scales. *Science*, 295(5564):2418–21, March 2002. ISSN 1095-9203. doi: 10.1126/science.1070821. URL http://www.ncbi.nlm.nih.gov/pubmed/11923529.

[29] Bartosz A. Grzybowski and George M. Whitesides. Three-Dimensional Dynamic Self-Assembly of Spinning Magnetic Disks: Vortex Crystals. *The Journal of Physical Chemistry B*, 106(6):1188–1194, February 2002. ISSN 1520-6106. doi: 10.1021/jp012819k. URL http://pubs.acs.org/doi/abs/10.1021/jp012819k.

[30] B. A. Grzybowski, H. A. Stone, and G. M. Whitesides. Dynamic self-assembly of magnetized, millimetre-sized objects rotating at a liquid-air interface. *Nature*, 405(6790):1033–6, June 2000. ISSN 1476-4687. doi: 10.1038/35016528. URL http://www.ncbi.nlm.nih.gov/pubmed/10890439.

[31] Job Boekhoven, Aurelie M Brizard, Krishna N K Kowlgi, Ger J M Koper, Rienk Eelkema, and Jan H van Esch. Dissipative self-assembly of a molecular gelator by using a chemical fuel. *Angewandte Chemie (International ed. in English)*, 49(28):4825–8, June 2010. ISSN 1521-3773. doi: 10.1002/anie.201001511. URL http://www.ncbi.nlm.nih.gov/pubmed/20512834.

[32] D. Klotsa, Michael Swift, R. Bowley, and P. King. Chain formation of spheres in oscillatory fluid flows. *Physical Review E*, 79(2):021302, February 2009. ISSN 1539-3755. doi: 10.1103/PhysRevE.79.021302. URL http://link.aps.org/doi/10.1103/PhysRevE.79.021302.

[33] Sharon C. Glotzer, Edmund Di Marzio, and M. Muthukumar. Reaction-Controlled Morphology of Phase-Separating Mixtures. *Physical Review Letters*, 74(11):2034–2037, March 1995. ISSN 0031-9007. doi: 10.1103/PhysRevLett.74.2034. URL http://link.aps.org/doi/10.1103/PhysRevLett.74.2034.

[34] Yanli Huo, Xiuli Jiang, Hongdong Zhang, and Yuliang Yang. Hydrodynamic effects on phase separation of binary mixtures with reversible chemical reaction. *The Journal of Chemical Physics*, 118(21):9830, 2003. ISSN 00219606. doi: 10.1063/1.1571511. URL http://link.aip.org/link/JCPSA6/v118/i21/p9830/s1&Agg=doi.

[35] Q. Tran-Cong and A. Harada. Reaction-induced ordering phenomena in binary polymer mixtures. *Physical review letters*, 76(7):1162–1165, February 1996. ISSN 1079-7114. URL http://www.ncbi.nlm.nih.gov/pubmed/10061649.

[36] K. Ichimura. Light-Driven Motion of Liquids on a Photoresponsive Surface. *Science*, 288(5471):1624–1626, June 2000. ISSN 00368075. doi: 10.1126/science.288.5471.1624. URL http://www.sciencemag.org/cgi/doi/10.1126/science.288.5471.1624.

[37] Joerg Lahann, Samir Mitragotri, Thanh-Nga Tran, Hiroki Kaido, Jagannathan Sundaram, Insung S. Choi, Saskia Hoffer, Gabor A. Somorjai, and Robert Langer. A reversibly switching surface. *Science*, 299(5605):371–4, January 2003. ISSN 1095-9203. doi: 10.1126/science.1078933. URL http://www.ncbi.nlm.nih.gov/pubmed/12532011.

[38] Prateek K. Jha, Vladimir Kuzovkov, Bartosz A. Grzybowski, and Monica Olvera de la Cruz. Dynamic self-assembly of photo-switchable nanoparticles. *Soft Matter*, 8(1):227, 2012. ISSN 1744-683X. doi: 10.1039/c1sm06662e. URL http://xlink.rsc.org/?DOI=c1sm06662e.

[39] Yanting Wang, S Teitel, and Christoph Dellago. Melting of icosahedral gold nanoclusters from molecular dynamics simulations. *The Journal of chemical physics*, 122(21):214722, June 2005. ISSN 0021-9606. doi: 10.1063/1.1917756. URL http://www.ncbi.nlm.nih.gov/pubmed/15974777.

[40] George M. Whitesides, J. Mathias, and C. Seto. Molecular self-assembly and nanochemistry: a chemical strategy for the synthesis of nanostructures. *Science*, 254(5036):1312–1319, November 1991. ISSN 0036-8075. doi: 10.1126/science.1962191. URL http://www.sciencemag.org/cgi/doi/10.1126/science.1962191.

[41] Matthew Tirrell. Modular materials by self-assembly. *AIChE Journal*, 51(9):2386–2390, September 2005. ISSN 0001-1541. doi: 10.1002/aic.10641. URL http://doi.wiley.com/10.1002/aic.10641.

[42] Yaakov Levy and José N. Onuchic. Water mediation in protein folding and molecular recognition. *Annual review of biophysics and biomolecular structure*, 35:389–415, January 2006. ISSN 1056-8700. doi: 10.1146/annurev.biophys.35.040405.102134. URL http://www.ncbi.nlm.nih.gov/pubmed/16689642.

[43] Anna Stradner, Helen Sedgwick, Frédéric Cardinaux, Wilson C. K. Poon, Stefan U. Egelhaaf, and Peter Schurtenberger. Equilibrium cluster formation in concentrated protein solutions and colloids. *Nature*, 432(7016):492–5, November 2004. ISSN 1476-4687. doi: 10.1038/nature03109. URL `http://www.ncbi.nlm.nih.gov/pubmed/15565151`.

[44] E O Budrene and H C Berg. Dynamics of formation of symmetrical patterns by chemotactic bacteria. *Nature*, 376(6535):49–53, July 1995. ISSN 0028-0836. doi: 10.1038/376049a0. URL `http://www.ncbi.nlm.nih.gov/pubmed/7596432`.

[45] Eshel Ben-Jacob, Haim Shmueli, Ofer Shochet, and Adam Tenenbaum. Adaptive self-organization during growth of bacterial colonies. *Physica A: Statistical Mechanics and its Applications*, 187(3-4):378–424, September 1992. ISSN 03784371. doi: 10.1016/0378-4371(92)90002-8. URL `http://linkinghub.elsevier.com/retrieve/pii/0378437192900028`.

[46] X. Jiang, M. Wang, David Y. Graham, and Mary K. Estes. Expression, self-assembly, and antigenicity of the Norwalk virus capsid protein. *Journal of Virology*, 66(11):6527–32, November 1992. ISSN 0022-538X. URL `http://www.pubmedcentral.nih.gov/articlerender.fcgi?artid=240146&tool=pmcentrez&rendertype=abstract`.

[47] R Kirnbauer, Janet Taub, Heather Greenstone, Richard Roden, M Dürst, Lutz Gissmann, Doug R Lowy, and John T Schiller. Efficient self-assembly of human papillomavirus type 16 L1 and L1-L2 into virus-like particles. *Journal of Virology*, 67(12):6929–36, December 1993. ISSN 0022-538X. URL `http://www.pubmedcentral.nih.gov/articlerender.fcgi?artid=238150&tool=pmcentrez&rendertype=abstract`.

[48] Rudolf Clausius. On the nature of the motion which we call heat. *Philosophical Magazine*, 14:108–127, 1857.

[49] J. Willard Gibbs. *Elementary principles in statistical mechanics : developed with especial reference to the rational foundation of thermodynamics*. Charles Scribner's Sons, New York, 1902.

[50] J. C. Maxwell. V. Illustrations of the dynamical theory of gases.Part I. On the motions and collisions of perfectly elastic spheres. *Philosophical Magazine Series 4*, 19(124), 1860. doi: 10.1080/14786446008642818.

[51] Ludwig Boltzmann. Weitere Studien über das Wärmegleichgewicht unter Gasmolekülen. *Wiener Berichte*, 66:275–370, 1872.

[52] Ludwig Boltzmann. Über die Beziehung zwischen dem zweiten Hauptsatz der mechanischen Wärmetheorie und der Wahrscheinlichkeitsrechnung respektive den Sätzen über das Wärmegleichgewicht. *Wiener Berichte*, 76:373–435, 1877.

[53] G Riess. Micellization of block copolymers. *Progress in Polymer Science*, 28(7):1107–1170, July 2003. ISSN 00796700. doi: 10.1016/S0079-6700(03)00015-7. URL http://linkinghub.elsevier.com/retrieve/pii/S0079670003000157.

[54] Arthur T. Winfree. Spiral waves of chemical activity. *Science*, 175(4022):634–6, February 1972. ISSN 0036-8075. doi: 10.1126/science.175.4022.634. URL http://www.ncbi.nlm.nih.gov/pubmed/17808803.

[55] D. A. Egolf, I. V. Melnikov, Werner Pesch, and R. E. Ecke. Mechanisms of extensive spatiotemporal chaos in Rayleigh-Benard convection. *Nature*, 404 (6779):733–6, April 2000. ISSN 1476-4687. doi: 10.1038/35008013. URL http://www.ncbi.nlm.nih.gov/pubmed/10783880.

[56] Vincenzo Palermo and Paolo Samorì. Molecular self-assembly across multiple length scales. *Angewandte Chemie (International ed. in English)*, 46(24):4428–32, January 2007. ISSN 1433-7851. doi: 10.1002/anie.200700416. URL http://www.ncbi.nlm.nih.gov/pubmed/17497615.

[57] Rajagopalan Thiruvengadathan, Venumadhav Korampally, Arkasubhra Ghosh, Nripen Chanda, Keshab Gangopadhyay, and Shubhra Gangopadhyay. Nanomaterial processing using self-assembly-bottom-up chemical and biological approaches. *Reports on progress in physics. Physical Society (Great Britain)*, 76 (6):066501, June 2013. ISSN 1361-6633. doi: 10.1088/0034-4885/76/6/066501. URL http://www.ncbi.nlm.nih.gov/pubmed/23722189.

[58] Job Boekhoven, Jos M. Poolman, Chandan Maity, Feng Li, Lars van der Mee, Christophe B. Minkenberg, Eduardo Mendes, Jan H. van Esch, and Rienk Eelkema. Catalytic control over supramolecular gel formation. *Nature Chemistry*, 5(5):433–7, May 2013. ISSN 1755-4349. doi: 10.1038/nchem.1617. URL http://www.ncbi.nlm.nih.gov/pubmed/23609096.

[59] Claudio Castellano, Santo Fortunato, and Vittorio Loreto. Statistical physics of social dynamics. *Reviews of Modern Physics*, 81(2):591–646, May 2009. ISSN 0034-6861. doi: 10.1103/RevModPhys.81.591. URL http://link.aps.org/doi/10.1103/RevModPhys.81.591.

[60] R. Aditi Simha and Sriram Ramaswamy. Hydrodynamic Fluctuations and Instabilities in Ordered Suspensions of Self-Propelled Particles. *Physical Review Letters*, 89(5):058101, July 2002. ISSN 0031-9007. doi: 10.1103/PhysRevLett.89.058101. URL http://link.aps.org/doi/10.1103/PhysRevLett.89.058101.

[61] Herbert Levine, Wouter-Jan Rappel, and Inon Cohen. Self-organization in systems of self-propelled particles. *Physical Review E*, 63(1):1–4, December 2000. ISSN 1063-651X. doi: 10.1103/PhysRevE.63.017101. URL http://link.aps.org/doi/10.1103/PhysRevE.63.017101.

[62] Gunnar Rückner and Raymond Kapral. Chemically Powered Nanodimers. *Physical Review Letters*, 98(15):150603, April 2007. ISSN 0031-9007. doi: 10.1103/PhysRevLett.98.150603. URL http://link.aps.org/doi/10.1103/PhysRevLett.98.150603.

[63] Aparna Baskaran and M. Cristina Marchetti. Hydrodynamics of self-propelled hard rods. *Physical Review E*, 77(1):011920, January 2008. ISSN 1539-3755. doi: 10.1103/PhysRevE.77.011920. URL http://link.aps.org/doi/10.1103/PhysRevE.77.011920.

[64] Benjamin G. Levine, John E. Stone, and Axel Kohlmeyer. Fast Analysis of Molecular Dynamics Trajectories with Graphics Processing Units-Radial Distribution Function Histogramming. *Journal of computational physics*, 230(9):3556–3569, May 2011. ISSN 0021-9991. doi: 10.1016/j.jcp.2011.01.048. URL http://www.pubmedcentral.nih.gov/articlerender.fcgi?artid=3085256&tool=pmcentrez&rendertype=abstract.

[65] Arshad Kudrolli, Geoffroy Lumay, Dmitri Volfson, and Lev Tsimring. Swarming and Swirling in Self-Propelled Polar Granular Rods. *Physical Review Letters*, 100(5):058001, February 2008. ISSN 0031-9007. doi: 10.1103/PhysRevLett.100.058001. URL http://link.aps.org/doi/10.1103/PhysRevLett.100.058001.

[66] M. DOrsogna, Y. Chuang, A. Bertozzi, and L. Chayes. Self-Propelled Particles with Soft-Core Interactions: Patterns, Stability, and Collapse. *Physical Review Letters*, 96(10):104302, March 2006. ISSN 0031-9007. doi: 10.1103/PhysRevLett.96.104302. URL http://link.aps.org/doi/10.1103/PhysRevLett.96.104302.

[67] Guillaume Grégoire and Hugues Chaté. Onset of Collective and Cohesive Motion. *Physical Review Letters*, 92(2):025702, January 2004. ISSN 0031-9007. doi: 10.1103/PhysRevLett.92.025702. URL http://link.aps.org/doi/10.1103/PhysRevLett.92.025702.

[68] András Czirók, H. Eugene Stanley, and Tamás Vicsek. Spontaneously ordered motion of self-propelled particles. *Journal of Physics A: Mathematical and General*, 30(5):1375–1385, March 1997. ISSN 0305-4470. doi: 10.1088/0305-4470/30/5/009. URL http://iopscience.iop.org/0305-4470/30/5/009http://stacks.iop.org/0305-4470/30/i=5/a=009?key=crossref.8fe1e9929d2eeb6471532eda8a3fb67b.

[69] Nguyen H. P. Nguyen, Eric Jankowski, and Sharon C. Glotzer. Thermal and athermal three-dimensional swarms of self-propelled particles. *Physical Review E*, 86(1):011136, July 2012. ISSN 1539-3755. doi: 10.1103/PhysRevE.86.011136. URL http://link.aps.org/doi/10.1103/PhysRevE.86.011136.

[70] Matthew F. Copeland and Douglas B. Weibel. Bacterial swarming: a model system for studying dynamic self-assembly. *Soft Matter*, 5(6):1174, 2009.

ISSN 1744-683X. doi: 10.1039/b812146j. URL http://xlink.rsc.org/?DOI=b812146j.

[71] Fernando Peruani and Luis Morelli. Self-Propelled Particles with Fluctuating Speed and Direction of Motion in Two Dimensions. *Physical Review Letters*, 99 (1):010602, July 2007. ISSN 0031-9007. doi: 10.1103/PhysRevLett.99.010602. URL http://link.aps.org/doi/10.1103/PhysRevLett.99.010602.

[72] I. Llopis and I. Pagonabarraga. Dynamic regimes of hydrodynamically coupled self-propelling particles. *Europhysics Letters (EPL)*, 75 (6):999–1005, September 2006. ISSN 0295-5075. doi: 10.1209/epl/i2006-10201-y. URL http://stacks.iop.org/0295-5075/75/i=6/a=999?key=crossref.5232916178295ab8f0e39fc611fc35e5.

[73] Takao Ohta and Takahiro Ohkuma. Deformable Self-Propelled Particles. *Physical Review Letters*, 102(15):154101, April 2009. ISSN 0031-9007. doi: 10.1103/PhysRevLett.102.154101. URL http://link.aps.org/doi/10.1103/PhysRevLett.102.154101.

[74] Hua Ke, Shengrong Ye, R. Lloyd Carroll, and Kenneth Showalter. Motion analysis of self-propelled Pt-silica particles in hydrogen peroxide solutions. *The Journal of Physical Chemistry A*, 114(17):5462–7, May 2010. ISSN 1520-5215. doi: 10.1021/jp101193u. URL http://www.ncbi.nlm.nih.gov/pubmed/20387839.

[75] Pulak K. Ghosh, Vyacheslav R. Misko, Fabio Marchesoni, and Franco Nori. Self-Propelled Janus Particles in a Ratchet: Numerical Simulations. *Physical Review Letters*, 110(26):268301, June 2013. ISSN 0031-9007. doi: 10.1103/PhysRevLett.110.268301. URL http://link.aps.org/doi/10.1103/PhysRevLett.110.268301.

[76] Wilson C. K. Poon. From Clarkia to Escherichia and Janus: the physics of natural and synthetic active colloids. pages 317–386, June 2013. URL http://arxiv.org/abs/1306.4799.

[77] Stephen J. Ebbens and Jonathan R. Howse. In pursuit of propulsion at the nanoscale. *Soft Matter*, 6(4):726, 2010. ISSN 1744-683X. doi: 10.1039/b918598d. URL http://xlink.rsc.org/?DOI=b918598d.

[78] Tamás Vicsek, András Czirók, Eshel Ben-Jacob, Inon Cohen, and Ofer Shochet. Novel Type of Phase Transition in a System of Self-Driven Particles. *Physical Review Letters*, 75(6):1226–1229, August 1995. ISSN 0031-9007. doi: 10.1103/PhysRevLett.75.1226. URL http://link.aps.org/doi/10.1103/PhysRevLett.75.1226.

[79] Jeremie Palacci, Stefano Sacanna, Asher Preska Steinberg, David J. Pine, and Paul M. Chaikin. Living crystals of light-activated colloidal surfers. *Science*, 339 (6122):936–40, February 2013. ISSN 1095-9203. doi: 10.1126/science.1230020. URL http://www.ncbi.nlm.nih.gov/pubmed/23371555.

[80] Sanjib Das, Priyadarshi Ranjan, Pradipta Sankar Maiti, Gurvinder Singh, Gregory Leitus, and Rafal Klajn. Dual-responsive nanoparticles and their self-assembly. *Advanced Materials*, 25(3):422–6, January 2013. ISSN 1521-4095. doi: 10.1002/adma.201201734. URL http://www.ncbi.nlm.nih.gov/pubmed/22933327.

[81] D. Klotsa, Michael Swift, R. Bowley, and P. King. Interaction of spheres in oscillatory fluid flows. *Physical Review E*, 76(5):056314, November 2007. ISSN 1539-3755. doi: 10.1103/PhysRevE.76.056314. URL http://link.aps.org/doi/10.1103/PhysRevE.76.056314.

[82] Rafal Klajn, Kyle J M Bishop, and Bartosz A. Grzybowski. Light-controlled self-assembly of reversible and irreversible nanoparticle suprastructures. *Proceedings of the National Academy of Sciences of the United States of America*, 104(25):10305–9, June 2007. ISSN 0027-8424. doi: 10.1073/pnas.0611371104. URL http://www.pubmedcentral.nih.gov/articlerender.fcgi?artid=1965508&tool=pmcentrez&rendertype=abstract.

[83] Sharon C. Glotzer, Dietrich Stauffer, and Naeem Jan. Monte Carlo simulations of phase separation in chemically reactive binary mixtures. *Physical Review Letters*, 72(26):4109–4112, June 1994. ISSN 0031-9007. doi: 10.1103/PhysRevLett.72.4109. URL http://link.aps.org/doi/10.1103/PhysRevLett.72.4109http://www.ncbi.nlm.nih.gov/pubmed/10056384.

[84] S. Toxvaerd. Molecular dynamics simulations of phase separation in chemically reactive binary mixtures. *Physical Review E*, 53(4):3710–3716, April 1996. ISSN 1063-651X. doi: 10.1103/PhysRevE.53.3710. URL http://link.aps.org/doi/10.1103/PhysRevE.53.3710.

[85] Miho Motoyama. Morphology of Binary Mixtures Which Undergo Phase Separation during Chemical Reactions. *Journal of the Physics Society Japan*, 65 (7):1894–1897, July 1996. ISSN 0031-9015. doi: 10.1143/JPSJ.65.1894. URL http://jpsj.ipap.jp/link?JPSJ/65/1894/.

[86] Miho Motoyama and Takao Ohta. Morphology of Phase-Separating Binary Mixtures with Chemical Reaction. *Journal of the Physics Society Japan*, 66(9):2715–2725, September 1997. ISSN 0031-9015. doi: 10.1143/JPSJ.66.2715. URL http://cat.inist.fr/?aModele=afficheN&cpsidt=2055505http://jpsj.ipap.jp/link?JPSJ/66/2715/.

[87] K. Furtado and J. Yeomans. Lattice Boltzmann simulations of phase separation in chemically reactive binary fluids. *Physical Review E*, 73(6):066124, June 2006. ISSN 1539-3755. doi: 10.1103/PhysRevE.73.066124. URL http://link.aps.org/doi/10.1103/PhysRevE.73.066124.

[88] Qui Tran-Cong, Junji Kawai, and Kouichi Endoh. Modes selection in polymer mixtures undergoing phase separation by photochemical reactions. *Chaos*

(Woodbury, N.Y.), 9(2):298–307, June 1999. ISSN 1089-7682. doi: 10.1063/1.166406. URL http://www.ncbi.nlm.nih.gov/pubmed/12779827.

[89] Yuka Tabe and Hiroshi Yokoyama. Coherent collective precession of molecular rotors with chiral propellers. *Nature Materials*, 2(12):806–9, December 2003. ISSN 1476-1122. doi: 10.1038/nmat1017. URL http://www.ncbi.nlm.nih.gov/pubmed/14625540.

[90] Kimiko Makino, Satoshi Yamamoto, Keiji Fujimoto, Haruma Kawaguchi, and Hiroyuki Ohshima. Surface Structure of Latex Particles Covered with Temperature-Sensitive Hydrogel Layers. *Journal of Colloid and Interface Science*, 166(1):251–258, August 1994. ISSN 00219797. doi: 10.1006/jcis.1994.1291. URL http://linkinghub.elsevier.com/retrieve/pii/S0021979784712914.

[91] M Okubo and H Ahmad. Adsorption of enzymes onto submicron-sized temperature-sensitive composite polymer particles and its activity. *Colloids and Surfaces A: Physicochemical and Engineering Aspects*, 153(1-3):429–433, August 1999. ISSN 09277757. doi: 10.1016/S0927-7757(98)00464-6. URL http://linkinghub.elsevier.com/retrieve/pii/S0927775798004646.

[92] JH Kim and M Ballauff. The volume transition in thermosensitive core-shell latex particles containing charged groups. *Colloid & Polymer Science*, 277(12):1210–1214, December 1999. ISSN 0303-402X. doi: 10.1007/s003960050512. URL http://link.springer.com/article/10.1007/s003960050512http://link.springer.com/10.1007/s003960050512.

[93] N. Dingenouts, C. Norhausen, and M. Ballauff. Observation of the Volume Transition in Thermosensitive CoreShell Latex Particles by Small-Angle X-ray Scattering. *Macromolecules*, 31(25):8912–8917, December 1998. ISSN 0024-9297. doi: 10.1021/ma980985t. URL http://pubs.acs.org/doi/abs/10.1021/ma980985t.

[94] J. Brady. Stokesian Dynamics. *Annual Review of Fluid Mechanics*, 20(1):111–157, January 1988. ISSN 00664189. doi: 10.1146/annurev.fluid.20.1.111. URL http://www.annualreviews.org/doi/abs/10.1146/annurev.fl.20.010188.000551http://fluid.annualreviews.org/cgi/doi/10.1146/annurev.fluid.20.1.111.

[95] Daan Frenkel and Berend Smit. *Understanding Molecular Simulation: From Algorithms to Applications*. Academic Press, San Diego, CA, 2 edition, 2001. ISBN 978-0-12-267351-1.

[96] John D. Weeks. Role of Repulsive Forces in Determining the Equilibrium Structure of Simple Liquids. *The Journal of Chemical Physics*, 54(12):5237, 1971. ISSN 00219606. doi: 10.1063/1.1674820. URL http://link.aip.org/link/?JCP/54/5237/1&Agg=doi.

[97] Stephen Whitelam and Phillip L Geissler. Avoiding unphysical kinetic traps in Monte Carlo simulations of strongly attractive particles. *The Journal of chemical physics*, 127(15):154101, October 2007. ISSN 0021-9606. doi: 10.1063/1.2790421. URL http://www.ncbi.nlm.nih.gov/pubmed/17949126.

[98] Paul Steinhardt, David Nelson, and Marco Ronchetti. Bond-orientational order in liquids and glasses. *Physical Review B*, 28(2):784–805, July 1983. ISSN 0163-1829. doi: 10.1103/PhysRevB.28.784. URL http://link.aps.org/doi/10.1103/PhysRevB.28.784.

[99] J. D. Landau and F. M. Lifshitz. *Quantum Mechanics*. Pergamon, New York, 1965.

[100] Antonio F. Osorio Vivanco, Igal Szleifer, and Sharon C. Glotzer. Dissipative Self-Assembly of Switchable Colloids Driven Far-From-Equilibrium. 2013.

[101] Jaap J. D. de Jong, P. Ralph Hania, Audrius Pugzlys, Linda N. Lucas, Maaike de Loos, Richard M. Kellogg, Ben L. Feringa, Koos Duppen, and Jan H. van Esch. Light-driven dynamic pattern formation. *Angewandte Chemie (International ed. in English)*, 44(16):2373–6, April 2005. ISSN 1433-7851. doi: 10.1002/anie.200462500. URL http://www.ncbi.nlm.nih.gov/pubmed/15761897.

[102] Matthias Ballauff and Yan Lu. Smart nanoparticles: Preparation, characterization and applications. *Polymer*, 48(7):1815–1823, March 2007. ISSN 00323861. doi: 10.1016/j.polymer.2007.02.004. URL http://linkinghub.elsevier.com/retrieve/pii/S0032386107001243.

[103] Trung Dac Nguyen and Sharon C. Glotzer. Reconfigurable assemblies of shape-changing nanorods. *ACS Nano*, 4(5):2585–94, May 2010. ISSN 1936-086X. doi: 10.1021/nn901725b. URL http://www.ncbi.nlm.nih.gov/pubmed/20408583.

[104] Trung Dac Nguyen, Eric Jankowski, and Sharon C. Glotzer. Self-assembly and reconfigurability of shape-shifting particles. *ACS Nano*, 5(11):8892–903, November 2011. ISSN 1936-086X. doi: 10.1021/nn203067y. URL http://www.ncbi.nlm.nih.gov/pubmed/21950837.

[105] Oleg Gang and Yugang Zhang. Shaping phases by phasing shapes. *ACS Nano*, 5 (11):8459–65, November 2011. ISSN 1936-086X. doi: 10.1021/nn2041363. URL http://www.ncbi.nlm.nih.gov/pubmed/22103256.

[106] Yugang Zhang, Fang Lu, Daniel van der Lelie, and Oleg Gang. Continuous Phase Transformation in Nanocube Assemblies. *Physical Review Letters*, 107(13):2–5, September 2011. ISSN 0031-9007. doi: 10.1103/PhysRevLett.107.135701. URL http://link.aps.org/doi/10.1103/PhysRevLett.107.135701.

[107] Yanli Huo, Hongdong Zhang, and Yuliang Yang. Effects of Reversible Chemical Reaction on Morphology and Domain Growth of Phase Separating Binary Mixtures with Viscosity Difference. *Macromolecular Theory and Simulations*, 13 (3):280–289, April 2004. ISSN 1022-1344. doi: 10.1002/mats.200300021. URL http://doi.wiley.com/10.1002/mats.200300021.

[108] Jacob Christensen, Ken Elder, and Hans Fogedby. Phase segregation dynamics of a chemically reactive binary mixture. *Physical Review E*, 54(3): R2212–R2215, September 1996. ISSN 1063-651X. doi: 10.1103/PhysRevE.54.R2212. URL http://www.ncbi.nlm.nih.gov/pubmed/9965444http://link.aps.org/doi/10.1103/PhysRevE.54.R2212.

[109] Y Oono and S Puri. Study of phase-separation dynamics by use of cell dynamical systems. I. Modeling. *Physical Review A*, 38(1):434–453, July 1988. ISSN 0556-2791. doi: 10.1103/PhysRevA.38.434. URL http://link.aps.org/doi/10.1103/PhysRevA.38.434.

[110] Joshua A. Anderson, Chris D. Lorenz, and A. Travesset. General purpose molecular dynamics simulations fully implemented on graphics processing units. *Journal of Computational Physics*, 227(10):5342–5359, May 2008. ISSN 00219991. doi: 10.1016/j.jcp.2008.01.047. URL http://linkinghub.elsevier.com/retrieve/pii/S0021999108000818.

[111] John W. Cahn. On spinodal decomposition. *Acta Metallurgica*, 9(9):795–801, September 1961. ISSN 00016160. doi: 10.1016/0001-6160(61)90182-1. URL http://linkinghub.elsevier.com/retrieve/pii/0001616061901821.

[112] Sanjay Puri and Vinod Wadhawan. *Kinetics of Phase Transitions*. CRC Press, 2009. ISBN 978-0849390654.

[113] W. Humphrey, A. Dalke, and K. Schulten. VMD: visual molecular dynamics. *Journal of Molecular Graphics*, 14(1):33–8, 27–8, February 1996. ISSN 0263-7855. URL http://www.ncbi.nlm.nih.gov/pubmed/8744570.

[114] Marek Grzelczak, Jan Vermant, Eric M. Furst, and Luis M. Liz-Marzán. Directed self-assembly of nanoparticles. *ACS Nano*, 4(7):3591–605, July 2010. ISSN 1936-086X. doi: 10.1021/nn100869j. URL http://www.ncbi.nlm.nih.gov/pubmed/20568710.

[115] Yan Gao and Zhiyong Tang. Design and application of inorganic nanoparticle superstructures: current status and future challenges. *Small (Weinheim an der Bergstrasse, Germany)*, 7(15):2133–46, August 2011. ISSN 1613-6829. doi: 10.1002/smll.201100474. URL http://www.ncbi.nlm.nih.gov/pubmed/21626691.

[116] Yanhu Wei, Shuangbing Han, Jiwon Kim, Siowling Soh, and Bartosz A. Grzybowski. Photoswitchable catalysis mediated by dynamic aggregation of

nanoparticles. *Journal of the American Chemical Society*, 132(32):11018–20, August 2010. ISSN 1520-5126. doi: 10.1021/ja104260n. URL http://www.ncbi.nlm.nih.gov/pubmed/20698662.

[117] S. Chandrasekhar. *Liquid Crystals*. Cambridge University Press, second edi edition, 1992. ISBN 978-0521427418.

[118] Barrett Comiskey, J. D. Albert, Hidekazu Yoshizawa, and Joseph Jacobson. An electrophoretic ink for all-printed reflective electronic displays. *Nature*, 394 (July):253–255, 1998. doi: 10.1038/28349.

[119] Antonio F. Osorio Vivanco, Monica Olvera de la Cruz, and Sharon C. Glotzer. Optimized Assembly Speed in Dissipative Systems of Photo-Switchable Colloids. pages 1–12, 2013.

[120] Younan Xia, Yujie Xiong, Byungkwon Lim, and Sara E. Skrabalak. Shape-controlled synthesis of metal nanocrystals: simple chemistry meets complex physics? *Angewandte Chemie (International ed. in English)*, 48(1):60–103, January 2009. ISSN 1521-3773. doi: 10.1002/anie.200802248. URL http://www.pubmedcentral.nih.gov/articlerender.fcgi?artid=2791829&tool=pmcentrez&rendertype=abstract.

[121] Rachel K Smith, Penelope a Lewis, and Paul S Weiss. Patterning self-assembled monolayers. *Progress in Surface Science*, 75(1-2):1–68, June 2004. ISSN 00796816. doi: 10.1016/j.progsurf.2003.12.001. URL http://linkinghub.elsevier.com/retrieve/pii/S0079681603001382.

[122] Katsuhiko Ariga, Jonathan P Hill, and Qingmin Ji. Layer-by-layer assembly as a versatile bottom-up nanofabrication technique for exploratory research and realistic application. *Physical chemistry chemical physics : PCCP*, 9(19):2319–40, May 2007. ISSN 1463-9076. doi: 10.1039/b700410a. URL http://www.ncbi.nlm.nih.gov/pubmed/17492095.

[123] Shawn M. Douglas, Hendrik Dietz, Tim Liedl, Björn Högberg, Franziska Graf, and William M. Shih. Self-assembly of DNA into nanoscale three-dimensional shapes. *Nature*, 459(7245):414–8, May 2009. ISSN 1476-4687. doi: 10.1038/nature08016. URL http://www.pubmedcentral.nih.gov/articlerender.fcgi?artid=2688462&tool=pmcentrez&rendertype=abstract.

[124] Igor S. Aranson. Active colloids. *Physics-Uspekhi*, 56(1):79–92, January 2013. ISSN 1063-7869. doi: 10.3367/UFNe.0183.201301e.0087. URL http://stacks.iop.org/1063-7869/56/i=1/a=79?key=crossref.08927423854c8de3743eaac303a47720.

[125] Xiaojiang Zhang, Kenneth D. Harris, Nathanael L. Y. Wu, Jeffrey N. Murphy, and Jillian M. Buriak. Fast assembly of ordered block copolymer nanostructures through microwave annealing. *ACS Nano*, 4(11):7021–9, November 2010. ISSN

1936-086X. doi: 10.1021/nn102387c. URL http://www.ncbi.nlm.nih.gov/pubmed/20964379.

[126] Hongmei Huang, Jeffrey N. Anker, Kemin Wang, and Raoul Kopelman. Magnetically assisted and accelerated self-assembly of strawberry-like nano/microparticles. *The Journal of Physical Chemistry B*, 110(40):19929–34, October 2006. ISSN 1520-6106. doi: 10.1021/jp062070j. URL http://www.ncbi.nlm.nih.gov/pubmed/17020379.

[127] Sun Choi, Inkyu Park, Zhao Hao, Hoi-ying N. Holman, Albert P. Pisano, and Tarek I. Zohdi. Ultrafast self-assembly of microscale particles by open-channel flow. *Langmuir : the ACS journal of surfaces and colloids*, 26(7):4661–7, April 2010. ISSN 1520-5827. doi: 10.1021/la903492w. URL http://www.ncbi.nlm.nih.gov/pubmed/19921822.

[128] Sun Choi, Arash Jamshidi, Tae Joon Seok, Ming C. Wu, Tarek I. Zohdi, and Albert P. Pisano. Fast, high-throughput creation of size-tunable micro/nanoparticle clusters via evaporative self-assembly in picoliter-scale droplets of particle suspension. *Langmuir : the ACS journal of surfaces and colloids*, 28 (6):3102–11, February 2012. ISSN 1520-5827. doi: 10.1021/la204362s. URL http://www.ncbi.nlm.nih.gov/pubmed/22260193.

[129] T. Witten and L. Sander. Diffusion-Limited Aggregation, a Kinetic Critical Phenomenon. *Physical Review Letters*, 47(19):1400–1403, November 1981. ISSN 0031-9007. doi: 10.1103/PhysRevLett.47.1400. URL http://link.aps.org/doi/10.1103/PhysRevLett.47.1400.

[130] M. Y. Lin, H. M. Lindsay, D. A. Weitz, R. Klein, R. C. Ball, and P. Meakin. Universal diffusion-limited colloid aggregation. *Journal of Physics: Condensed Matter*, 2(13):3093–3113, April 1990. ISSN 0953-8984. doi: 10.1088/0953-8984/2/13/019. URL http://stacks.iop.org/0953-8984/2/i=13/a=019?key=crossref.c2320b20e7ca4837bdbf297341418de7.

[131] Tamás Vicsek. Pattern Formation in Diffusion-Limited Aggregation. *Physical Review Letters*, 53(24):2281–2284, December 1984. ISSN 0031-9007. doi: 10.1103/PhysRevLett.53.2281. URL http://link.aps.org/doi/10.1103/PhysRevLett.53.2281.

[132] Dimitri Gidaspow and Lu Huilin. Equation of state and radial distribution functions of FCC particles in a CFB. *AIChE Journal*, 44(2):279–293, February 1998. ISSN 00011541. doi: 10.1002/aic.690440207. URL http://doi.wiley.com/10.1002/aic.690440207.

[133] J. S. van Duijneveldt and Daan Frenkel. Computer simulation study of free energy barriers in crystal nucleation. *The Journal of Chemical Physics*, 96(6): 4655, 1992. ISSN 00219606. doi: 10.1063/1.462802. URL http://link.aip.org/link/JCPSA6/v96/i6/p4655/s1&Agg=doi.